

Wilhelm Bergesen

Optimization of the Energy Management System of a Solar Car

Master's thesis in Electric Power Engineering

Supervisor: Steve Völler

June 2023

Wilhelm Bergesen

Optimization of the Energy Management System of a Solar Car

Master's thesis in Electric Power Engineering
Supervisor: Steve Völler
June 2023

Norwegian University of Science and Technology
Faculty of Information Technology and Electrical Engineering
Department of Electric Power Engineering





Kunnskap for en bedre verden

DEPARTMENT OF ELECTRICAL ENERGY

TET4900 - ELECTRICAL ENERGY AND ENERGYSYSTEMS,
MASTERS THESIS

Optimization of the Energy Management System of a Solar Car

Author:
Wilhelm Bergesen

Supervisor:
Steve Völler

19.06.2023

Abstract

The World Solar Challenge is a solar car event where fully self-sufficient, grid-disconnected, solar-powered electric vehicles race across Australia, only assisted by a low-capacity energy storage system. The solar cars function like tiny mobile microgrids. Solar cars are highly specialized systems and require thorough research before constructing a functioning one.

This thesis aims to investigate everything related to the energy management system for a solar car participating in the World Solar Challenge's Challenger class. This includes determining the solar profile for the route, calculating the expected energy production of the solar car's photovoltaic generators, determining the energy consumption for a solar car during a race, and determining which components would be best to construct a high-performance solar car from. The study would also explore how best to utilize the low-capacity energy storage system. These tasks were approached through an extensive literature study, an investigation of previous contestants, and the creation of a Python library named `scpylib`.

`scpylib` was built to simulate a solar car driving from Darwin to Adelaide like a participant of the World Solar Challenge would. `scpylib` retrieves solar irradiance and other weather data from PVGIS based on a map. It then calculates the expected output of the photovoltaics. Finally it runs a race simulation, where the performance is calculated through a mathematical model of the solar car based on travel speed and the photovoltaic output data.

The literature study and simulations found that a solar car with the following characteristics would be the most viable choices for a new solar car team. The car should have a monohull shape, as it has proven to be the best-performing in recent years. The microgrid topology should consist of a lithium-ion battery, monocrystalline silicon photovoltaic cells, a maximum power point tracker DC-DC converter, and a three-phase three-level inverter. Alternatives would be a lithium-sulfur battery and perovskite-based photovoltaic cells. However, they are not yet commercially available, and their performance in such a niche high-temperature area, like the World Solar Challenge, is yet to be seen.

The simulations' results determine that the simulation model is realistic, despite its many simplifications. The load model is simplified by only calculating the energy consumption at cruising speeds, and the acceleration phase is neglected. It also behaves unrealistically at low solar car speeds, but this is not an issue due to neglecting of the acceleration phase. `scpylib` is currently incapable of running simulations based on too many data points within the map file. This is primarily due to its method of preparing and storing data. Workarounds to this problem have been proposed, but simulation times would increase by a large margin.

The retrieved data is based on real measurements, validating the simulations' realism. However, race strategizing and optimizing become more difficult due to this. Utilizing weather forecasts to influence simulations becomes unreliable as the solar irradiance from the retrieved data is likely already influenced by sky coverage. The proposed method of avoiding this would be to standardize the data, then manipulate it during simulations.

This thesis will prove helpful to solar car teams starting out, as information about a vast field of study has been compiled into this one document, serving as an introduction and a guide. `scpylib` will also serve as a viability analysis tool with building blocks for more advanced future simulations.

Sammendrag

The World Solar Challenge er et solcellebilkonkurranse der fullstendig selvforsynte, nettfrakoblede, solcelledrevne elektriske kjøretøy kjører om kapp på tvers av Australia, kun hjulpet av et energilagringssystem med lav kapasitet. Solcellebilene fungerer som små mobile mikronett. Solcellebiler er svært spesialiserte systemer og krever grundig forskning før man kan konstruere en fungerende solcellebil.

Denne avhandlingen har som mål å undersøke alt som er relatert til energistyringssystemet for en solcellebil som deltar i World Solar Challenge i "Challenger" klassen. Dette inkluderer å bestemme solprofilen for ruten, beregne forventet energiproduksjon for en solcellebils solcelleanlegg, bestemme energiforbruket til en solcellebil under et løp, og bestemme hvilke komponenter som ville være best egnet til å konstruere en høyt ytende solcellebil. Studien vil også utforske hvordan man best kan utnytte energilagringssystemet. Disse oppgavene ble utført gjennom omfattende litteraturstudier, undersøkelser av tidligere deltakere og opprettelsen av et Python-bibliotek kalt "scpylib".

"scpylib" ble utviklet for å simulere en solcellebil som kjører fra Darwin til Adelaide, på samme måte som en deltaker i World Solar Challenge ville gjort det. "scpylib" henter solinnstråling og annen værdata fra PVGIS basert på et kart. Deretter beregner den forventet produksjon fra solcelleanlegget. Til slutt kjører den en løpssimulering, der ytelsen beregnes ved hjelp av en matematisk modell av solcellebilen basert på kjørehastighet og data om solcelleanleggets produksjon.

Litteraturstudien og simuleringene konkluderte med at en solcellebil med følgende egenskaper ville være de beste valgene for et nytt solcellebilt team. Bilen bør ha en skrogform (monohull), da denne typen bil har vist seg å ha best ytelse de siste årene. Mikronett-topologien bør bestå av et litium-ion-batteri, monokrystallinske silisium solceller, en DC-DC-konverter for maksimal effekt-punktsparing og en trefaset trelags omformer. Alternativer kunne være et litium-svovel-batteri og solceller basert på perovskitt. Imidlertid er disse alternativene ennå ikke kommersielt tilgjengelige, og deres ytelse i en slikt nisjeområde med høye temperaturer som World Solar Challenge er ennå ikke sett.

Resultatene fra simuleringene viser at simuleringen er realistisk, til tross for mange forenklinger. Lastmodellen forenkles ved å bare beregne energiforbruket ved cruise fart, og akselerasjonsfasen blir neglisjert. Den oppfører seg også urealistisk ved lave hastigheter, men dette er ikke et problem på grunn av neglisjeringen av akselerasjonsfasen. "scpylib" er for øyeblikket ikke i stand til å kjøre simuleringer basert på for mange datapunkter innenfor kartfilen. Dette skyldes hovedsakelig dens metode for forberedelse og lagring av data. Det er foreslått løsninger på dette problemet, men simuleringstiden ville øke betydelig.

De innhentede dataene er basert på virkelige målinger, noe som bekrefter simuleringenes realisme. Imidlertid blir løpsstrategier og optimalisering mer utfordrende på grunn av dette. Bruk av værmeldinger for å påvirke simuleringer blir upålitelig ettersom solinnstrålingen fra de innhentede dataene allerede sannsynligvis er påvirket av skydekke. Den foreslåtte metoden for å unngå dette er å standardisere dataene og deretter manipulere dem under simuleringer.

Denne avhandlingen vil være nyttig for solcellebil team som starter ut, da informasjon om et bredt studieområde er samlet i dette dokumentet som en introduksjon og guide. "scpylib" vil også fungere som et verktøy for levedyktighetsanalyse med byggeklosser for mer avanserte simuleringer i fremtiden.

Acknowledgement

I would like to express my gratitude to my supervisor Steve Völler, for granting me direction and providing feedback on my report. He has been readily available, be through meetings or email. I would also like to acknowledge his great taste in T-shirt motifs.

I would like to express my gratitude to my family. For cheering me on through the five years i've spent in Trondheim, and always being there when i come home

Next, i would like to thank my girlfriend for being so supportive and kind. She has always been ready to cheer me up.

I would also like to thank my flatmates for the most positively chaotic living conditions i've experienced, and I will miss never knowing what shenanigans to expect when i return from a long day at the university.

Lastly i would like to thank my fellow students at room F-325 (also known as the sewer-hall). We shared many laughs and conversations, and have gone through several of the tribulations the F-block presented. Be it leakage from the ceiling, loud construction noises, or extreme indoor temperatures.

Acronyms

AC Asymmetric Catamaran. ix, 5, 16, 30, 54
DoD Depth of Discharge. 19, 28
ESS Energy Storage System. ix, x, xii, 7, 18–21, 28–31, 38, 49, 50, 53, 54, 56–59
EV Electric Vehicle. 1, 7, 18
LP Load Profile. 22
MH Monohull. 5, 30, 53, 54, 56, 58
MJ Multi-Junction. 13, 30, 54, 58
MPP Maximum Power Point. 16, 21, 55, 58
NTNU Norwegian University for Science and Technology. 26
PMSM Permanent Magnet Synchronous Motor. 1, 21
PV Photovoltaic. ix, x, xii, 1–3, 6, 8, 9, 11–18, 20, 21, 26, 28, 30, 31, 37, 38, 41, 46, 52–59
PVGIS Photovoltaic Geographical Information System. 26
PWM Pulse Width Modulation. 21
SC Solar Car. ix–xii, 1–3, 5, 7–9, 13, 15, 16, 18, 20–24, 26–34, 37, 38, 41, 45–59, 67, 81–88
scpylib Solar car python library. 33
SI	. Solar Irradiance. ix–xii, 9, 10, 13, 15, 16, 26–28, 31, 33, 36, 37, 41, 42, 44, 50, 52, 53, 55–59, 68–73
SoC State of Charge. x, 18, 19, 31, 38, 50, 54, 57
WSC	World Solar Challenge. ix–xii, 1–6, 15, 18, 24, 27, 28, 30, 42–44, 46, 54–56, 58, 59, 67, 73, 80

Nomenclature

CuGaSe₂ Copper Gallium Selenium

CuInSe₂ Copper Indium Selenium.

Li – ion Lithium-ion. Common chemical structure of rechargeable batteries

Li – polymer Lithium-ion polymer, also abbreviated as LiPo, is a type of rechargeable batteries that use a solid polymer electrolyte instead of a liquid electrolyte.

Li – S Lithium-Sulfur. A high energy density rechargeable battery chemical structure

LiFePO₄ Lithium iron phosphate. A rechargeable battery chemistry that is characteristically safe and durable.

CdTe Cadmium Telluride. A thin film solar technology.

GaAs Gallium Arsenide

Table of Contents

List of Figures	ix
List of Tables	xii
1 Introduction	1
1.1 Background	1
1.2 Objective	1
1.3 Project Boundaries	2
1.4 Structure of the Thesis	2
2 The World Solar Challenge	3
2.1 History	3
2.1.1 Other solar challenges	5
2.2 Rules and regulations	6
2.2.1 Photovoltaic Cells and Solar Collectors	6
2.2.2 Energy Storage System	6
2.3 Nordlys NTNU	7
3 Theoretic Background	8
3.1 Micro-grids	8
3.2 Photovoltaic-Cells	9
3.2.1 Solar irradiance	9
3.2.2 Basic semiconductor physics and band-gap energy	11
3.2.3 Tilt angle and azimuth	13
3.2.4 Power Generation	15
3.3 Energy Storage System	18
3.3.1 Basic electrochemical battery physics	18
3.3.2 Battery reliability, efficiency, and safety	18
3.3.3 Capacity, charge- and discharge rate	19
3.3.4 Heating	19
3.4 Power electronics	20
3.5 The motor	21
3.6 The Solar Car's Mechanics	22
3.6.1 Incline	22
3.6.2 Drag	23

3.6.3	Rolling resistance	24
3.6.4	Work and power	24
3.7	Dynamic Model and Load Profile	24
4	Methodology	26
4.1	Software	26
4.2	Solar profile of the route	27
4.2.1	Map	27
4.3	Energy Production	28
4.4	Energy Consumption	28
4.5	Energy Storage System Inclusion	28
4.6	Optimization and predictive simulation	29
4.7	Choice of Suitable Components	29
4.7.1	Shape	30
4.7.2	Photovoltaics and Power Electronics	30
4.7.3	Compatible Energy Storage System	30
4.8	Simplifications	31
4.8.1	Electric circuit calculations	31
4.8.2	Load profile	32
4.9	Simulation baseline	32
5	Codebase	33
5.1	Architecture	33
5.2	Simplifications and limitations	41
5.2.1	Energy consumption	41
6	Results	42
6.1	Solar Profile	42
6.2	Energy generation	45
6.3	Energy consumption	46
6.4	Choice of suitable components	49
6.5	Solar car simulation	49
7	Discussion	52
7.1	Weather data	52
7.1.1	Solar Irradiance Data	52
7.1.2	Wind	52

7.2	Photovoltaic generation	53
7.2.1	Array orientation	53
7.2.2	Temperature	53
7.2.3	Electrical dynamics	53
7.3	The Solar Car's energy consumption	53
7.4	Choice of Components	54
7.5	Codebase	55
7.5.1	Energy Storage System Utilization Strategy	56
7.6	Future work	56
7.6.1	Electric analysis	56
7.6.2	Solar car shape	56
7.6.3	Load model	56
7.6.4	Simulation improvements	57
7.6.5	Data Processing and Standardization	57
8	Conclusion	58
	Bibliography	60
	Appendix	66
A	Previous contestants	66
B	Plots	68
B.1	Hourly Solar Irradiation Data	68
B.2	Average SI value throughout the route	74
B.3	Hourly Temperature	74
B.4	Average temperature	80
B.5	PV output	81
B.6	Average PV output per day throughout the route.	86
B.7	Load	87

List of Figures

1	The Quiet Achiever. Worlds first practical SC powered entirely by PV-cells.	3
2	Three different contestants from the original WSC in 1987.	4
3	The route map for the WSC. Starting out in Darwin and ending in Adelaide, with 9 landmarks in-between.	4
4	The SCs WSC showcases on their website as examples for their classes.	5
5	Examples of modern SC shapes.	5
6	Nordlys' logo from their website: https://www.nordlysntnu.no/	7
7	Illustration of a microgrid. The collection of buildings in the center serves as the load with other microgrid features surrounding it. It can also be noted that the illustration showcases a microgrid with an optional network connection. [1]	8
8	An example of a modern SC with an overlay of its components. Black lines for power flow, and blue dotted lines for electrical signals.	9
9	Single-line diagram for the SC.	9
10	World solar radiation map. [2]	10
11	Long term averages for Global Horizontal Irradiation in Australia [3].	10
12	Graph depicting the solar spectral irradiance experienced at the upper atmosphere and at sea level. The graph also shows values specific to silicon PVs. [4]	11
13	[5]	12
14	Band diagram of a semiconductor. Silicon at $0^{\circ}K$ has zero electrons in the conduction band, making it a perfect insulator. [5]	12
15	PV array facing south at a fixed tilt. The array faces south with an azimuth angle of 0° . [6]	14
16	The effect of PV panel tilt on solar energy capture. [6]	14
17	PV tilt of an SC driving up an incline. The effective tilt equals the incline added to the tilt of the PVs on the SC.	14
18	Screenshots from areas along the route taken using google maps. The vast majority of the route looks like 18b and 18d.	15
19	Two simple illustrations of an AC-shaped SC from an eagle-eye perspective. The illustration showcases how cockpit placement can affect the total SI hitting the PV panels on the SC by shading them depending on relative orientation to the sun.	16
20	The maximum power point of a PV cell. [7]	17
21	IV-characteristic graph depicting how changes in temperature affect the cell. [8]	17
22	The quadrant concept. [9]	20
23	The gravitational- and normal forces on a object on an incline. f is resistance, Θ being the incline and $mg\sin\Theta$ is the sum of the gravitational- and normal forces. [10]	23
24	Elevation profile from measurements done by the Stanford Solar Car team [11].	27
25	The ESS discharge regulation coefficient with a wide scope.	29
26	The ESS discharge regulation within expected SC performance.	29

27	The efficiency of the SC's electric circuit.	31
28	Structure of the main folder of scpylib.	33
29	Most relevant contents of pvlib for SCs.	34
30	The map functions folder.	35
31	Chart depicting the SI data retrieving scripts architecture.	36
32	Chart depicting the PV output calculation process.	37
33	Chart depicting the architecture of Race_simulation.py.	38
34	Flowchart depicting a race simulation using Race_simulation.py.	39
35	The hourly SI for the starting point 35a and destination 35b for the WSC. The data is for a TMY.	42
36	Average SI for the landmarks along the route in October during a TMY.	42
37	The wind speed for the starting point and destination for the WSC. The data is for a TMY.	43
38	Average wind speed for the landmarks along the route in October during a TMY.	43
39	Maximum wind speed for the landmarks along the route in October during a TMY.	44
40	The temperature for the starting point and destination for the WSC. The data is for a TMY.	44
41	Average temperature for the landmarks along the route in October during a TMY.	45
42	Maximum temperature for the landmarks along the route in October during a TMY.	45
43	The PV output of the SC for the starting point and ending of destination for the WSC. The data is for a TMY. The graph looks identical	46
44	Average PV output for the landmarks along the route in October during a TMY. The average value includes nighttime in the calculation.	46
45	The load of the SC between 0 and 130 km/h, with steps in incline between 0° and 4°.	47
46	The load of the SC between 0 and 130 km/h, with steps in wind speed between 0m/s and 10m/s	47
47	The load of the SC between 0 and 130 km/h, with steps in wind speed between -2.5m/s and -12.5m/s. The load is still positive at Velocity = 0m/s, and increases close to linearly up to around the 30km/h mark. This being due to how the load is calculated in the code. The load behaves properly once the SC speed equals the wind speed.	48
48	The load of the SC between 0 and 130 km/h, with steps in temperature between 15°C and 35°C.	48
49	The speed of the simulated SC through the race. The velocity at the end of day 1 is 46.5km/h. The low points are during the final hour of the race before the end of the daily nine legal driving hours, when the SI is at its lowest.	50
50	The ESS's SoC throughout the race.	50
51	The progress of the simulated SC as a function of time. The race ends at the end of the fourth day.	51
52	Hourly SI-data for Darwin during October. The data is from a TMY.	68

53	Hourly SI-data for Katherine during October. The data is from a TMY.	68
54	Hourly SI-data for Daly Waters during October. The data is from a TMY.	69
55	Hourly SI-data for Tennant Creek during October. The data is from a TMY.	69
56	Hourly SI-data for Barrow Creek during October. The data is from a TMY.	70
57	Hourly SI-data for Alice Springs during October. The data is from a TMY.	70
58	Hourly SI-data for Kulgera during October. The data is from a TMY.	71
59	Hourly SI-data for Coober Pedy during October. The data is from a TMY.	71
60	Hourly SI-data for Glendambo during October. The data is from a TMY.	72
61	Hourly SI-data for Port Augusta during October. The data is from a TMY.	72
63	Average SI per day in October throughout the WSC route. The data is from the TMY PVGIS.	73
62	Hourly SI-data for Adelaide during October. The data is from a TMY.	73
64	Hourly ambient air temperature for Darwin during October. The data is from a TMY.	74
65	Hourly ambient air temperature for Katherine during October. The data is from a TMY.	75
66	Hourly ambient air temperature for Daly Waters during October. The data is from a TMY.	75
67	Hourly ambient air temperature for Tennant Creek during October. The data is from a TMY.	76
68	Hourly ambient air temperature for Barrow Creek during October. The data is from a TMY.	76
69	Hourly ambient air temperature for Alice Springs during October. The data is from a TMY.	77
70	Hourly ambient air temperature for Kulgera during October. The data is from a TMY.	77
71	Hourly ambient air temperature for Coober Pedy during October. The data is from a TMY.	78
72	Hourly ambient air temperature for Glendambo during October. The data is from a TMY.	78
73	Hourly ambient air temperature for Port Augusta during October. The data is from a TMY.	79
74	Hourly ambient air temperature for Adelaide during October. The data is from a TMY.	79
75	The average temperature for the entire route for the WSC during a TMY.	80
76	Relative air drag coefficient through the route. 1.0 being the air-drag coefficient for 30°Celsius.	80
77	PV output of the SC throughout October in Darwin during a TMY.	81
78	PV output of the SC throughout October in Katherine during a TMY.	81
79	PV output of the SC throughout October in Daly Waters during a TMY.	82
80	PV output of the SC throughout October in Tennant Creek during a TMY.	82

81	PV output of the SC throughout October in Barrow Creek during a TMY.	83
82	PV output of the SC throughout October in Alice Springs during a TMY.	83
83	PV output of the SC throughout October in Kulgera during a TMY.	84
84	PV output of the SC throughout October in Coober Pedy during a TMY.	84
85	PV output of the SC throughout October in Glendambo during a TMY.	85
86	PV output of the SC throughout October in Port Augusta during a TMY.	85
87	PV output of the SC throughout October in Adelaide during a TMY.	86
88	Average PV-output per day throughout the route in october during a TMY. . . .	86
89	The load for the SC with steps in incline.	87
90	The load for the SC with steps in windspeed.	87
91	The load for the SC with steps in air temperature.	88

List of Tables

1	WSC class distinctions.	5
2	The allowable total cell mass of rechargeable electrochemical cells.	6
3	Lithium-ion battery cells with size designator restrictions. The number of cells equal to the allowable total cell mass divided by individual cell weight.	7
4	Different PV cell materials's and chemical compositions's bandwidth energy and corresponding maximum wavelength. Multijunction cells's properties not listed. . .	13
5	ESS C-rate effects on performance and duration.	19
6	Air density based on temperature. [12]	23
7	Size of SI data files retrieved based on amount of locations.	27
8	Values from the Stanford Solar Car Team map file.	28
9	The parameters for the top three performing cars of the WSC between 2011-2019. Some data is inaccessible due to teams being competitively secretive.	30
10	Constant values for simulating the SC.	32
11	Excerpt from the retrieved weather data. The data is for October during a TMY. .	44
12	The simulation results depending on battery C-rate. The optimal C-rate for these racing conditions is between 0.0525 and 0.05, where the ESS is depleted just as the SC passes the finish line.	49
13	SC-data for all the finishing contestants for the WSC 2019 and 2017. It should be noted that this list only includes finishing teams. The total number of entries into the challenger class would be approximately 30 each year.	67

1 Introduction

1.1 Background

In recent years, there has been a growing global concern about the detrimental effects of fossil fuels on the environment, including air pollution and climate change. A typical passenger vehicle emits about 4.6 metric tons of carbon dioxide yearly [13]. The developments in Electric Vehicle (EV) technologies are beneficial in reducing the total amount of carbon dioxide released into the atmosphere. Lithium battery- and Permanent Magnet Synchronous Motor (PMSM) technology improvements have helped extend EVs' energy storage capabilities, range, and dynamic capabilities, such as speed and acceleration. However, EVs still need to be charged with power from the grid. This increase in load has introduced new challenges when it comes to grid stability and energy planning. Simultaneous EV charging may lead to grid congestion and higher power peaks [14]. Though renewable sources are becoming a significant part of power generation, more than 60% of global electric energy comes from burning fossil fuels [15]. Peaking power plants are also usually gas turbines [16]. Thus more carbon will be released due to EV charging-induced power peaks. Therefore, we must explore other charging options to achieve the UN's Sustainable Development Goals 7, 9, and 13 [17].

- Affordable and clean energy
- Industry, innovation, and infrastructure
- Climate action

A potential solution would be self-charging cars equipped with Photovoltaics (PV), commonly known as Solar Cars (SC). By harnessing the Sun's power through integrated PVs, SCs can generate clean, renewable energy while on the move, reducing the reliance on the grid. The concept is not entirely new, as solar-powered vehicles date back to the 1980s when Australia held the first World Solar Challenge (WSC). To compete in such an event with an SC, a sound foundational understanding of SCs dynamics and PVs is needed. Furthermore, one part of that understanding comes from knowledge of the vehicle's route and the components best suited to traverse such environments.

1.2 Objective

The previous paragraph specified the need for knowledge regarding SC racing, and this thesis seeks to attain it. However, the technical field of SC racing is broad and consists of multiple disciplines. So this thesis will conduct research regarding an SC's energy management system. We can specify this thesis' search for knowledge further by dividing its field of research into four key objectives::

1. Generate a solar profile along the road for the race
2. Calculate the energy production from the solar profile for different solar cell settings during the race
3. Calculate the estimated energy consumption of the car, based on e.g., components, car shape, and outer factors (road conditions, speed, etc.) in combination with a storage unit
4. Choose suitable components

We can engage in a more informed approach to constructing an SC by achieving these goals. The goals listed above will primarily be referred to as Solar Profile, Energy Production, Energy Consumption, and Suitable Component Choice.

1.3 Project Boundaries

The scope of this master's thesis project is centered around the comprehensive energy management of an SC, specifically designed to participate in the prestigious WSC. The project primarily consists of a theoretical study, without incorporating physical models, aiming to achieve the objectives listed in the previous subsection. Though the project will delve into the technical aspects of the electric system and run calculations regarding PV-based energy generation, no specifics about the system's electric specifics will be considered. This precludes calculations regarding voltage levels, current drawn, specific components' impedance, switching frequency, and the like. However, these topics will be researched and discussed as they will be important in choosing suitable components.

The project will also focus solely on the WSC and its specifics. Therefore, there will be little to no consideration for the SC's performance in any other arena. While the focus remains on the WSC, the project does not extend into the physical construction or implementation of the SC, remaining within the realm of theoretical analysis and simulation. The study will also disregard the economic aspect and the financing of constructing a physical SC. But it will consider commercial availability when choosing components.

1.4 Structure of the Thesis

The thesis contains eight chapters, including this one and an appendix.

The first chapter is the one you are currently reading. This chapter introduces the reader to SC racing and the challenges this thesis addresses. It also defines the scope of the thesis by specifying the objectives and boundaries.

The second chapter explains the concept of SC racing as a competition. It also goes over the WSC's history as the world's first SC race and the motivations behind its creation. The chapter then delves into the relevant rules and regulations for the objectives of this thesis.

The third chapter contains relevant theory. Its purpose is to give the reader an understanding of the theory regarding PVs, power electronics, and electric drives. The chapter also covers some of the natural phenomena that affect the performance of an SC and its parts.

The fourth chapter explains the methodology. It tells the reader how the knowledge gathered in the third chapter will be used to solve the challenges and reach thesis objectives. It tells the reader which software will be used and why. It also contains data from previous contestants from the WSC. It also presents the simplifications made.

The fifth chapter presents the codebase. It presents to the user the library developed for the project's duration. It explains the codebase architecture and its functionalities and outputs. The chapter also delves more into how the simplifications presented in the fourth chapter affect the functions.

The sixth chapter presents the results. This chapter presents how inputs affect the output of the functions within the codebase. The outputs presented are predictions of how an SC behaves based on the phenomena presented in chapter three. **The sixth chapter also presents the chosen components of the SC.**

The seventh chapter is for discussion. In it, the results presented in the sixth chapter are discussed. It also discusses the future steps towards a working physical SC and how the created codebase can be used to determine component choices and test racing strategies. It also discusses the ramifications of the simplifications specified in the fourth chapter.

The eighth chapter is the conclusion chapter. This chapter concludes the thesis based on the matters discussed in the seventh chapter.

The entirety of the codebase is submitted as a zip file. As this thesis is a continuation of the specialization project written in the fall of 2022, some parts of Chapters 2 and 3 are reused and/or rewritten for this thesis, and are cited with the following source [18].

2 The World Solar Challenge

2.1 History

The Bridgestone World Solar Challenge¹, formerly known as the World Solar Challenge (WSC) pre-2013, is an international SC event in Australia. The event has its roots in the 1980s. It started with the adventurer Hans Tholstrup and former racing driver Larry Perkins crossing Australia from west to east in their homemade SC, The Quiet Achiever.



Figure 1: The Quiet Achiever. Worlds first practical SC powered entirely by PV-cells.

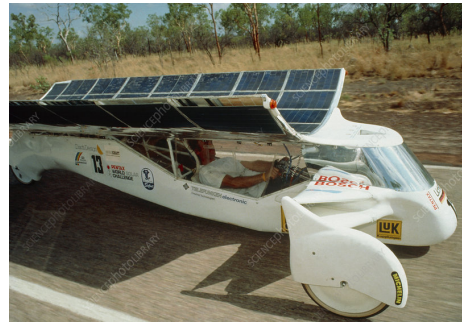
Inspired by their achievement, Hans urged others to explore the boundaries of sun-powered transport, thus founding the WSC. Five years later, in 1987, the first official WSC event was held. During the event, all the competing cars were to race from Darwin in northern Australia, through the Outback, then to Adelaide in southern Australia. Entrants from the 1987 event can be seen in Figure 2. After 1987, the event was held again every three years until 1999 and every second year after that.

The event is still about technological innovation within personal transport. The event continues to push participating teams to develop better designs for SCs and utilize new PV technologies. The technological development is evident in the WSC's rule and regulation evolution. In 1987, there was a single competing class. Participants in this racing class were allowed $8.0m^2$ of solar collectors. In 2005 several teams experienced a handicap from the South Australia speed limit of 110km/h. This was due to teams discovering more optimal aerodynamic designs and developments within PV technologies. It was generally agreed upon that Tholstrup's original challenge of traversing Australia in a purely solar-powered vehicle was well met and exceeded. Thus the organizers introduced two classes in 2007: The Challenger and the Adventure class. The new Adventure class was meant to encourage a practical design for an SC, while the Challenger class remained the same in concept. However, new restrictions and requirements were introduced to the Challenger class. The most notable one was that the total solar collector area was reduced to $6m^2$. In 2013 the Cruiser class was introduced. This class expanded upon the ideas from the original Adventure class of a more practical SC. The Cruiser class is for SCs designed with practicality and commercial market viability in mind. The Adventure class became a non-competitive class for all SCs, which fit the road safety criteria, but not the other regulations for the Cruiser- and Challenger classes. Further developments in battery capacity and PV cells have led to further restrictions and rule changes, and it's also expected to do so sometime in the future [19]. Examples from the different classes can be seen in Figure 4.

¹<https://worldsolarchallenge.org/>



(a) Example one [20]



(b) Example two [21]



(c) Example three [21]

Figure 2: Three different contestants from the original WSC in 1987.



Figure 3: The route map for the WSC. Starting out in Darwin and ending in Adelaide, with 9 landmarks in-between.



(a) Challenger



(b) Cruiser



(c) Adventure

Figure 4: The SCs WSC showcases on their website as examples for their classes.

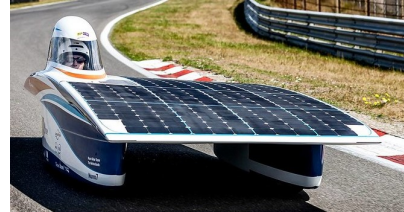
WSC class specifics		
Challenger	Cruiser	Adventure
Single seat	Two or more seats	Any number of seats
Competitive	Competitive	Non competitive
Solely judged by finishing time	Judged by several factors	No judges
Maximum of $4.0m^2$ of Solar collector	Maximum of $5.0m^2$ of Solar collector	No specified limit
Energy Storage System restrictions	No Energy Storage System restrictions	No Energy Storage System restrictions
Specified car occupant weight	Specified car occupant weight	No specified car occupant weight

Table 1: WSC class distinctions.

The general shape of an SC has changed since the first WSC. The two top-performing shapes for an SC currently are a Monohull/Bullet car (MH) and Asymmetric Catamaran (AC). Examples of both can be seen in Figure 5. MH-shaped SCs usually have the cockpit in the center of the front end. The AC-shaped SCs, however, usually have them on one side in the back portion. They also usually have a thin bridge between the cockpit side and the other wheeled side, hence the name. Other shapes may be more suited for the challenge that may be discovered in the future with changes to the rules and regulations, but as of right now, these two dominate the leaderboards.



(a) Monohull



(b) Asymmetric Catamaran

Figure 5: Examples of modern SC shapes.

2.1.1 Other solar challenges

Inspired by the first WSC, other countries started to host solar car events. Other notable events are the American Solar Challenge², the Dell-Winston School Solar Car Challenge³, and the South African Solar Challenge⁴. Several more events are hosted around the world regularly, with their own routes, specifications, and characteristics. One of the main differences between the WSC and some of the other events is the classes. Some of the events host drag and track races, which are usually a lot shorter than the endurance run experienced in the WSC. [22]

²<https://www.americansolarchallenge.org/>

³<https://www.solarcarchallenge.org/challenge/>

⁴<https://www.solarchallenge.org.za/>

2.2 Rules and regulations

Knowing the present rules and regulations is essential to design the optimal car for the challenge. The WSC provides a document specifying the limitations of the participating car and its driver. Chapter two, "Solar Car Regulations," is the most relevant chapter for the scope of this paper. [23]

2.2.1 Photovoltaic Cells and Solar Collectors

The regulations specify that the maximum total PV-cell area is $4.0m^2$ for the challenger class. *"The cell area calculations must be based on flat, unconnected cells. For cells that are overlapped, the cell area is defined as the exposed surface area of the cell. Cell area includes active material, busbars, fingers, and connection pads."* [23, p. 20].

The regulations also do not directly specify a maximum power output for the PVs. However, it limits the use of non-silicon PV-cells and alternative charging methods through these two rules two restrictions.

"2.4.1: A standard solar collector uses silicon photovoltaic cells without reflectors or concentrators. Teams wanting to use reflectors, concentrators or some other form of solar collector must send details of the proposed solar collector to the event organiser for approval.

The power generated by a proposed non-standard solar collector should be no more than the power generated by a standard solar collector. The materials should have low environmental toxicity; this precludes the use of GaAs, CdTe and CuInSe₂. Teams wishing to use non-silicon materials of low environmental toxicity, such as perovskites or organic solar cells, should contact the event organiser. Where the solar collector employs reflectors or concentrators, the allowable aperture of the solar collector should not exceed that of a standard solar collector."

"2.4.4: All devices used for solar charging must be carried in the solar car. This includes stands, supports, and cables

One of the major rule changes in recent years is the preclusion of GaAs-based PV technologies. The significance of this change will be presented and discussed in chapters 4 and 7, respectively.

2.2.2 Energy Storage System

The car may store energy. Electrochemical cells are allowed, and the organizers must approve other forms of storage. Tables 2 and 3 display the limits to battery storage. The energy can only be stored in a maximum of 2 packs. For safety reasons, batteries are cannot operate outside of the manufacturer's specifications. Those specifications being minimum and maximum electric and thermal conditions.

Electrochemical cell chemistry ⁵	Allowable total cell mass (kg)
Li-S	15.00
Li-ion	20.00
Li-polymer	20.00
<i>LiFePO₄</i>	36.00

Table 2: The allowable total cell mass of rechargeable electrochemical cells.

⁵See nomenclature for chemistries

Cell size designator ⁶	Deemed cell mass (kg)	Maximum number of cells allowed
18650	0.0476	420
20700	0.0634	315
21700	0.0701	285

Table 3: Lithium-ion battery cells with size designator restrictions. The number of cells equal to the allowable total cell mass divided by individual cell weight.

The general rule of thumb the event organizers use when defining the maximum battery is that the total cell mass should add up to the equivalent capacity of 5kWh. The idea behind the ESS storage limit was: *”If a 1kW car traveled our route from Darwin to Adelaide in 50 hours, the energy consumption would be 50kWh. From that, it would be reasonable to allow a 10% stored energy capacity (5kWh) to cope with hills, cloudy conditions or to have the ability to overtake another vehicle safely.”* [25].

Other limits apply to storage systems, such as primary batteries and capacitors. Capacitors can only store up to 10.0Wh. Primary batteries used to:

- power a real-time clock when the SC is turned off
- retain data when the SC is turned off
- power wireless tire pressure monitors

do not count as a part of the ESS as long as the capacity doesn’t exceed 2.0Wh.

[18]

2.3 Nordlys NTNU

Several universities and businesses send teams worldwide to compete in these events. However, Norway has never founded an SC team as of the start of the project period for this thesis.

Student organizations for competing technology and engineering teams have grown at NTNU in recent years. There are teams for everything from underwater drones, cybersecurity and long-distance endurance cars, but no SC team. Through the efforts of a student with experience in Shift Hyperloop (Competing within hyper-loop-technology) and DNV Fuel Fighter (EV-efficiency), the process of founding Nordlys NTNU was set in motion. Some master specialization projects were proposed, and this thesis is the continuation of one of them. Since Nordlys is Norway’s first SC-team, it was thought to be fitting to compete in the original event in the Challenger class. The possibility of traveling to Australia will also attract motivated engineering students.



Figure 6: Nordlys’ logo from their website: <https://www.nordlysentnu.no/>

⁶The cell size designator is a way to describe cylindrical Li-ion cells. The number consists of two parts. The first two digits is the diameter of the cell in mm, and the last 3 are the height in tenths of a mm. E.g. an 18650 is 18mm in diameter and 65mm tall. [24]

3 Theoretic Background

SC-racing is a complicated combination of several engineering fields. The theory section lays the groundwork for the subsequent sections, emphasizing energy management and the electric aspect of SCs. By drawing on concepts and theories from existing literature, we aim to establish a robust theoretical foundation for our study. We explore relevant models and theories while also analyzing empirical data within the context of the goals set by Nordlys NTNU.

3.1 Micro-grids

Microgrids are smaller electrical grids that utilize local power sources to supply a smaller area. The area in question could be a neighborhood, an island, or an industrial plant. These grids can be completely self-sufficient (islanded mode) or be supplied from the larger electrical grid (grid-connected mode). The power source may be renewable or fossil fuels [26]. The core functionalities are no matter what area it serves: "power generation, power storage, control, manage and measure, convert, and consume" [27]. An illustration of a typical microgrid with several power sources can be seen in Figure 7.

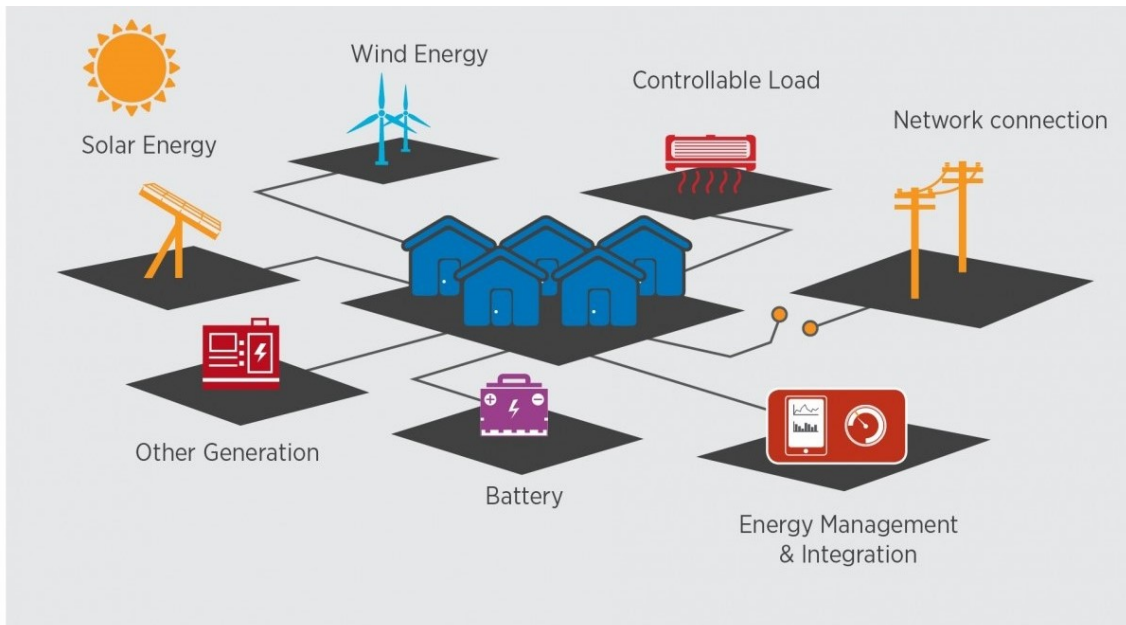


Figure 7: Illustration of a microgrid. The collection of buildings in the center serves as the load with other microgrid features surrounding it. It can also be noted that the illustration showcases a microgrid with an optional network connection. [1]

An SC is a unique microgrid. The scale is tiny compared to other microgrids, the load can experience large fluctuations, and it is mobile. Because it is mobile and because of regulations specified in [23], the entire grid is permanently disconnected from the main grid. However, the topology resembles a PV grid operating in islanded mode. An illustration depicting an SC with its microgrid components highlighted can be seen in Figure 8. A single-line diagram for the SC grid topology can be seen in Figure 9. [18]

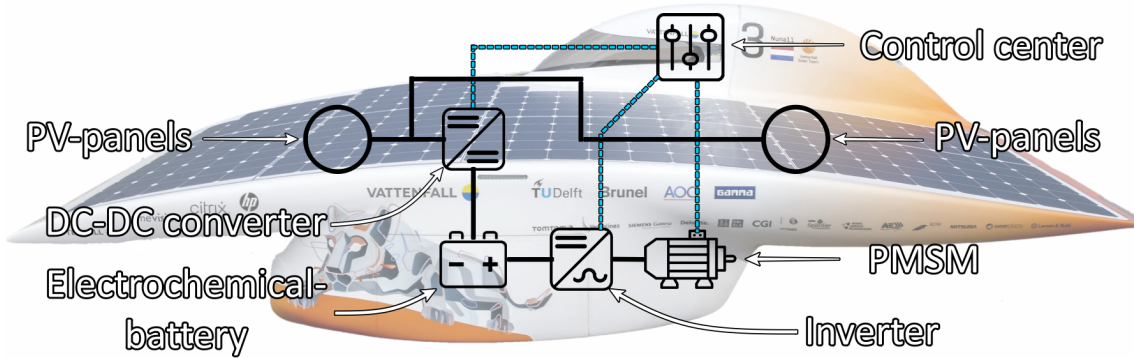


Figure 8: An example of a modern SC with an overlay of its components. Black lines for power flow, and blue dotted lines for electrical signals.

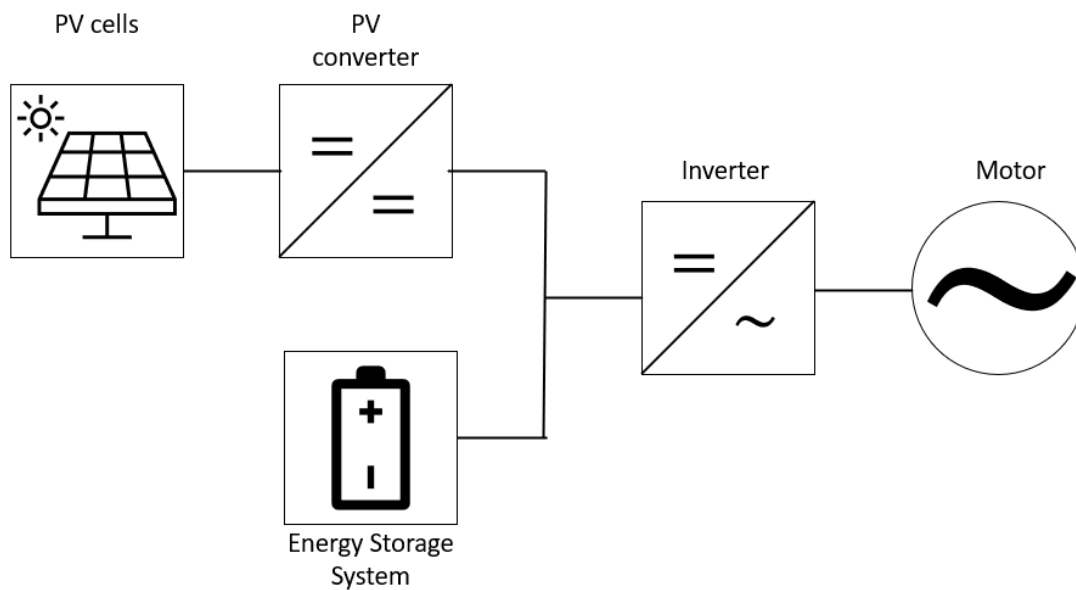


Figure 9: Single-line diagram for the SC.

3.2 Photovoltaic-Cells

A Photovoltaic (PV)-cell, or solar cell, is an electronic device that converts energy from incoming light directly into electric energy. As PV cells will be the only energy source for the SC, their efficiency and reliability will be crucial for adequate performance. Their efficiency as a power source depends on several factors, ranging from material properties to implementation and usage [28, 5]. [18]

3.2.1 Solar irradiance

Irradiance is the amount of photonic energy transferred onto a surface per second [29]. Solar irradiance SI refers to the energy coming from the Sun. In general, SI is measured in W/m^2 . It is usually integrated over a specific period to measure radiant energy, as SI varies depending on local factors. Such as atmospheric conditions, topological layout, time of day, and time of the year. Some areas might see great variance throughout a year due to the seasons and the earth's position

relative to the sun, which would affect the radiation angle and the day-night cycle. For Darwin and Adelaide in Australia during October, a regular day is between 06:32-18:43 and 06:54-19:18, respectively [30]. The annual radiant energy variance worldwide can be seen as illustrated in Figure 10, while the long-term averages for SI in Australia can be seen in Figure 11. [18]

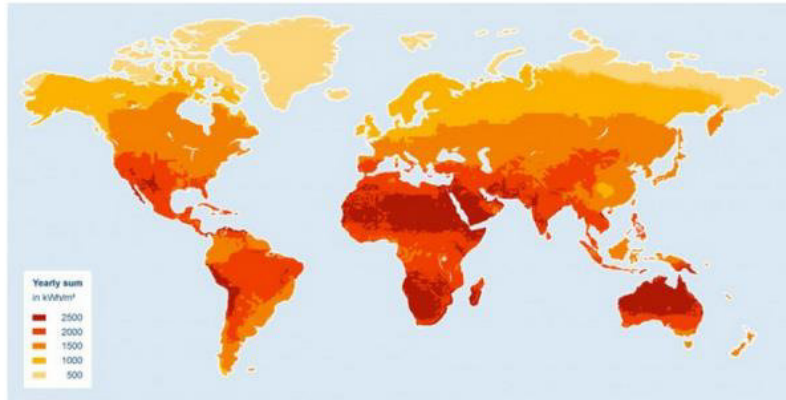


Figure 10: World solar radiation map. [2]

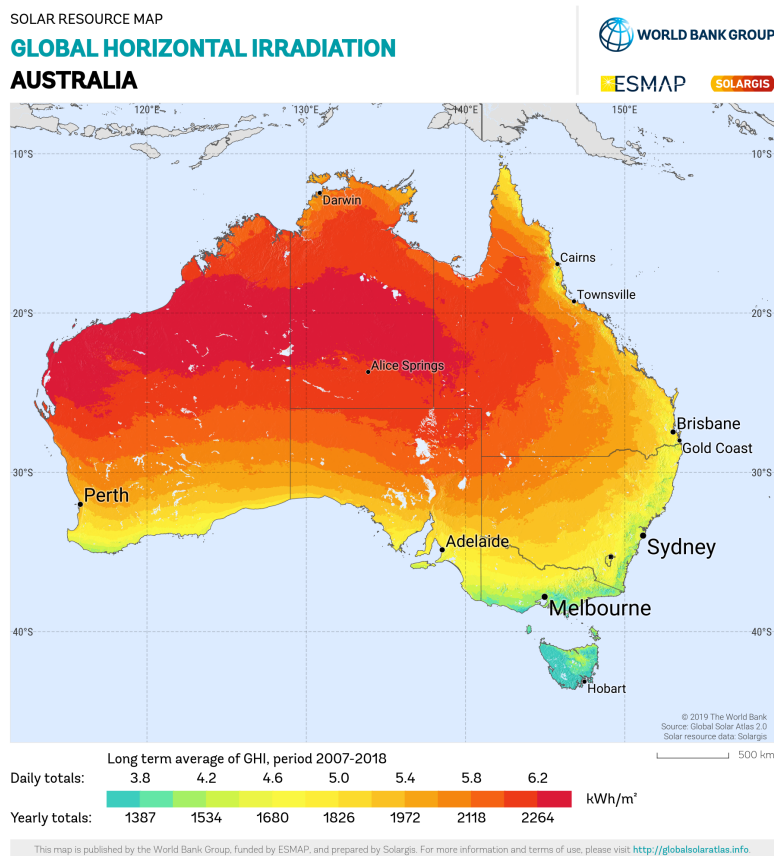


Figure 11: Long term averages for Global Horizontal Irradiation in Australia [3].

The SI can be observed to be distributed based on wavelength. Figure 12 depicts SI per wavelength of the sun. As shown in the figure, a significant portion of the total energy from the sun is within the visible light spectrum, which is between 380nm and 700nm. The Figure also shows that a large portion of the energy within the visible light range is absorbed by gases in the atmosphere. The infrared portion shows that certain bandwidths are almost completely absorbed by water vapor, carbon dioxide, and ozone in the atmosphere.

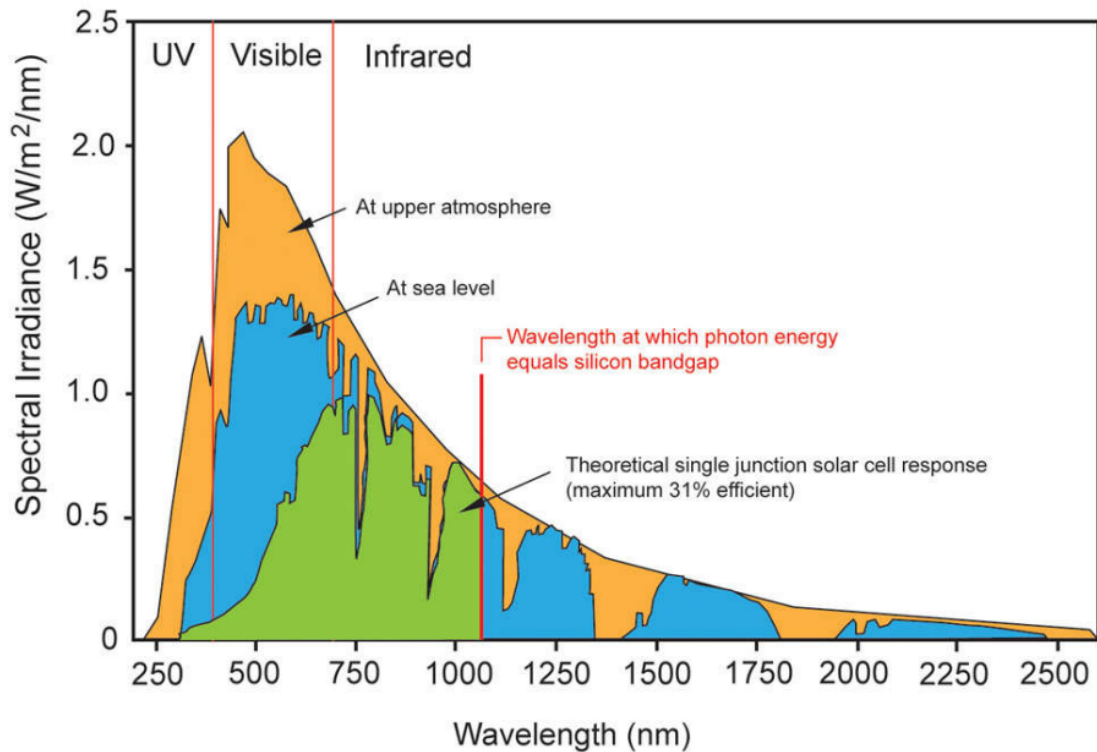


Figure 12: Graph depicting the solar spectral irradiance experienced at the upper atmosphere and at sea level. The graph also shows values specific to silicon PVs. [4]

3.2.2 Basic semiconductor physics and band-gap energy

PV cells are made from semiconducting materials, meaning that the material is more conductive than an insulator but less than an actual conductor. The technologies can be divided into thin-film and crystalline technologies. Crystalline technologies can be divided further into mono- and polycrystalline. The thin film type is generally the least efficient, and monocrystalline is the most efficient [6].

Silicon is the most used material in PV technology. About 95% of all PV modules sold are made from silicon. It is highly efficient and has a low cost, and modules usually have a long life [31]. Since silicon is the starting point for most of the world's PV technologies and semiconductors, it will serve as an example to explain the basics of PV functionalities.

Silicon is the 14th element on the periodic table. Thus it has 14 protons and neutrons in its nucleus and 14 orbital electrons. As valence electrons are the aspect of the element that matters in electronics, it is usual to draw a silicon atom with a +4 value on its nucleus and four valence electrons. An example is shown in Subfigure 13a. In pure crystalline silicon, each atom forms covalent bonds with four adjacent atoms in the three-dimensional tetrahedral pattern. A two-dimensional illustration can be seen in Subfigure 13b [5].

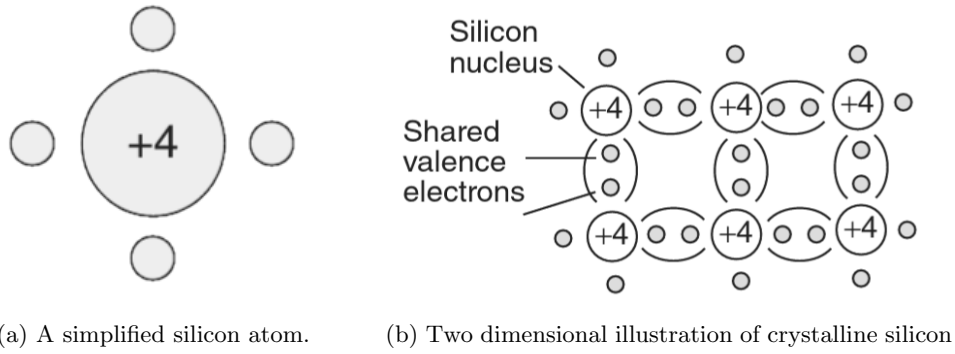


Figure 13: [5]

Silicon is a perfect electrical insulator at absolute zero Kelvin, unlike regular conductors. Some electrons might be excited enough to free themselves from their nuclei as temperature increases, allowing electric current to flow. Quantum physics explains the conductivity of semiconductors by using band diagrams like the one shown in Figure 14.

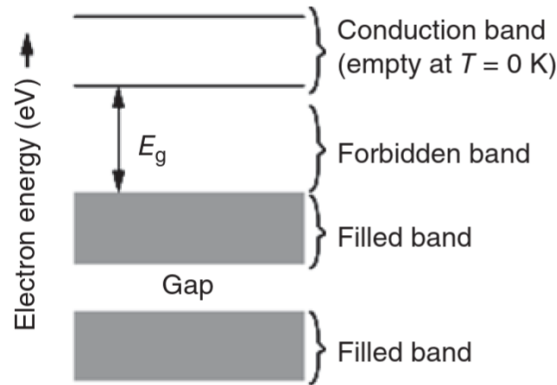


Figure 14: Band diagram of a semiconductor. Silicon at $0^\circ K$ has zero electrons in the conduction band, making it a perfect insulator. [5]

The gaps between energy bands are called forbidden bands. The most important forbidden band is the one separating the conduction band and the highest-filled band below it. The energy needed for an electron to free itself and jump from a filled band to the conduction band is called the band-gap energy (E_g). The unit used to quantify band-gap energy is usually electron volts (eV), where one electron volt is the energy an electron acquires when its voltage is increased by 1V. [5]. To find the spectral bandwidth of a PV cell, we must find the maximum wavelength a photon can have and still excite a valence electron [31, 32]. The energy of a photon can be calculated using Equation 1:

$$E = \frac{h \cdot c}{\lambda} \quad (1)$$

Where E is the photons energy, h is the Planck constant, c is the speed of light, and λ is the wavelength. By substituting E with E_g , we can find the maximum wavelength usable for a semi-conducting material. The maximum wavelength (λ_{max}) can be calculated using Equation 2:

$$\lambda_{max} = \frac{h \cdot c}{E_g} \quad (2)$$

Materials

As previously stated, silicon is the most used material in PV technology, with about 95% of all PV modules sold made from it. However, other highly efficient materials, such as perovskite and gallium arsenide, exist [33]. Each semiconducting material comes with its strengths and weaknesses. Some materials can be toxic and leave a negative environmental impact, but the negative impact can be nullified with proper re-purposing of PV cells [34, 35, 36]. Table 4 showcases different PV cell materials and their characteristics. Sources can be seen in ⁷.

Chemical composition	Si	a-Si	CdTe	<i>CuInSe₂</i>	<i>GuGaSe₂</i>	GaAs	Perovskite
Bandwidth energy [eV]	1.12	1.7	1.49	1.04	1.67	1.43	1.72
Maximum wavelength [nm]	1107	729	832	1192	742	867	722
Market efficiency [%]	25	7	22	13.5	9.7	29	25.5
Theoretical efficiency [%]	31	10	32	19.2	11.9	32	?
Race legality	Yes	Yes	No	No	Likely no ⁸	No	Yes

Table 4: Different PV cell materials’s and chemical compositions’s bandwidth energy and corresponding maximum wavelength. Multijunction cells’s properties not listed.

The table depicts other materials than Si to have a lower range. However, the cell response can still be quite high. As the green field in Figure 12 shows, silicon is less effective at absorbing low-wavelength SI. Other materials with a shorter maximum wavelength can be more efficient at using shorter wavelengths [44]. This brings us to Multi-Junction (MJ) PV cells. A PV cell does not have to be a single junction made from a single material. Different materials can be layered into MJ-cells increasing conversion efficiency by capturing a wider range of SI with a better cell response. [45].

As most of the materials listed in Table 4 are banned, must currently commercially available high-performance PV cells are precluded. Perovskite-based cells, however, have shown potential, both as a single junction cell and as part of an MJ cell. Single junction cells are predicted to reach the levels of monocrystalline Si-cells and might even surpass them, and they’ve already reached efficiencies up to 25.5% as part of an MJ-cell [46, 47, 48]. Perovskite will also be a more environmentally friendly than GaAs with proper recycling methods [36].

3.2.3 Tilt angle and azimuth

PV’s energy output is directly correlated to the tilt angle and azimuth angle. Tilt refers to the PV’s angle to the ground, and azimuth is the angle to the cardinal directions. A PV panel at 0°azimuth, located in the northern hemisphere, would have its surface area directly pointing south. A PV with 0°azimuth can be seen in Figure 15. The optimal usage of a PV cell would be to track the Sun’s position and adjust tilt and azimuth accordingly. An illustration of how solar capture would be affected by a PV’s tilt can be seen in Figure 16. An SC would be more restricted regarding solar tracking. The tilting of the PVs could obstruct the driver’s view or cause more air resistance. Figure 17 shows how an SC’s PV tilt is affected by the road it drives on.

⁷Monocrystalline silicon [37], Amorphous silicon [38], CdTe [39], CuInSe₂ [40], CuGaSe₂ [41], GaAs [42], Perovskite [43].

⁸As both *CuInSe₂* and GaAs are illegal, *GuGaSe₂* is most likely illegal too.

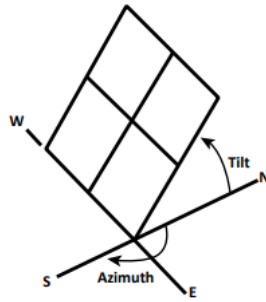


Figure 15: PV array facing south at a fixed tilt. The array faces south with an azimuth angle of 0° . [6]

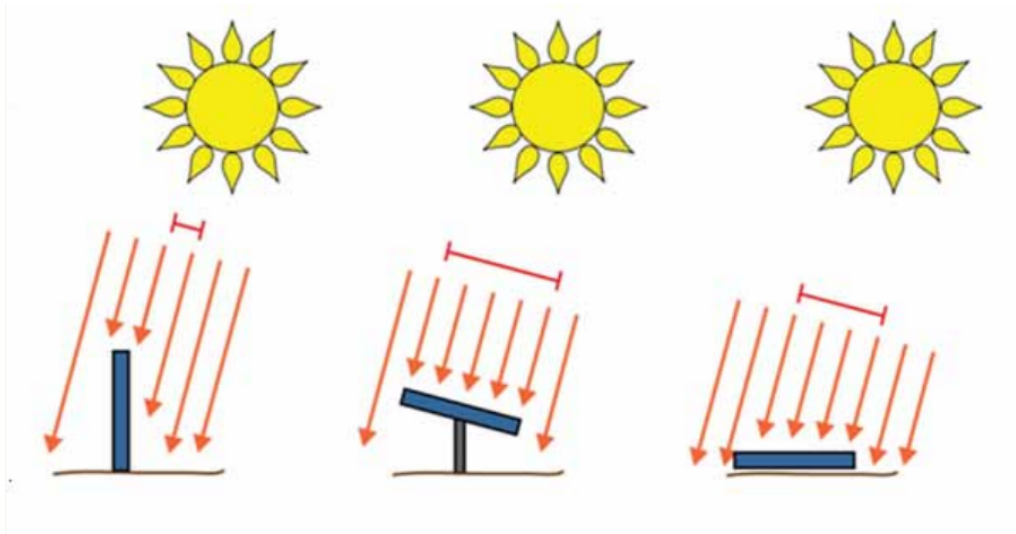


Figure 16: The effect of PV panel tilt on solar energy capture. [6]

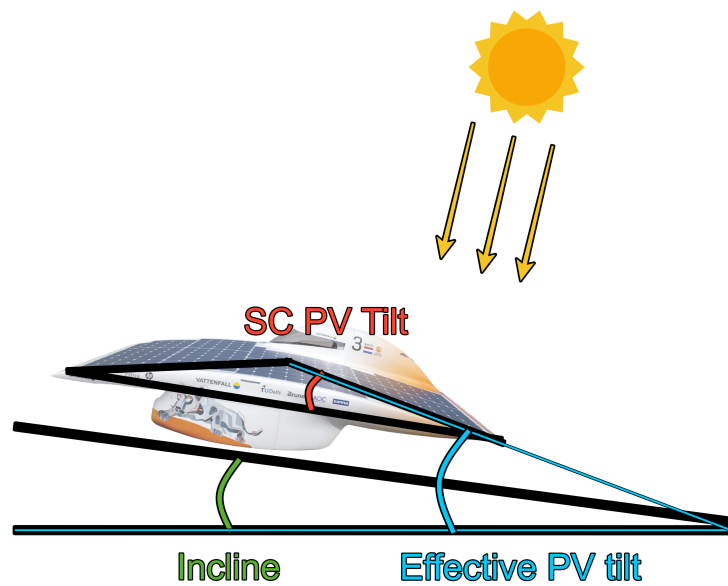


Figure 17: PV tilt of an SC driving up an incline. The effective tilt equals the incline added to the tilt of the PVs on the SC.

3.2.4 Power Generation

The power generation of PV cells can be calculated using Equation 3 [49].

$$P = \underline{A} \cdot r \cdot SI \cdot PR \quad (3)$$

Where \underline{A} is the effective surface area of the PV cell, r is the efficiency, SI is the solar irradiance, and PR is the performance ratio. \underline{A} depends on PV cell size and orientation relative to the Sun. The effect can be seen as illustrated in Figure 16. Further, r depends on the materials used, and SI on the weather conditions and locality. PR can vary depending on many factors, such as:

- Inverter losses
- Temperature losses
- Shadings
- Losses at weak radiation
- Dust, snow, etc

In general, it depends on environmental and installation factors [49]. [18] For an SC, some of the more important factors to account for are the first three listed. Due to the surrounding environment for the WSC, shadings from natural structures such as walls and trees are minimal. The structures around areas like Alice Springs also tend to be mostly trees, with nearby buildings being away from the main road. Most of the route will be in sparsely forested areas and deserts. Examples from the view of the road can be seen in Figure 18.



(a) Darwin, close to the starting line.



(b) Close to Edith.



(c) Main road past Alice Springs



(d) Close to Coober Pedy

Figure 18: Screenshots from areas along the route taken using google maps. The vast majority of the route looks like 18b and 18d.

The main shading the SC may experience will be from its geometry. Due to the rules regarding vision, the cockpit will always be the highest point on the vehicle. Therefore, the placement of the

cockpit relative to the Sun will partly shade the PV panels to an extent. An illustration of cockpit shading can be seen in Figure 19.

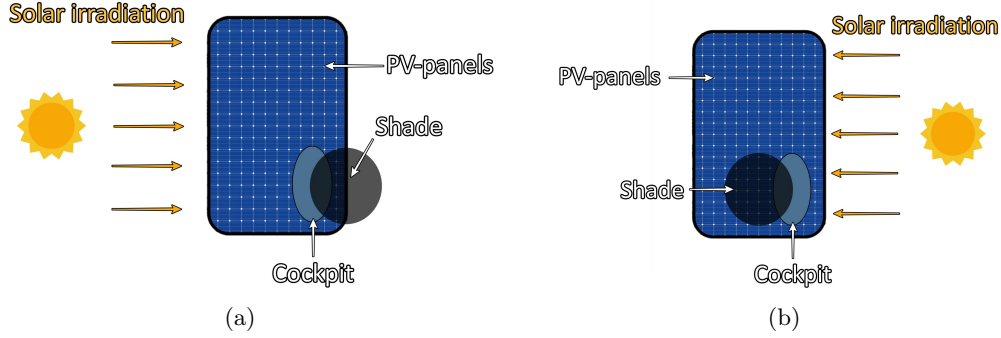


Figure 19: Two simple illustrations of an AC-shaped SC from an eagle-eye perspective. The illustration showcases how cockpit placement can affect the total SI hitting the PV panels on the SC by shading them depending on relative orientation to the sun.

Inverter losses depend on which inverter is chosen, how it is installed, and how it is used. The exact losses can only be calculated if the parameters of the chosen inverter are known, the voltage is known, and the current is known. The types of losses include conduction losses and switching losses. The specifics of those will be explained in subsection 3.4.

The third one, temperature losses, is a complex topic as temperature affects most of a semiconductor's material parameters. To examine the temperature losses of a PV cell, one can use the general equation for power output based on voltage and current ($P = VI$). The change in open circuit voltage can be represented with Equation 4.

$$\frac{dV_{OC}}{dT} = \frac{V_{G0} - V_{OC}}{T} - \gamma \frac{k}{q} \quad (4)$$

Where V_{OC} is the open circuit voltage, T is the PV cell temperature in Kelvin, V_{G0} is the linearly extrapolated bandgap energy open circuit voltage from absolute zero, γ is a constant for the temperature dependency of the PV cell, k is the Boltzmann's constant, and q is electronic charge.

The short circuit current (I_{SC}) increases per increase in cell temperature. Since the increase in temperature lowers the bandgap energy, a larger range of SI can excite the valence electrons. This increase is marginal, however. The change in I_{SC} for silicon is about 0.06% per $^{\circ}C$ difference between $25^{\circ}C$ and cell temperature. [8]

The output power can be represented with an IV-characteristics graph. An IV-graph depicts the correlation between V_{OC} and I_{SC} . We can also read the Maximum Power Point (MPP) from an IV graph. The MPP is the operating voltage and current that results in the highest electrical power output [7]. An illustration of the concept of MPP can be seen in Figure 20. As the cell temperature changes, the IV graph also transforms. A change in IV-characteristic can be seen illustrated in Figure 21. We can see how an increased temperature will result in a lower V_{OC} and lower I_{SC} . If we were to find the MPP for both curves, we would find that:

$$MPP_{lowtemp} > MPP_{hightemp}$$

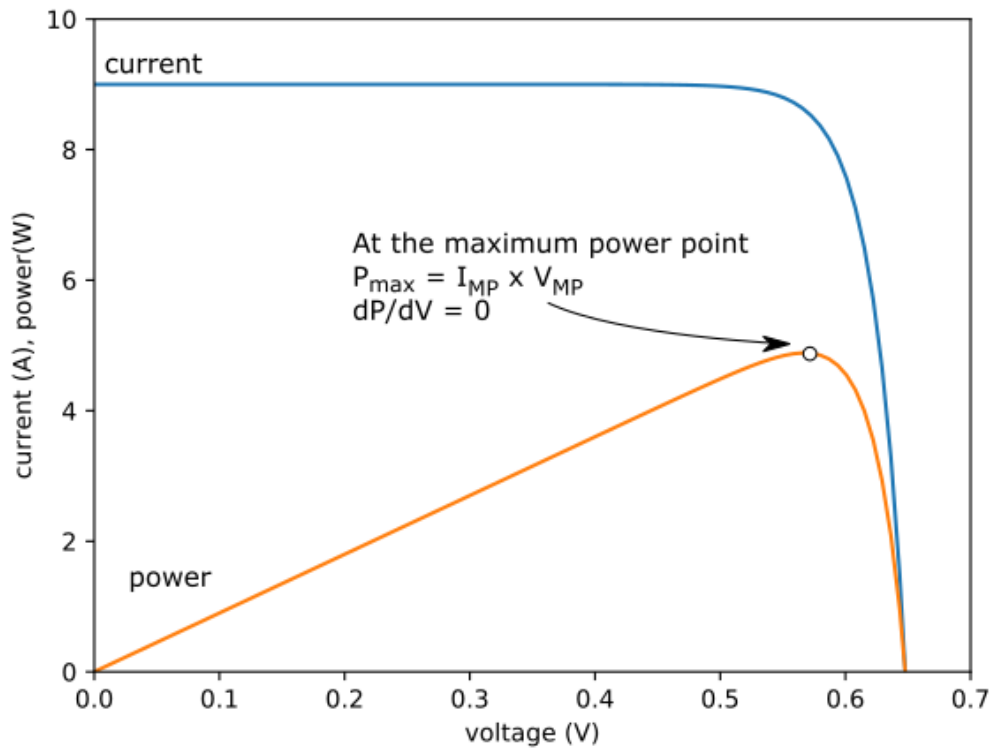


Figure 20: The maximum power point of a PV cell. [7]

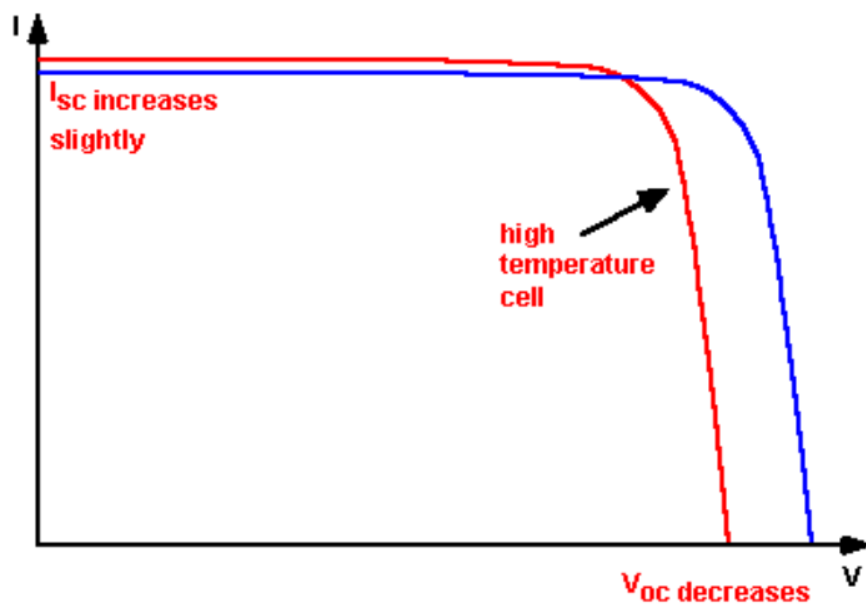


Figure 21: IV-characteristic graph depicting how changes in temperature affect the cell. [8]

It is also worth noting that γ from equation 4 is affected by the semiconducting material used for the PV cell. Thus the optimal semiconducting material varies depending on its expected operating temperature.

3.3 Energy Storage System

PVs are variable power sources since their production is directly tied to the availability of sunlight. Their production does not account for the magnitude of the load it powers. Thus they can both under and over-perform. Though an SC is more likely to demand equal or more power than its PVs can deliver, phenomena like traffic congestion and speed limits limit the potential output of the system, which may result in higher power production than usage. PVs voltage levels are also tied to their power output. Thus, an ESS is required as its more predictable voltage levels will help tackle the irregularities from the PVs energy production [50]. In the context of the WSC, an ESS is also essential for the safe overtaking of other vehicles [25]. The only option for an electrical ESS in such a small mobile system is electrochemical secondary batteries. There are many different makeups of secondary batteries, but the most commonly used by earlier competitors are listed in Table 2.

A typical EV has a lithium-ion battery, with a capacity of around 40kWh, with some having up to 100kWh [51]. The SC is limited to the dimensions displayed in Tables 2 and 3. As of 2020, a Li-ion battery would have an energy density of 250Wh/kg [52]. Li-S is the only type of battery listed with a higher energy density than Li-ion. It has an incredibly high theoretical energy density of 2567Wh/kg. It has a realized density of 300-600Wh/kg [53]. Operational high energy density Li-S batteries are not yet commercially available to the public. However, the market is developing rapidly, and low-cost- high-energy Li-S batteries might soon be on the market [54]. [18]

3.3.1 Basic electrochemical battery physics

"The most important characteristics of a battery are determined by the voltage of their cells, the current capable of supplying over a given time (measured in Ah), the time constants and its internal resistance. The electrodes that supply or receive power are called positive electrodes (e_p) and negative electrodes (e_n) respectively. Inside the battery, the ions are transported between the negative and positive electrodes through an electrolyte. The electrolyte can be liquid, solid or gaseous." [55, p. 305]. The electromotive force E_0 is the voltage difference between the electrode potentials for an open external circuit or at no load, defined as:

$$E_0 = E_{e_p} - E_{e_n} \quad (5)$$

3.3.2 Battery reliability, efficiency, and safety

Electrochemical batteries are like PVs in that they have varying voltage levels they are much more predictable. This makes them suitable to base the hardware voltage of the SC on [56]. In Equation 5, we see the open circuit no-load voltage of the battery. But during the initial discharge of the battery, the voltage can be parameterized as:

$$V_0 = E_0 - \eta \cdot I \cdot R_0 \quad (6)$$

Where V_0 is the terminal voltage, I is the current consumption of the connected load, R_0 is the battery cell's internal resistance, and η is the polarization factor. The polarization factor is a summarizing simplification of the complex chemical processes happening between the electrodes within the battery. As the voltage may vary depending on the State of Charge SoC, a more descriptive expression would be the one seen in Equation 7:

$$V_i = E_0 - \eta \cdot I \cdot R_i \quad (7)$$

where V_i and R_i can be presented by Equations 8 and 9.

$$V_i = V_0 - K_v Q_d \quad (8)$$

$$R_i = R_0 + K_R Q_d \quad (9)$$

The voltage V_i decreases linearly with the discharge Q_d , and the internal resistance R_i increases linearly with Q_d . K_v and K_R are constants that reflect the characteristics of a battery and can be determined through testing [55].

A battery's efficiency can be categorized into charge efficiency, discharge efficiency, and round-trip efficiency. As the name implies, charge efficiency is how many units of energy are stored in a battery compared to how many units of energy are put in, and discharge is the same but out of the battery. Round trip efficiency refers to how much electrical energy is regained per unit put into the battery [57]. The energy flow of a battery can be calculated using 10, 11, and 12.

$$E_{battery} = \eta_{charge} E_{charge} \quad (10)$$

$$E_{discharge} = \eta_{discharge} E_{battery} \quad (11)$$

$$E_{round-trip} = \eta_{charge} \eta_{discharge} E_{charge} = \eta_{round-trip} E_{charge} \quad (12)$$

The round-trip efficiency is not a constant value. It is subject to change due to ambient- and internal temperatures. The efficiency of Li-ion batteries may decrease by 25% if charged at 40°C. The ideal temperature lies at 20°C [58, 59]. A secondary battery may also have its maximum capacity reduced from usage. The reduction depends on ambient temperature and Depth of Discharge (DoD) [60, 61]. [18]

3.3.3 Capacity, charge- and discharge rate

Two crucial characteristics of ESSs include their storage capacity and operating C-rate, which are fundamental when selecting suitable ESSs. Storage capacity is often measured in units of Ampere-hours (Ah) or Watt-hours (Wh), and the conversion between the two can be achieved by employing Ohm's law based on the ESS terminal voltage. On the other hand, C-rate indicates the discharge or charge rate of an ESS relative to its capacity. It is represented as a multiple of the ESS's rated capacity. For instance, an ESS with a rated capacity of 1Ah and a C-rate of 1C discharges at a rate of 1A and depletes it after one hour of operation. Similarly, an ESS with the same capacity and a C-rate of 2C discharges at a rate of 2A and depletes after 30 minutes. More examples can be seen in Table 5. An ESS will degrade faster when it operates at higher C-rates. High C-rate operation might also lead to cell failure [62].

Capacity [Ah]	C-rate	Operating current [A]	Time until depletion
1	0.2	0.2	5 hours
	0.5	0.5	2 hours
	1	1	1 hour
	2	2	30 minutes
	5	5	12 minutes

Table 5: ESS C-rate effects on performance and duration.

3.3.4 Heating

Battery heating is a complex process. Internally generated heat consists of Joule heat and reaction heat. Both are affected by temperature, battery aging, SoC, and operating current. The reaction

heat refers to the heat generated during the electrochemical process of transferring electrons and ions between the electrodes and the electrolyte. Joule heat is the result of current flowing through the battery' internal resistance [63]. The Joule heat can be roughly estimated using Equation 13.

$$P_{battery-heat} = I^2 \cdot R_i \quad (13)$$

$P_{battery-heat}$ is the momentary heat development in the battery, I is the charge/discharge current, and R_i is the internal resistance.

3.4 Power electronics

An essential part of an energy system utilizing renewable resources is power electronics. As seen in Figure 9, the SC's electrical system features an inverter and a converter. A *converter* is an electrical device that can convert a DC power source voltage to a different DC load voltage. The voltage can be stepped up or down, and voltage levels may vary depending on the application. An *inverter* is another electrical device capable of inverting a DC into an AC [64]. The voltages from the ESS and PV cells would be compatible with the power converters. Furthermore, with the inverter, a dc system connected ac-motor becomes possible.

When choosing converter and inverter types, a deciding factor is which quadrants the load is required to operate in. Regarding power electronics, quadrants refer to which operating mode the inverter/converter can operate in on the U-I plane. The quadrant concept can be seen as illustrated in Figure 22.

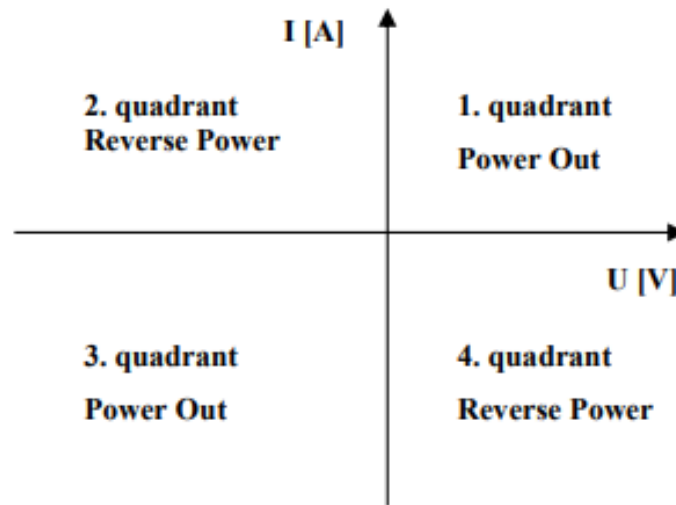


Figure 22: The quadrant concept. [9]

Buck-boost converter

A buck-boost converter is a DC-DC power converter. Depending on the input, it can be used as both a step-up and a step-down converter. It can be used for standalone PV grids and electric drives. Though, as of 2020, their use in PV applications is still being researched. [65]

Half-bridge converter

A half-bridge converter is a combination of buck- and boost converters. The half-bridge converter can step the source voltage up or down for the load. It is also capable of operating in both the first and fourth quadrants. Thus, it can supply the load with power and feed power back into the voltage source. It can only generate positive output voltages.

Three-level three-phase inverter

An inverter can invert DC into AC by switching the voltage source on and off. The output signal may resemble a wave by regulating the on and off periods through Pulse Width Modulation (PWM). Furthermore, by switching the output voltage into a negative one, then regulating the signal through PWM, one can get the negative part of the waveform. Thus a sinusoidal waveform can be achieved. However, using a standard two-level three-phase topology, one would get undesired capacitive currents from the DC link when switches occur. The capacitive currents will limit the speed at which a switch from positive to negative can occur. However, by introducing a neutral point to the DC-link, the output terminal can be switched between the negative via the neutral point and then to the positive point. This method will effectively halve the switching time, resulting in a more efficient converter topology [9].

Maximum Power Point Tracker

An MPP-Tracker is a DC-DC power converter that, in principle, ensures the connected PV generator always operates at MPP independently of the load [66]. The converter observes the output of the PV, then changes the system's impedance to ensure maximum power transfer.

Heating

The primary source of loss within power electronics is heating. A thermal model for the cooling system is needed when dimensioning semiconductors within electrical drives. Therefore, the power developed in the diodes needs to be calculated. The general commutation losses can be calculated using 14 or 15 if the current frequency is high [9].

$$P_D = U_{D0} \cdot I_D(t) + R_D \cdot I_D^2(t) \quad (14)$$

Where U_{D0} is the diode voltage, I_D is the diode current, and R_D is the resistor.

$$P_{D,avg} = U_{D0} \cdot I_{D,avg} + R_D \cdot I_{D,rms}^2 \quad (15)$$

Where U_{D0} is the diode voltage, I_D is the diode current, R_D is the resistor, $I_{D,avg}$ is the average current, and $I_{D,rms}$ is the root mean square value of the current. The voltage and resistor values are temperature dependant. To know the actual temperature change, the thermal characteristics of the specific semiconductor must be acquired. This is a value with the unit $^{\circ}K/W$, which is usually listed in the semiconductor manufacturer's datasheet.

DC-link converters

Depending on the usage of the ESS, its DC-DC converter can be neglected since the ESS would be the main power source during acceleration. The DC link would then be based on the ESS voltage. One should minimize the number of transistors between the energy source and the load [67, 56]. [18]

3.5 The motor

The motor is an essential part of an electric vehicle. It is solely responsible for propelling the vehicle forward. The actual method and mechanics behind how different types of motor work vary, depending on the power source and the motor's purpose. The main attribute that is essential for an SC motor is its efficiency. A Permanent Magnet Synchronous Motor (PMSM) is one of the most efficient motor types. It has a very high torque density and efficiency, is small in size, and is lightweight [68]. Factors that are all very important for an SC, where total system efficiency, weight, and acceleration capabilities matter. [18]

Another aspect it is important to consider when choosing a particular motor is **gears**. Gear grants us the ability to change the torque and speed of a motor [9]. A motor with a very high-rated speed might be geared for a higher torque with lower speeds, and vice versa. However, a gear also introduces a loss of mechanical energy. The total energy lost through a gear can be calculated using 16. The relationship between speed and torque can be expressed as shown in 17.

$$\eta_{gear} = \frac{P_{out}}{P_{in}} \quad (16)$$

Where η_{gear} is the dimensionless number for gear efficiency, P_{out} is the power out of the system, and P_{in} is the power put into the system.

$$T_{out} = \eta_{gear} \left(\frac{\omega_{in}}{\omega_{out}} \right) T_{in} \quad (17)$$

Where T_{out} is the output torque of the system, ω_{in} is the input speed, ω_{out} is the output speed, and T_{in} is the input torque. This can be simplified as:

$$T_{out} = \eta_{gear} i_{gear} T_{in} \quad (18)$$

Where i_{gear} is the gear ratio.

3.6 The Solar Car's Mechanics

The SC's mechanics is the basis of what the LP will be modeled after. The force required to accelerate the mass that is the SC and maintain its velocity. Thus we must first consider Newton's first and second laws of motion. [69]

1. *Every body continues in its state of rest, or of uniform motion in a straight line, unless it is compelled to change that state by forces impressed upon it.*
2. *The change of motion of an object is proportional to the force impressed; and is made in the direction of the straight line in which the force is impressed.*

The expression for the movement of the car can be derived from Newton's second law and can be seen in 19.

$$F = ma \quad (19)$$

Where m is the mass of the object and a the acceleration.

The one force driving the SC forward would be the rotational force of the motor. Therefore the SC will be limited by the external forces from the surroundings, internal counter forces such as friction on the rotor, and the motor's output. [18]

3.6.1 Incline

One of the forces applied to the SC would be the sum of the gravitational pull and normal force. The force will be parallel with the driving force from the wheels, with direction depending on the terrain being a de- or incline. Depending on the incline, this force will be referred to as $F_{incline}$ or $F_{decline}$. The force can be calculated through 20. An illustration of the forces can be seen in Figure 23.

$$F_{incline} = F_{decline} = mg \sin \Theta \quad (20)$$

Where m is the SC's mass, g is the gravitational constant, and Θ is the incline angle.

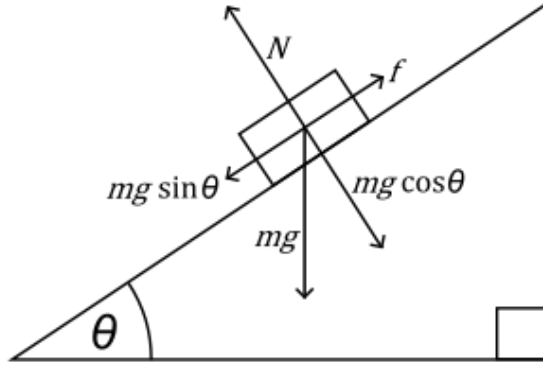


Figure 23: The gravitational- and normal forces on a object on an incline. f is resistance, Θ being the incline and $mg \sin \Theta$ is the sum of the gravitational- and normal forces. [10]

3.6.2 Drag

Another external force is drag. Drag is, in fluid dynamics, a force acting opposite to the relative motion of any object moving through a fluid (be it in gas or liquid form) [70]. In the case of SC-racing, air resistance would be more descriptive as the fluid in question would be the air. The drag force for high speed can be calculated through 21.

$$D = cv^2 \quad (21)$$

Where D is the drag force, c is the drag constant, and v is the relative velocity through the liquid. The drag constant can be calculated through 22.

$$c = \frac{C_d \rho A}{2} \quad (22)$$

Where C_d is the drag coefficient, ρ is the fluid's density, and A the object's cross-sectional area. The drag coefficient is a dimensionless number that the shape of the object and the Reynolds Number determines. The density of air is inversely related to temperature. Air density for the temperature range $15^\circ C - 40^\circ C$ can be seen in Table 6.

Temperature, T [$^\circ C$]	Air density, ρ [kg/m^3]
15	1.225
20	1.204
25	1.184
30	1.164
35	1.145
40	1.127

Table 6: Air density based on temperature. [12]

The drag coefficient for a standard personalized vehicle is around 0.25 to 0.30 [71]. However, the drag coefficient can be reduced and optimized. The drag coefficient can be found through estimations based on the geometrical shape of the object traveling through a liquid. However, it can oftentimes be found through measurement and using 22 [72].

$$D = \frac{C_d \rho A}{2} v^2 \quad (23)$$

The D becomes the largest counter force for an SC, as it increase by the velocity squared.

3.6.3 Rolling resistance

Rolling resistance, also known as rolling drag, is the resistance a vehicle must overcome to maintain speed. Rolling resistance is unavoidable but can be minimized. The main factor that affects rolling resistance is hysteresis. Hysteresis means that the recovered energy is less than the energy of deformation. In other words, the energy expenditure of the wheel's deformation and the ground it travels along cannot be fully recovered. When accounting for rolling resistance, a rolling coefficient is used. The rolling resistance, R , can be calculated using Equation 25.

$$R = C_{rr}N \quad (24)$$

C_{rr} is the rolling coefficient, and N is the normal force. The normal force can be seen in Figure 23, where it is shown to be equal to $mg\cos\Theta$. Thus the rolling resistance can be represented as:

$$R = C_{rr}mg\cos\Theta \quad (25)$$

The rolling coefficient for a regular car is about 0.015 [73]. However long distance endurance cars can have a lot lower values. Tires used by most SCs in the WSC is approximately 0.004 []. This results in the rolling resistance being the smallest part of the counter force acting on an SC.

3.6.4 Work and power

We know that speed is the distanced traveled by time in a static environment. Giving us:

$$v = \frac{S}{t} [m/s] \quad (26)$$

Where v is the velocity, S is the distance traveled, and t is the time the object spent traveling. Next we also know that work is defined as the energy transferred to an object by application of a force along a displacement. Thus giving us:

$$W = F \cdot S \quad (27)$$

Where W is the work, and F is the applied force. Further we also know that work is the energy transferred per unit time. Since 26 references displacement per unit time, we can insert it into 27 and we get:

$$P = \frac{W}{t} = F \cdot v \quad (28)$$

3.7 Dynamic Model and Load Profile

By combining the concepts from 3.6.1, 3.6.2 and Newton's second law of motion, we get a dynamic representation of the SC system.

$$F(t) = F_{incline} + D + R + F_{car} \quad (29)$$

By combining 21 and 22, we get 23.

$$F(t) = mg\sin\Theta + \frac{C_d\rho A}{2}v_{wind,relative}^2 + C_{rr}mg\cos\Theta + ma \quad (30)$$

The SC will stay at a constant pace for most of the route. Thus we know that $a = 0$, and the model can be simplified to be:

$$F(t) = mg\sin\Theta + mgC_{rr}\cos\Theta + \frac{C_d\rho A}{2}v_{wind,relative}^2 \quad (31)$$

Then we apply 28 to 31 and get a dynamic model based on the energy needed.

$$P(t) = mgv\sin\Theta + mgvC_{rr}\cos\Theta + \frac{C_d\rho A}{2}v_{wind,relative}^3 \quad (32)$$

[18]

4 Methodology

4.1 Software

The task of running calculations for an SC can be done with several softwares. Some of the desired attributes of the chosen software in this context is:

- Availability
- User-friendliness
- Effectiveness in reaching Nordlys's goals

As Nordlys is an organization mainly staffed and run by students, the software would preferably be free. It should also be something most future members could easily learn or already have an affinity for before joining. The chosen language to address the thesis topic presented in section 1.2 is *Python*.

Python

Python can do a wide array of tasks and run scientific- and mathematical calculations, access websites, manage data storage, etc. It is free and can use several distribution applications. It is also possible to download existing libraries from the internet for free, potentially reducing the workload. Most engineering students at NTNU also have some experience with Python programming through an introductory course or other courses. The chosen distribution is *Anaconda*.

Anaconda Spyder

Anaconda is a distribution platform that provides a wide array of tools and libraries specifically tailored for data science and machine learning. It includes several packages used for this thesis, including NumPy and Pandas. It also aims to simplify package management and deployment for user-friendliness [74]. One of the Integrated Development Environments (IDE) that are included in Anaconda is *Spyder*.

"Spyder is a free and open source scientific environment written in Python, for Python, and designed by and for scientists, engineers and data analysts. It features a unique combination of the advanced editing, analysis, debugging, and profiling functionality of a comprehensive development tool with the data exploration, interactive execution, deep inspection, and beautiful visualization capabilities of a scientific package." [75]

Spyder is a user-friendly IDE that makes reading and comprehending code easy. It has a clear layout and makes the task of correctly path scripts easier. It also makes it easier to install packages and libraries. One such library is *pvlb*.

pvlb

"pvlb Python is a community-supported tool that provides a set of functions and classes for simulating the performance of photovoltaic energy systems."[76]. The library is extensive, with functions and inbuilt modules for PVs, DC-DC converters, Inverters, and more. It also has several IO tools to retrieve and process external data and convert it into DataFrames. The DataFrames can then be converted into csv files or other formats as needed. *pvlb* will be needed, as its IO tools are essential for the library created to solve this thesis's objectives.

PVGIS

Photovoltaic Geographical Information System (PVGIS) is an online tool providing free and open access to SI- and weather data from a given geographical location, and PV electric energy generation for a given PV kWp capacity. PVGIS will mainly be used through an inbuilt *pvlb* function for retrieving pandas DataFrames with SI data.

scpylib

Solar car Pythonlibrary (*scpylib*) is the library created by the author of this thesis. It was created to achieve the main objectives of this thesis. It is a collection of mostly original modules that

solve specific tasks required to simulate an SC. Its architecture, functionalities, characteristics, and limitations will be specified in Chapter 5.

4.2 Solar profile of the route

As stated in 4.1, our first objective will be achieved by using Python. The solar profile will be made from SI data for the locations along the route. A script for accessing PVGIS and procedural creation of csv files containing hourly weather- and SI data will be made. The retrieved data will be for a typical meteorological year (TMY) and a given year. The data will also be sliced down to only include values for October since the WSC is always arranged during that month. The TMY data will be used to run the simulations for this thesis. The module retrieving data from a specific year will be included for its potential use by Nordlys. A more detailed explanation of the code is given in the next section, 5.

4.2.1 Map

A proper map is required to retrieve adequately accurate SI data. However, SI data retrieval can be quite computationally demanding, depending on the number of data points for the map. A map with 11 landmarks retrieves 7722kb of data, which gets sliced down to 644kb. More examples can be seen in Table 7. Thus a simple map will be used for the main functions of the code. An accurate map created by previous contestants through measurement will be included in scpylib for elevation profile calculations and future simulations. The elevation profile from the measured data can be seen in Figure 24.

Locations	Data retrieved	Resulting sliced data
1	643.5kb	58.5kb
11	7722kb	644kb
100	70.2Mb	5850kb
1'000	702Mb	58.5Mb
204'878 ⁹	8.537Tb	711.4Gb

Table 7: Size of SI data files retrieved based on amount of locations.

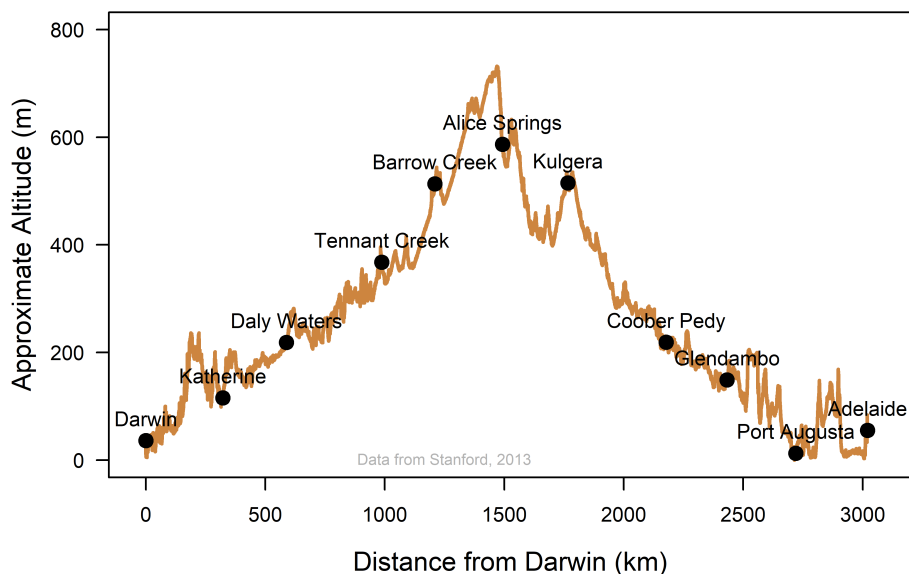


Figure 24: Elevation profile from measurements done by the Stanford Solar Car team [11].

⁹The amount of measurements included in the map file from Stanford Solar Car team. [11]

Table 8 contains data which is easily retrievable within the map file created by Stanford Solar Car Team. They are values that are relevant for teams participating the WSC. They are important to consider as standards to meet when dimensioning an SC.

Highest point of elevation =	732m
Incline towards that point =	0.0244°
Sharpest incline = 11.45°	

Table 8: Values from the Stanford Solar Car Team map file.

The sharpest incline value is for a stretch between Darwin and Katherine (Hayes Creek Hill). The incline values used in the simulation are much closer to the

4.3 Energy Production

The second objective will be achieved using a Python code base. The route will be divided into stretches. A module in scpylib will retrieve the necessary SI data and saves them as different .csv files. This way, SI data for the specific location the SC is at during a specific time will be easily retrievable for PV output calculations. The specific momentary power generation will be calculated with equation 3.

4.4 Energy Consumption

Like objective 2, objective 3 will be achieved through a script in scpylib. The script, containing functions modeled after equation 32, will calculate the load as a function of vehicle velocity and relative windspeed. Another script will then solve for the corresponding speed for a given PV output. The scripts mentioned will illustrate the SC's behavior at increasing speeds, and solve for the resultant speed at a given PV output. As shown in equation 32 for the dynamic model, the acceleration is neglected, which will impact the results.

4.5 Energy Storage System Inclusion

The ESS will be modeled with a simple energy-balancing script. The script will assume a constant internal resistance and roundtrip efficiency. The script also neglects capacity loss due to DoD, ambient temperature, and Joule heat. A specific c-rate will be set, and the energy drawn from the ESS will be based on it. As the load increases exponentially, a function that will decrease the battery's output non-linearly based on SC speed within expected travel speeds will be used.

The function used will be:

$$y = 1 - \frac{(v_{\frac{km}{h}} - 40)}{90} * \sin\left(\frac{v_{\frac{km}{h}} - 40}{90} * \frac{\pi}{2}\right)$$

A plot of the function can be seen in Figure 25. Figure 26 displays the function within the expected SC speed range. The ESS will be fully charged at the start of each simulation. Charging through the race will only happen outside legal driving hours, when the SC stands still.

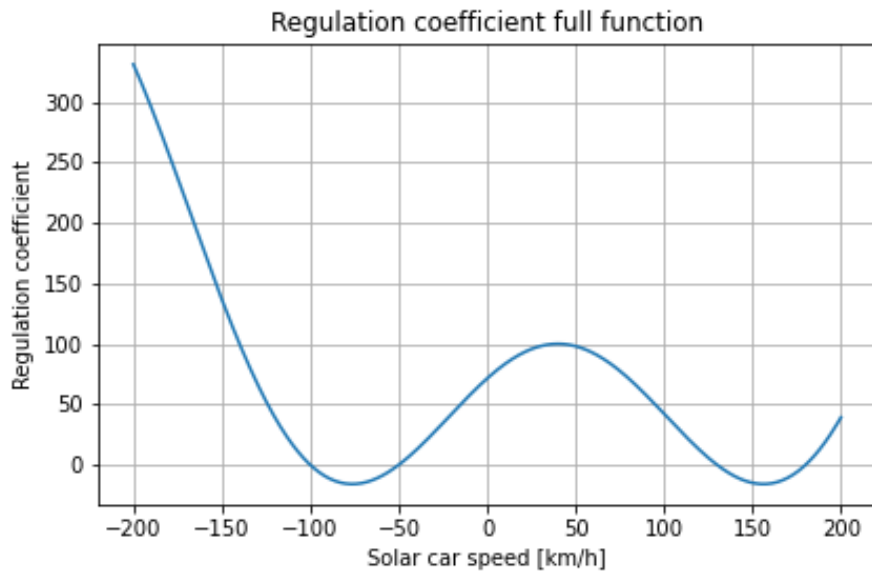


Figure 25: The ESS discharge regulation coefficient with a wide scope.

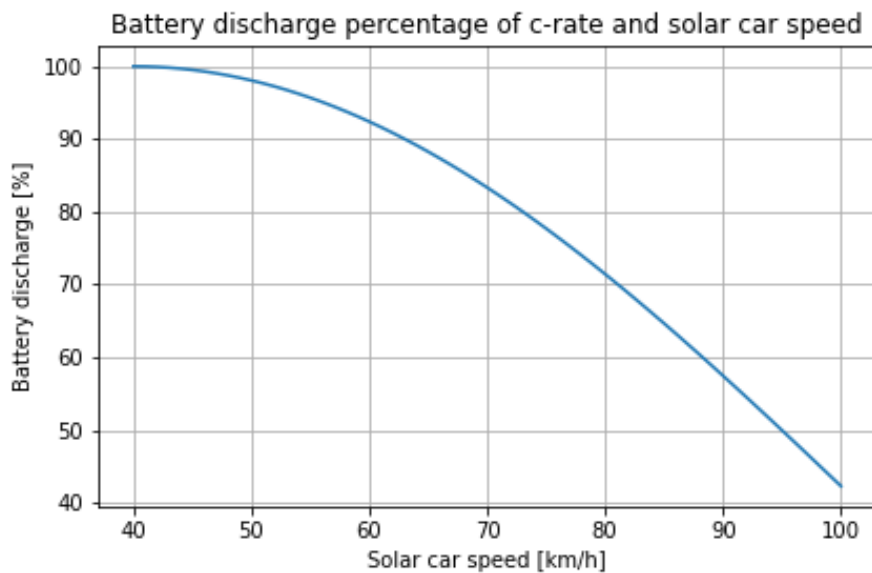


Figure 26: The ESS discharge regulation within expected SC performance.

4.6 Optimization and predictive simulation

The simulations run during the project period of this thesis will be static due to time constraints. Though methods of computer-based optimization and live simulation will be discussed. Strategies for ESS utilization will also be discussed due to its importance on a physical SC's performance during a race.

4.7 Choice of Suitable Components

To help achieve our fourth objective of choosing suitable components, we must first examine previous contestants. As they are competitive teams, some of them can be very secretive. Thus,

some information will be hard to come by. Data about the three highest-ranking contestants for the past five years can be seen in Table 9.

Year	Placement	Weight [kg]	Shape	PV-cell area [m^2]	PV-cell type	Efficiency [%]	ESS-capacity [kWh]	ESS-chemistry	References
2019	1	135	AC	2.64	MJ	28-32	5.3	Li-ion	[77, 78]
	2	142	MH	4.0	Si	23.7	5.0	LiPo	[79]
	3	-	MH	-	MJ-GaAs	-	-	-	[80]
2017	1	141	AC	2.64	MJ-GaAs	-	-	-	[81]
	2	-	MH	-	MJ-GaAs	-	-	-	[82]
	3	-	AC	2.64	MJ	-	5.0	-	[83, 84]
2015	1	-	AC	6.0	Si	22.5	5.1	Li-ion	[81]
	2	149	AC	6.0	Si	22	-	Li-ion	[85]
	3	160	AC	6.0	Si	23.2	5.0	Li-ion	[79]
2013	1	190	AC	6.0	Si	22.5	5.3	Li-ion	[81]
	2	149	OS	6.0	Si	22.5	5.2	Li-ion	[79]
	3	139	OS	6.0	Si	-	-	Li-ion	[86]
2011	1	134	OS	6.0	Si	22	5.0	Li-ion	[79]
	2	140	OS	6.0	M-Si	22	5.0	Li-ion	[81]
	3	-	OS	6.0	-	-	-	Li-ion	

Table 9: The parameters for the top three performing cars of the WSC between 2011-2019. Some data is inaccessible due to teams being competitively secretive.

Data from all the contestants for the 2019 event and 2017 can be seen in A13. The components will be chosen based on both the tables mentioned and other possible technologies mentioned in Chapter 3.

4.7.1 Shape

As we can be seen in Table 9, the top-performing shapes have evolved from symmetric multi-bodied SCs into MHs and ACs. The change to the AC shape being dominant can be attributed to Nuna 7's first place in 2013, despite it being 28% heavier than the second place. Then we can see how MH-shaped SCs develop and become the majority of the top performers by 2019. This is more obvious if we look at all the finishing SCs depicted in A13, where most of the list is MH-shaped SCs.

Thus the best choice would be some form of MH-shaped SC.

4.7.2 Photovoltaics and Power Electronics

All the previous contestants have maximized the PV-cell area no matter the chosen shape. Thus all calculations will be made using $4.0m^2$ of legal PV-cells. In 2019, the better-performing contestants utilized MJ-GaAs PV-cells. But that is no longer an option due to the rules listed in 2.2.1.

Very few teams specify their SC's wiring or the parameters of the power electronics. Thus we will choose components based on information from Chapter 3.

4.7.3 Compatible Energy Storage System

When choosing a compatible ESS, one must consider the points about C-rate stated in 3.3.3. As the total capacity is set to be a maximum of 5kWh, the discharge rate should be an appropriate one capable of fully depleting the ESS when it reaches the finish line while also achieving the shortest finishing time. scpylib will be used to determine a fitting C-rate by running simulations and optimizing for the fastest finishing time. The metric for measuring performance will be average travel speed.

4.8 Simplifications

Due to the interdisciplinary nature of designing and modeling an SC, several simplifications had to be made during the creation of scpylib. There are also several assumptions being made when determining the input variables. The assumptions are made with regard to previous contestants and values found in Chapter 3.

4.8.1 Electric circuit calculations

Relevant theory for calculating the specifics of an SC and its components is presented but not utilized. This thesis merely presents how one could calculate losses for electrical components. But since no specific components are chosen, the exact efficiency is impossible to calculate. Therefore the conversion efficiency from PV output to motor output is assumed to be 90%. We also assume that

$$\eta_{charge} = \eta_{discharge} = 95\%$$

is true. The system can be thought of as presented in Figure 27.

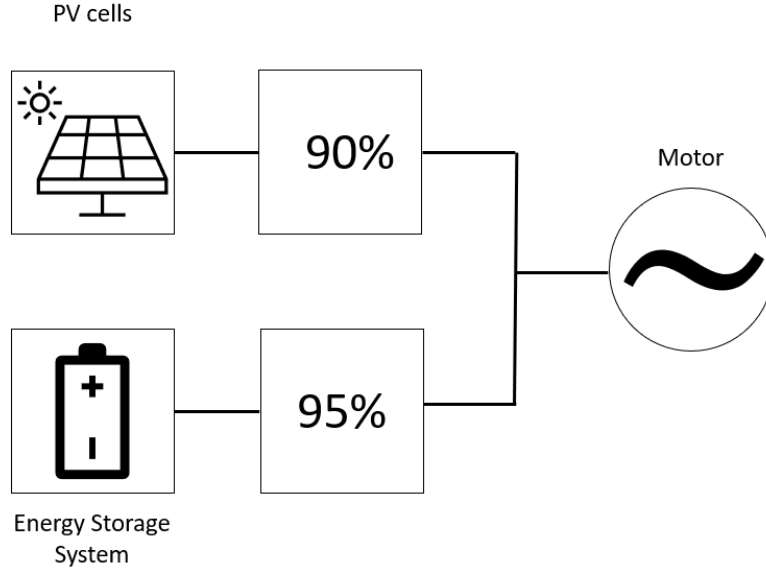


Figure 27: The efficiency of the SC's electric circuit.

The values for energy through the system will be entirely based on the calculated output of the PVs from the retrieved SI data. Due to the generally flat shape of the SC, the output is assumed not to be affected by PV tilt or azimuth. An SC's pv system might have a tilt of 10° . If we are to calculate the effect of a tilt of that magnitude, we get that:

$$\underline{A}_{PV} = A_{PV} \cdot \cos(10^\circ) = 0.9848A_{PV} \approx A_{PV}$$

Thus we will assume the system has a tilt of 0° .

Heating and temperature sensitivity

Since no current calculations are made, heat development in the ESS and the power electronic components will be disregarded. However, it will be discussed in Chapter 7. Other aspects, such as changes in PV efficiency due to cell temperature, will also be disregarded.

Energy Storage System

As previously stated and illustrated, the ESS will have a constant round-trip efficiency. And since no electrical calculations are being made, changes in voltage due to changes in SoC will not affect the efficiency.

4.8.2 Load profile

The energy consumption of the SC will suffer some inaccuracies due to simplifications and assumptions. Most testing will be done with a static wind speed. Several tests will be run with varying static wind speeds and some with the data provided by the TMY data from PVGIS.

The load calculations in the simulations will be based on weather data for a TMY. This includes values for wind speed, wind direction, and temperature.

4.9 Simulation baseline

The baseline for the simulation input used to simulate the SC is listed in Table 10.

Solar car dimensions		PV-dimensions		ESS-dimensions	
Car mass	200kg	Area	$4.0m^2$	Capacity	5.0kWh
Total mass	280kg	Efficiency	22%	η_{charge}	95%
Drag coefficient	0.09	Performance rating	1.0	$\eta_{discharge}$	95%
Rolling coefficient	0.004				

Table 10: Constant values for simulating the SC.

The chosen start date is 15th October, since it is the middle of the month.

5 Codebase

The created code base is called "Solar Car Python library," or `scpylib` for short. `scpylib` is created with the purpose of helping future members of the SC racing team Nordlys NTNU. The codebase contains scripts to create a detailed SI map for a given start location and destination. It also provides simulation tools for SC racing.

5.1 Architecture

The general architecture of `scpylib` is depicted in Figure 28. It contains some data folders and several functions address various aspects of an SC.

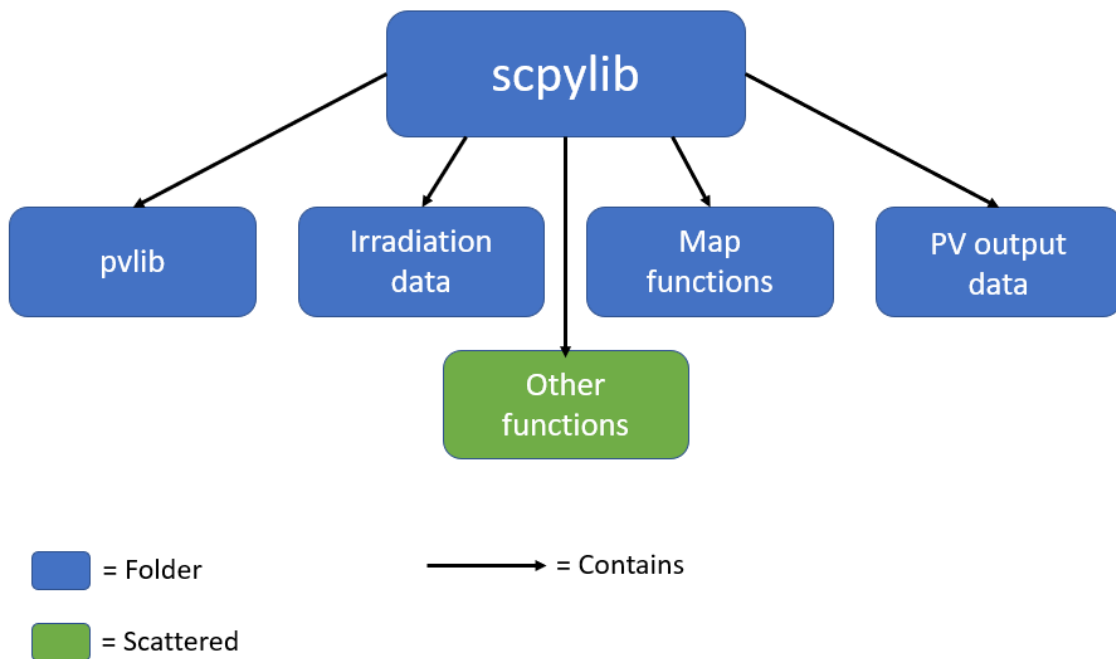


Figure 28: Structure of the main folder of `scpylib`.

pvlib is the one imported library within **scpylib**. It is mostly just imported to use the IOtool **pvgis**, as stated in 4.1. The contents of **pvlib** can be summed up with Figure 29. Though only the **pvgis** tool is used, other folders containing potentially applicable tools for SCs are listed.

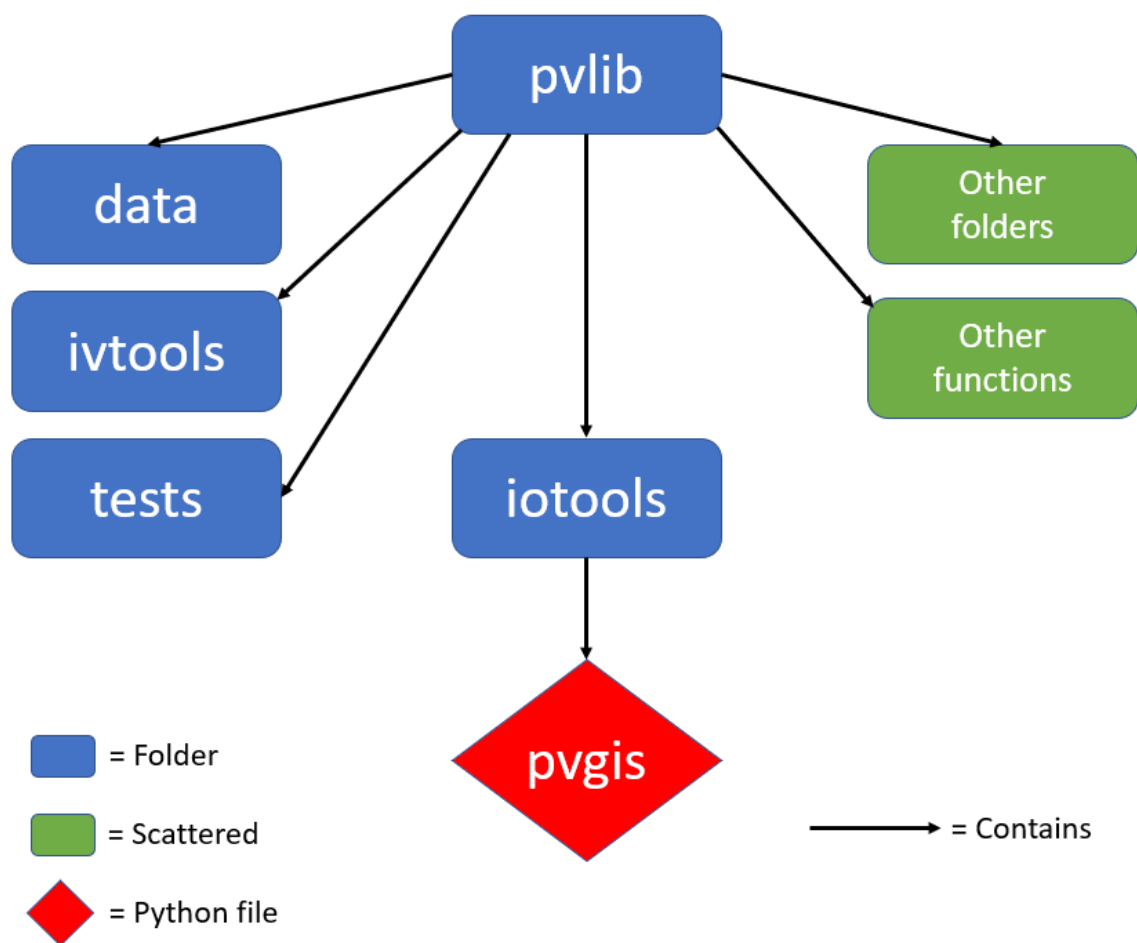


Figure 29: Most relevant contents of **pvlib** for SCs.

One of the essential parts of scpylib is the **map functions**. The **Map_creation.py** script imports an Excel file containing a column of names. The first row contains the starting location, the last row is the destination, and the rows between are landmarks. The script then uses functions from **Google_maps_api.py** to create a Google Maps trip based on the names. The script then expands the first column of the Excel file with additional locations based on the established route. The script then adds columns for the locations' latitude, longitude, and elevation. The script also creates a column for the distance to the following location. The script then calculates the incline of the stretch to the following location based on distance and elevation difference. Then it uses a function from **Bearing.py** to calculate the bearing between the coordinates of one location and the next. A copy of the map file is then saved and exported to the main scpylib folder. The map functions folder also contains a file called **Elevation_profile.py**, which plots the route's elevation. A chart depicting the map functions folder can be seen in Figure 30.

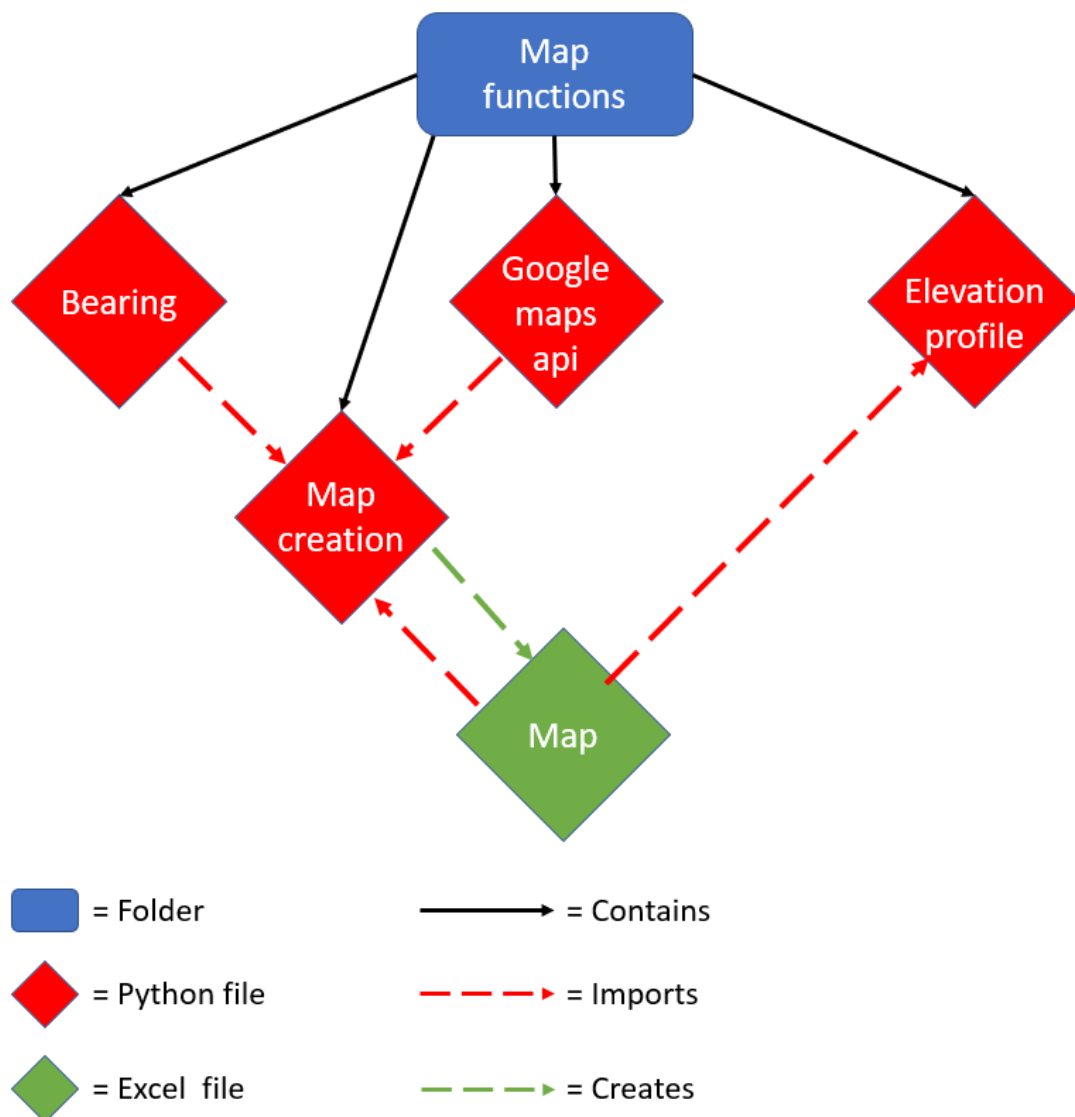


Figure 30: The map functions folder.

The next step of a complete map containing **SI data** is retrieving it using the PVGIS IOtool from pvlib. The data can be retrieved in the TMY format or recorded values from a specific timeframe (one-year minimum). The retrieved data is in hourly values. The data is then archived as .csv files within the **Irradiation data folder**. A chart depicting the process can be seen in Figure 31.

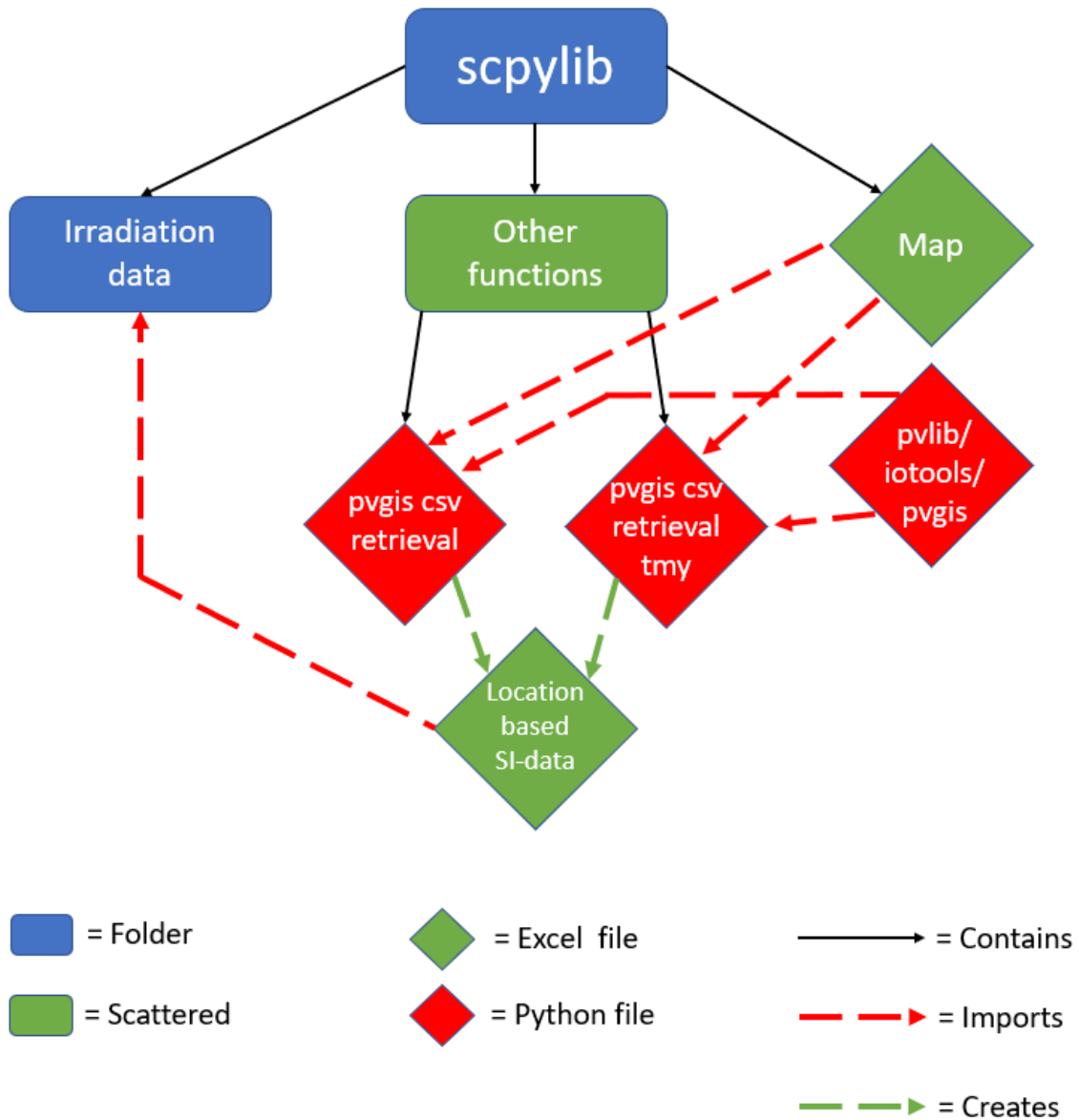


Figure 31: Chart depicting the SI data retrieving scripts architecture.

The next step in simulating an SC's performance is calculating the PVs' performance. The output will be calculated based on equation 3. There are two different output scripts, as the irradiation data files' format vary depending on how they were retrieved. A file called **Sky_coverage.py** also contains functions that modify the output based on sky coverage, as the name suggests. In the likeness of the input SI data, the output is saved as hourly data in .csv files. A chart depicting the process can be seen in Figure 32.

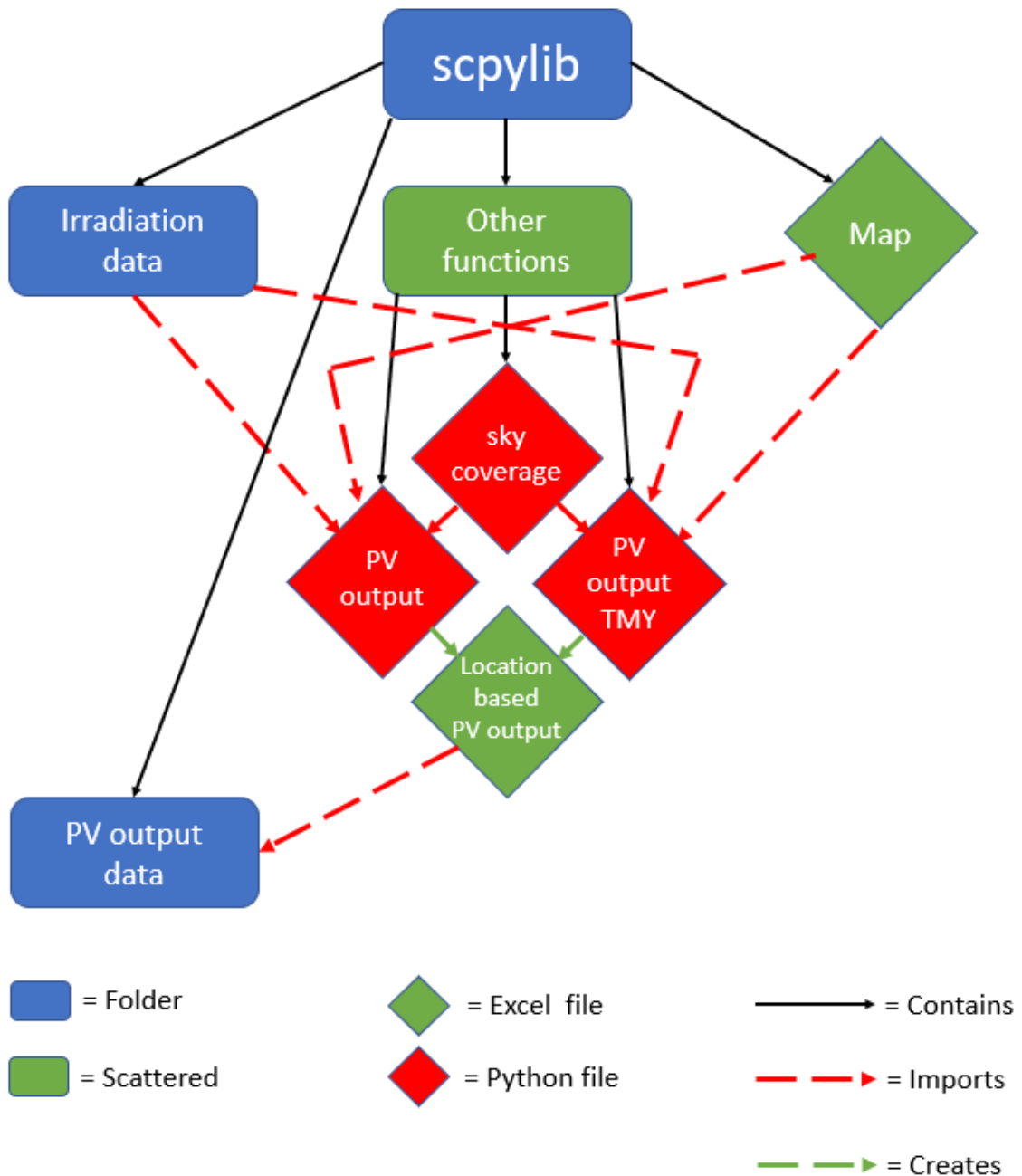


Figure 32: Chart depicting the PV output calculation process.

Finally, the culmination of the different processes is the **Race_simulation.py** file. It contains a script that utilizes outputs and functions from several other files. The file contains a script that runs a while loop to simulate an SC traveling the route. The script uses a location list created from the map file. The script then calculates the SC's speed depending on PV output per hour. The PV output is retrieved on csv files that are opened based on the SC's current location. The resultant velocity in km/h is then calculated based on setting output equal to the load equation 32, then solving the equation with the secant method.

Then the SC gets additional kinetic energy based on the ESS's SoC, C-rate, and the previous speed calculation. The speed is then recalculated in the same manner with the additional input energy.

The distance traveled then equals the velocity as the while loop cycles through hourly data, and velocity is given in km/h.

At the end of the loop, the current distance traveled is compared to the distance to the next location. Then at the beginning of the next loop, the location changes depending on if the next location is reached. A new set of PV-output data is then opened.

This continues until the destination is reached. A chart depicting an illustration of the code architecture can be seen in Figure 33, and a flow chart of a race simulation loop can be seen in 34.

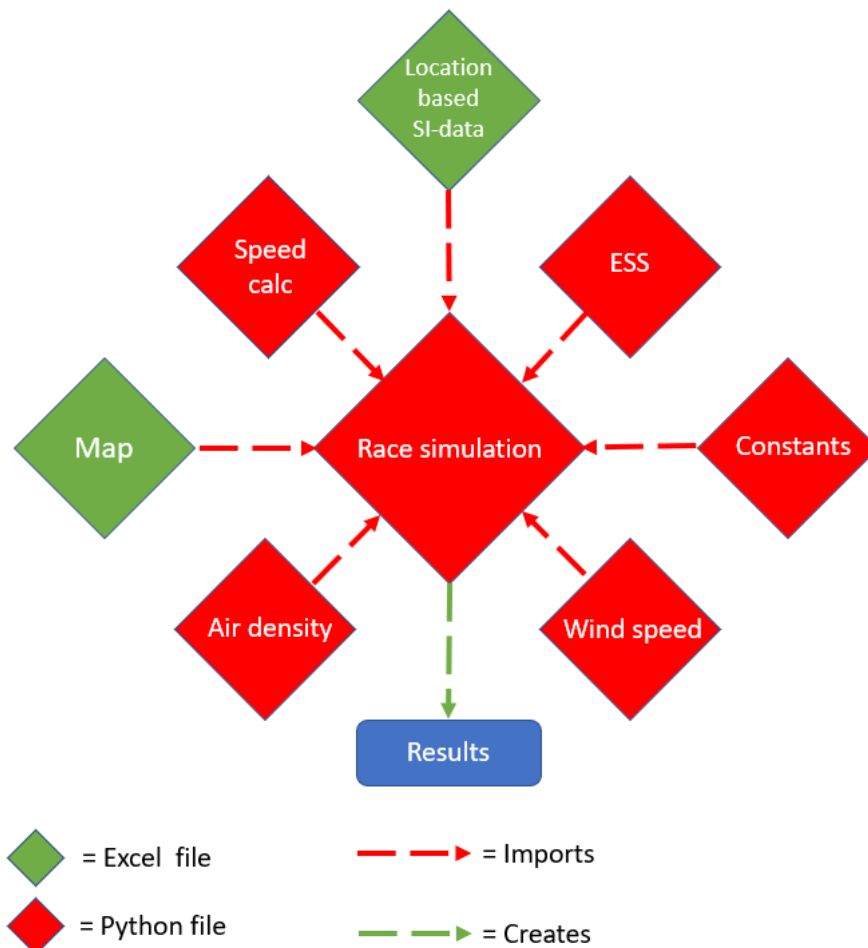


Figure 33: Chart depicting the architecture of `Race_simulation.py`.

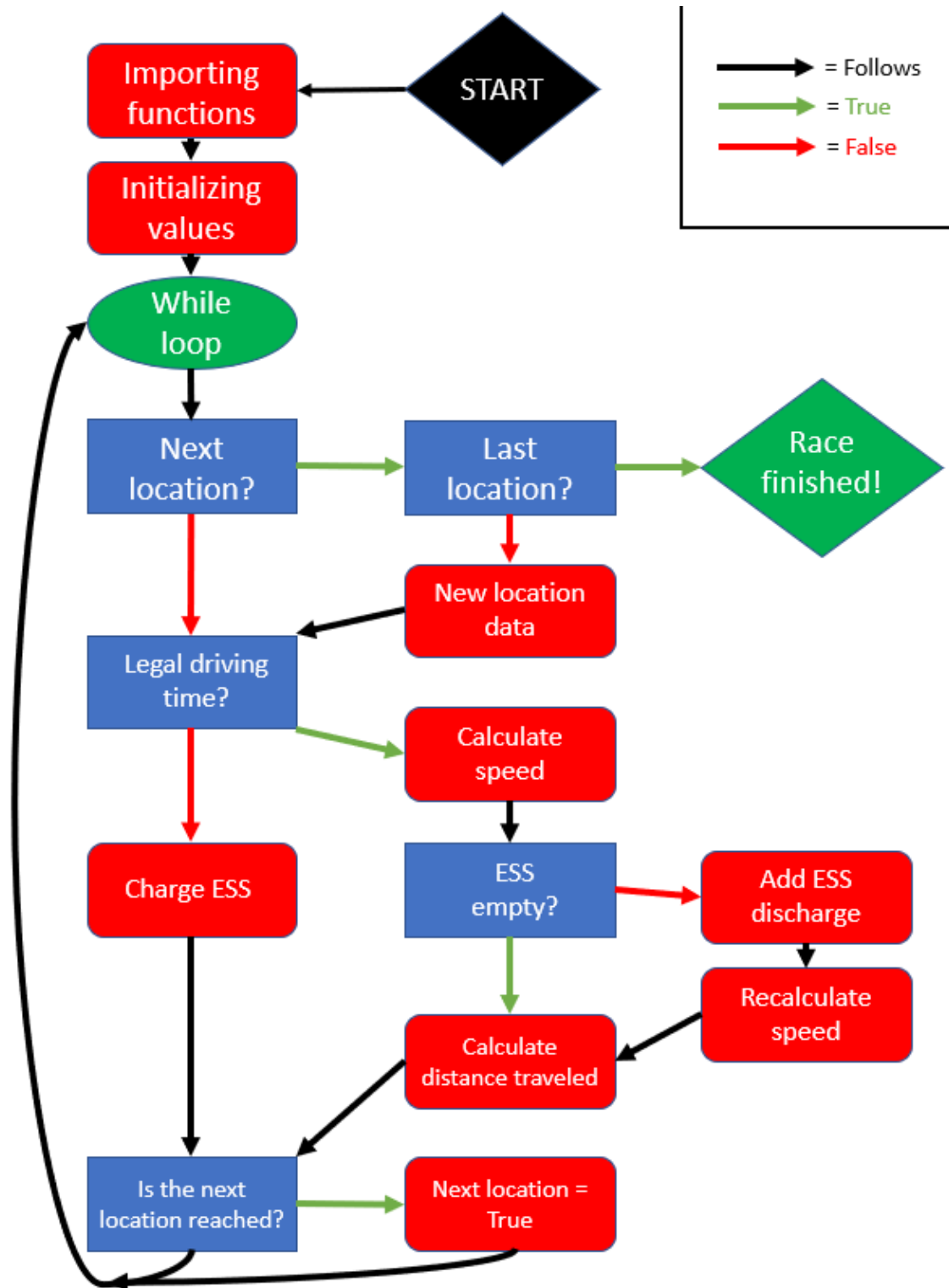


Figure 34: Flowchart depicting a race simulation using Race_simulation.py.

Below is an example of how each Python file is structured. They all start with importing the utilized functions from other files and constants for values such as gravitational acceleration. The map is opened and read. Then a list of location strings and a dictionary with values pertaining to the location names are made from the values within the map file. The final if statement contains calls to functions within the file, so the functions can be tested.

```
"""
Created on Day Month Date Hour:Minute:Second Year

@author: Wilhelm
"""

"""
This comment describes what the purpose of the particular script you're observing
is. It is also some of the thoughts behind its structure. If the modeling of a
calculation is mentioned in the thesis theory chapter, then it will also be described
in this comment as such:
    This script solves the mass-energy equivalence equation
     $E = mc^2$ 
"""

import pythonpackages as pp
import Constants
from Specific_Module import function

# Initializing a list and dictionary containing data from the Excel file
# kart.xlsx
from Map_list_and_dict import List_and_dict_builder
my_dict, location_list = List_and_dict_builder()

# Depending on the state of the script, some placeholder values will be defined
# with a specific value. Like for example windspeed when the load model
# is tested.

placeholder_value = 3.14

# Then the functions for the script is defined

# Functions may just define a specific value
def get_value(x):
    if x > 0:
        value = x
    return value

# Some may do a calculation based on the input
def calc_value(x):
    value += Constants.gravity * x
    return value

# Some may call on other functions within the script, but were made as two
# different functions for clarity's sake
def calc_some_stuff(x):
    y = get_value(x)
    new_value = calc_value(y)
    return new_value

# Then the last part is meant to test the functions
if __name__ == '__main__':

    test = calc_some_stuff()
```

5.2 Simplifications and limitations

5.2.1 Energy consumption

Equation 32 is used to determine the energy consumption of the SC in the simulations. The function used to present the loads behaviour is as such:

```
def get_load(v, v_wind, theta, rho):
    P = (m*Constants.g*math.sin(math.radians(theta)) +
         m*Constants.g*Crr*math.cos(math.radians(theta)) + ((Cd*rho*A)/2)*(v_wind+v)**2)*v
    return P
```

However, the way the equation is utilized in the simulations is through three other functions. The functions can be seen below.

```
# Defines the equation
def equation(v, v_wind, theta, rho, P):
    return (m*Constants.g*math.sin(theta) + m*Constants.g*Crr*math.cos(theta) + ((Cd*rho*A)/2)*(v_wind+v)**2)*v - P

# Solves the equation with the secant method
def secant_method(x0, x1, tol, v_wind, theta, rho, P):
    while abs(equation(x1, v_wind, theta, rho, P)) > tol:
        x2 = x1 - equation(x1, v_wind, theta, rho, P)*(x1 - x0)/(equation(x1, v_wind, theta, rho, P)
            - equation(x0, v_wind, theta, rho, P))
        x0, x1 = x1, x2
    return x2

# Calls the above functions and returns the speed both in m/s and km/h
def get_speed(v_wind, theta, rho, P):
    v_ms = secant_method(1, 2, 1e-6, v_wind, theta, rho, P)
    v_kmt = v_ms*3.6
    return v_ms, v_kmt
```

The way air drag is calculated means that winds moving at higher relative speeds, from behind, results in a greater load. In reality, the load should be lessened by it. This should be negligible, as the vehicle most likely will always have a greater velocity than the relative wind. This is the case due to the model not including the SC's acceleration, thus jumping from rest to full speed in a single calculation.

scpylib uses a simplified calculation for PV output. It uses equation 3 as a baseline, disregarding for current or voltage levels. The SI retrieved from PVGIS is for a flat surface on a 0° tilt. Thus, it cannot calculate the power output of an SC with PVs that are not uniformly flat surfaces.

6 Results

This chapter presents the retrieved SI- and weather data. It also presents the results of the race simulation. Most results are presented through plots. The plots are too numerous to present all of them in this chapter. Thus, most plots depict data for Darwin and Adelaide since they are the WSC's start and destination, respectively. All of the resulting plots can be seen in Appendix B.

6.1 Solar Profile

The solar profile also contain data for wind speed, wind direction, and ambient temperature. Values that are all relevant for the following two objectives of energy- production and consumption.

SI data were retrieved alongside other weather data and stored as csv files. The SI contents of the csv files can be plotted as shown in Figure 35.

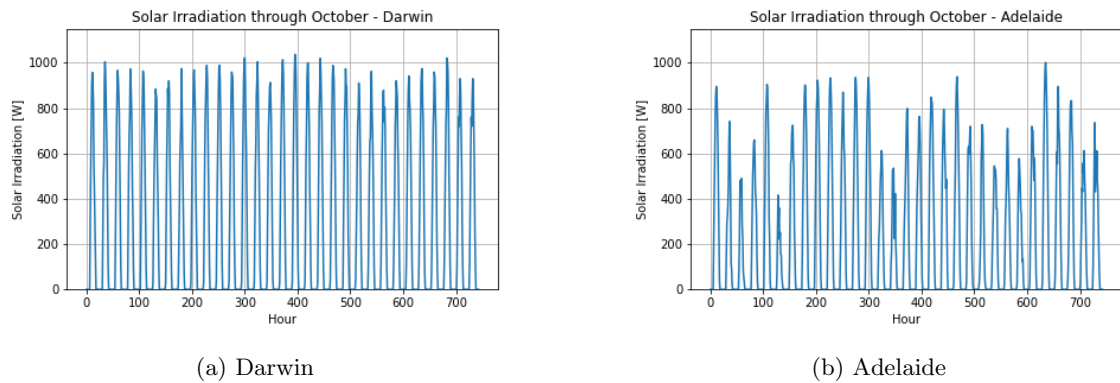


Figure 35: The hourly SI for the starting point 35a and destination 35b for the WSC. The data is for a TMY.

The average SI per day in October along the route for a TMY can be seen in 44.

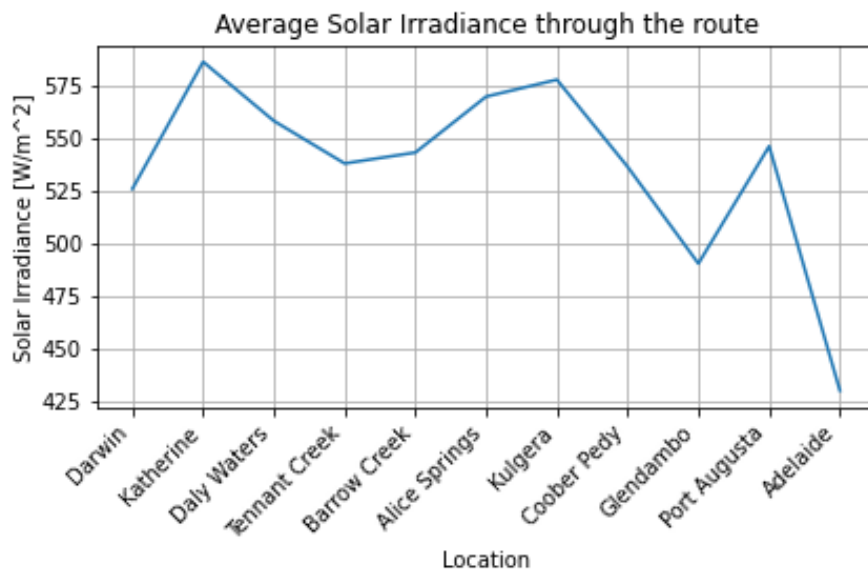


Figure 36: Average SI for the landmarks along the route in October during a TMY.

The csv files also contain weather data for wind speeds and wind direction. A plot depicting wind

speeds for Darwin and Adelaide can be seen in Figure 37, while the wind direction distribution can be seen in Table 11. All the plots for wind speed show the absolute value measured, disregarding wind direction.

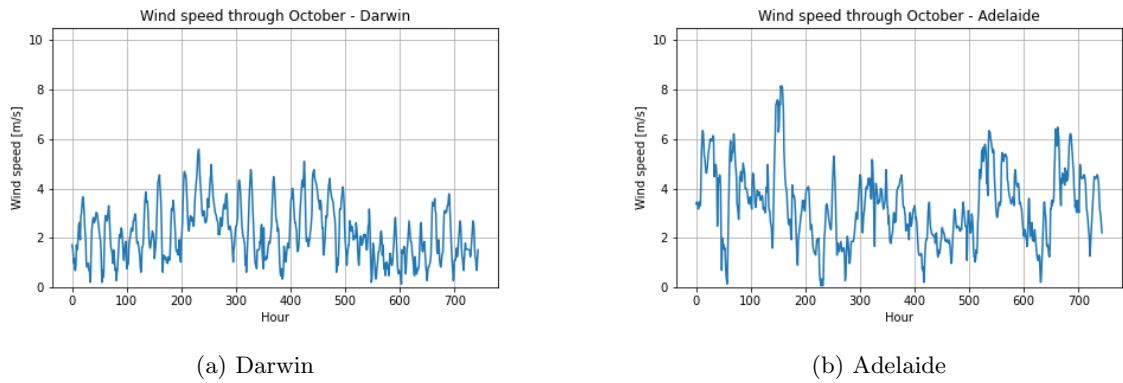


Figure 37: The wind speed for the starting point and destination for the WSC. The data is for a TMY.

The average wind speed per day in October along the route for a TMY can be seen in 38. The maximum wind speed can be seen in Figure 38.

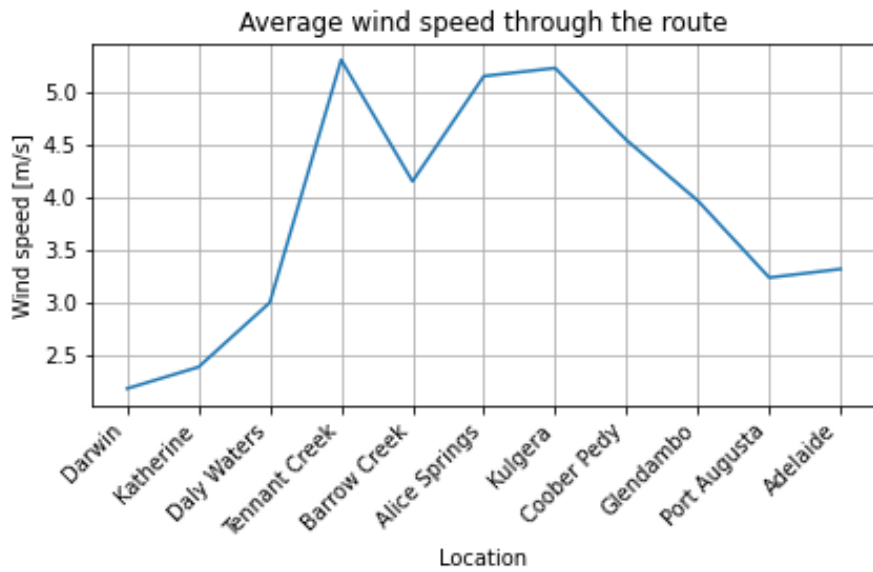


Figure 38: Average wind speed for the landmarks along the route in October during a TMY.

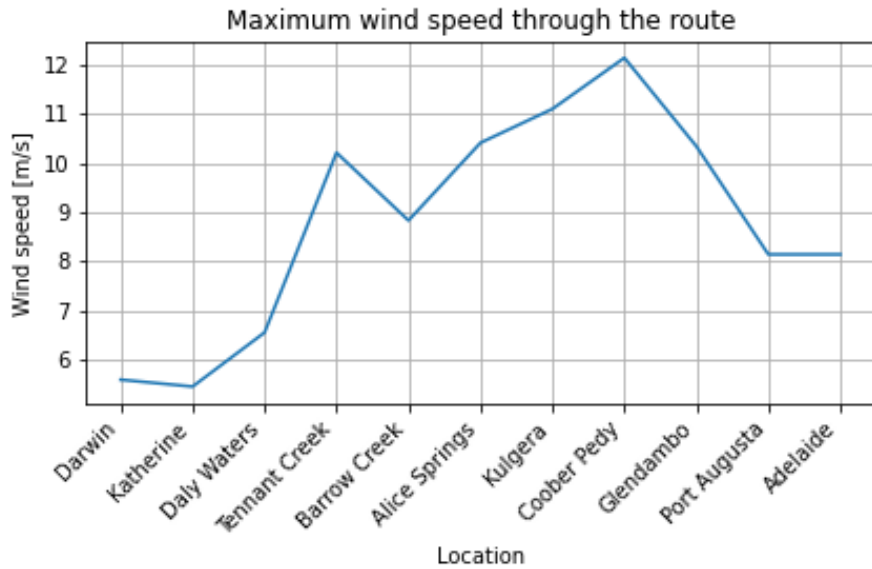


Figure 39: Maximum wind speed for the landmarks along the route in October during a TMY.

Table 11 depicts the amount of hours the wind originates from its respective direction. The percentage column depicts what percentage of the time during that month the wind originates from the respective direction.

Wind direction	Darwin		Adelaide	
	Hours	Percentage	Hours	Percentage
North	94	12.64	62	8.34
North-East	131	17.61	41	5.52
East	88	11.83	96	12.92
South-East	47	6.32	206	27.73
South	36	4.84	181	24.36
South-West	21	2.82	45	6.06
West	184	24.73	73	9.83
North-West	143	19.22	39	5.25

Table 11: Excerpt from the retrieved weather data. The data is for October during a TMY.

Similarly to SI and wind speed, the hourly temperature values for each location can be plotted as shown in 40.

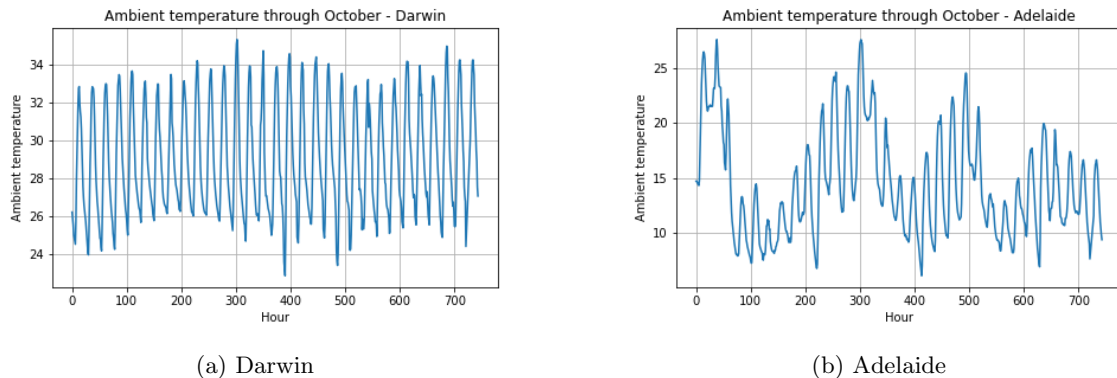


Figure 40: The temperature for the starting point and destination for the WSC. The data is for a TMY.

The average values and maximum values for temperatures for each location can be seen plotted in figures 75 and 42.

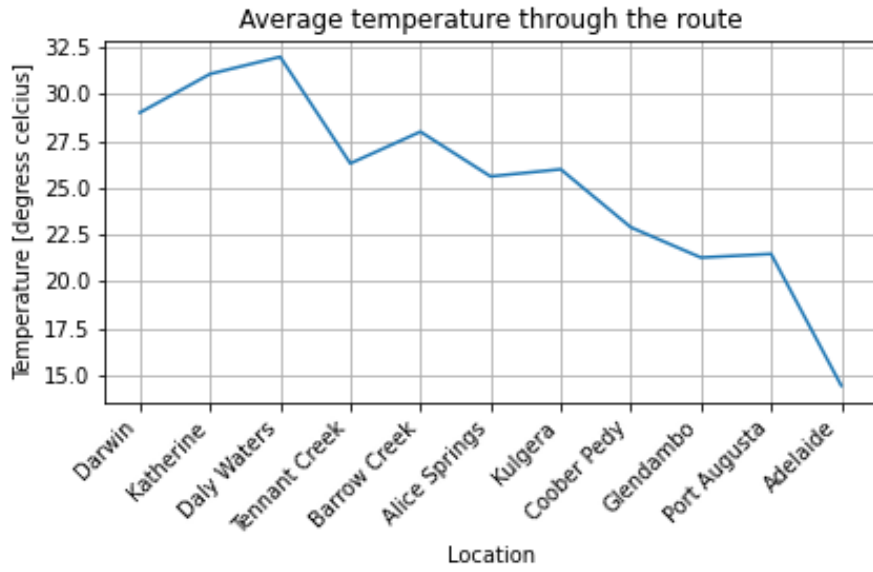


Figure 41: Average temperature for the landmarks along the route in October during a TMY.

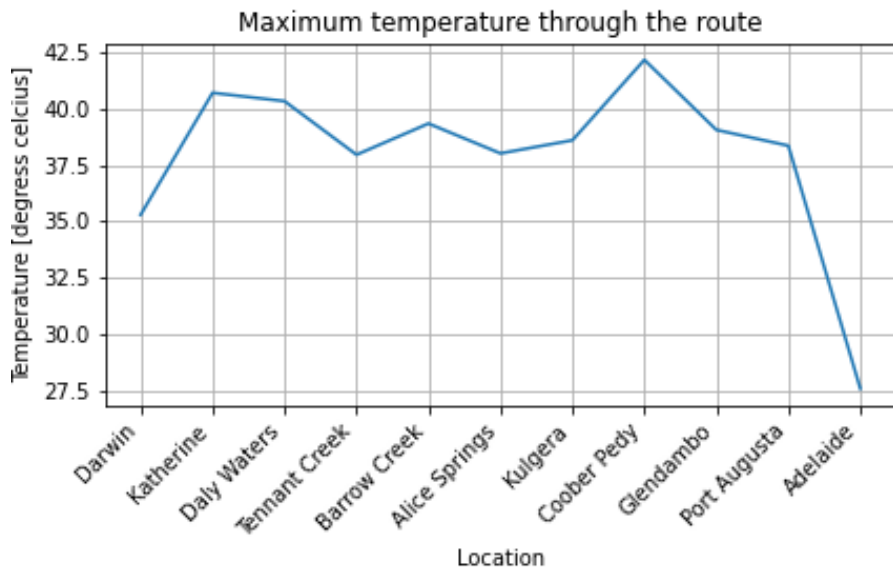
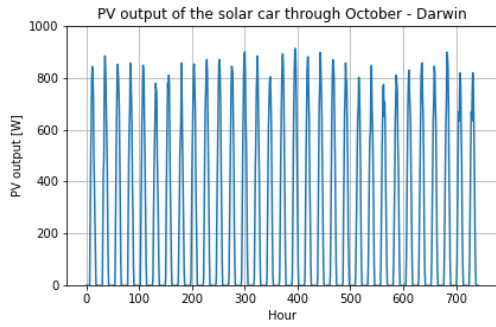


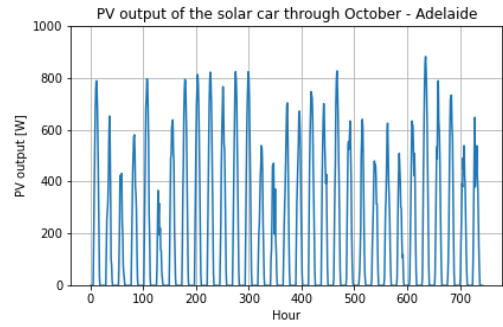
Figure 42: Maximum temperature for the landmarks along the route in October during a TMY.

6.2 Energy generation

The resultant energy output for the SC were calculated from data retrieved for the solar profile. A visual representation of the output in Darwin and Adelaide can be seen in Figure 43.



(a) Darwin



(b) Adelaide

Figure 43: The PV output of the SC for the starting point and ending of destination for the WSC. The data is for a TMY. The graph looks identical

The average PV output per day in October along the route for a TMY can be seen in 44.

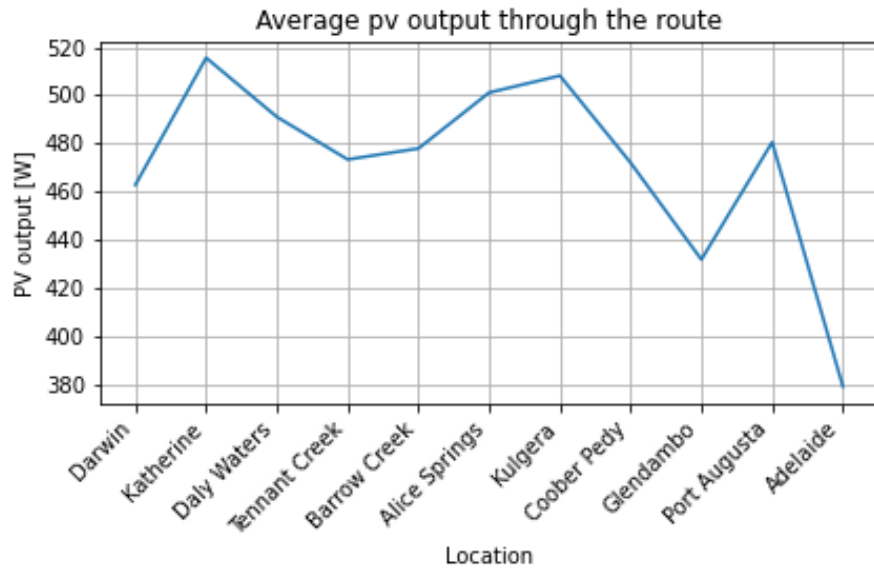


Figure 44: Average PV output for the landmarks along the route in October during a TMY. The average value includes nighttime in the calculation.

6.3 Energy consumption

The energy consumption of the SC with the input values from Table 10 from chapter 4 can be seen in figures 45-48.

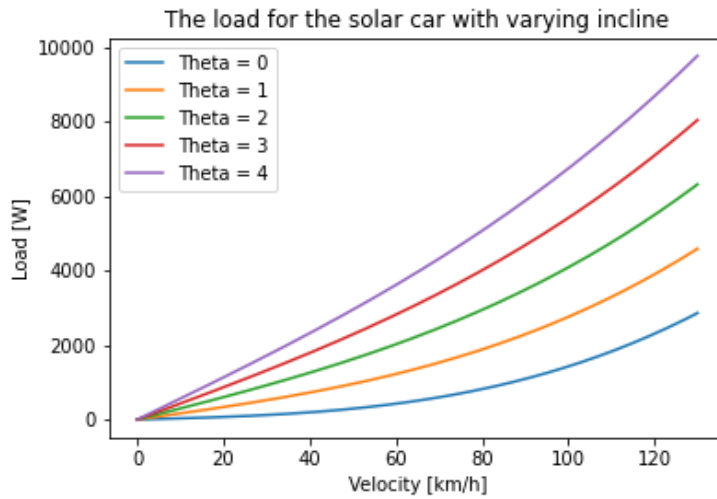


Figure 45: The load of the SC between 0 and 130 km/h, with steps in incline between 0° and 4°.

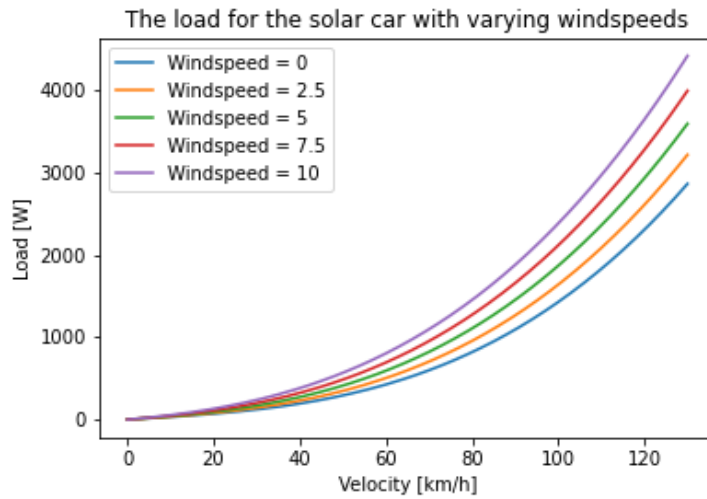


Figure 46: The load of the SC between 0 and 130 km/h, with steps in wind speed between 0m/s and 10m/s

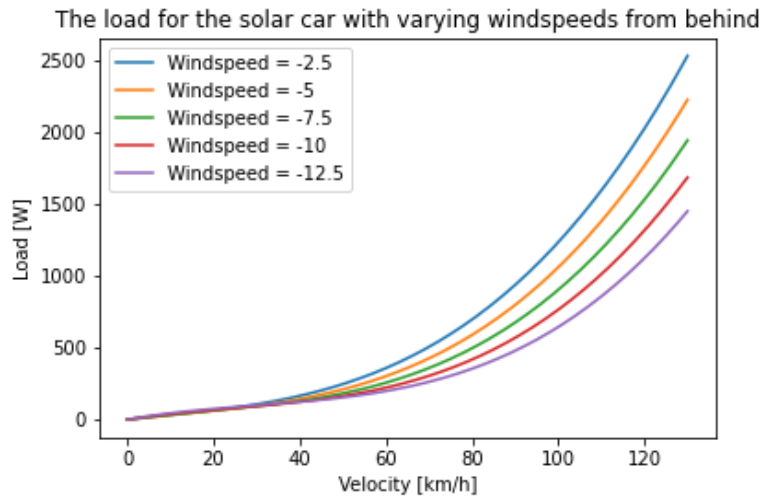


Figure 47: The load of the SC between 0 and 130 km/h, with steps in wind speed between -2.5m/s and -12.5m/s. The load is still positive at Velocity = 0m/s, and increases close to linearly up to around the 30km/h mark. This being due to how the load is calculated in the code. The load behaves properly once the SC speed equals the wind speed.

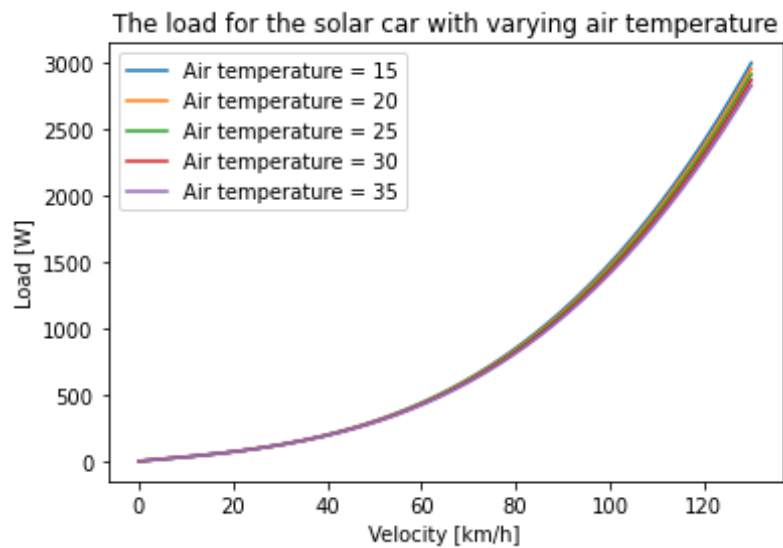


Figure 48: The load of the SC between 0 and 130 km/h, with steps in temperature between 15°C and 35°C.

6.4 Choice of suitable components

The performance of the simulated SC with varying ESS C-rates can be seen in Table 12. As stated in chapter 4 the C-rate was set to a specific value, then manually adjusted for to find the best outcome. The Table columns are the specified maximum C-rate, the resultant maximum discharge, the distance the SC traveled before the ESS was depleted the first time, and then the resultant average SC speed, respectively.

C-rate	Maximum discharge [W]	Distance reached at depletion [km]	Average SC speed [km/h]
1	5000	236	72.02
0.5	2500	337	73.12
0.1	500	1153	74.96
0.07	350	2230	75.33
0.06	300	2927	76.45
0.055	275	3045	76.57
0.0525	262.5	3075	76.90
0.05	250	Never fully depleted	77.20
0.01	50	Never fully depleted	69.34
0.005	25	Never fully depleted	67.94
0.001	5	Never fully depleted	67.33

Table 12: The simulation results depending on battery C-rate. The optimal C-rate for these racing conditions is between 0.0525 and 0.05, where the ESS is depleted just as the SC passes the finish line.

No detailed electrical analysis was made. Thus no final choices for other components were made. The topic will be discussed in the **next chapter**.

6.5 Solar car simulation

Figures 49-51, display the results from a solar car simulation. The start date was set to 15th October 00:00 and the C-rate to 0.0525. The C-rate being picked due to the results from Table 12. Figure 49 displays the cruising speed of the SC throughout the race. Each dip every nine hours is from the legal race time ending. The SC never has a speed of 0 in this plot and it experiences sharp increases in speed between two days. This is a result of the SC's acceleration not being accounted for.

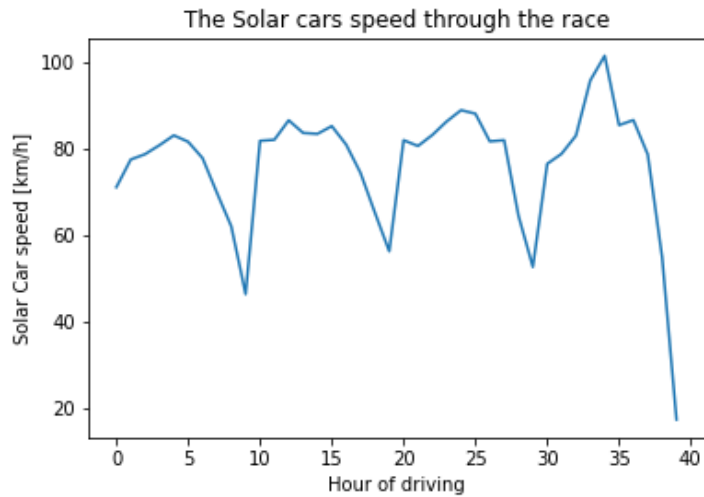


Figure 49: The speed of the simulated SC through the race. The velocity at the end of day 1 is 46.5km/h. The low points are during the final hour of the race before the end of the daily nine legal driving hours, when the SI is at its lowest.

Figure 50 depicts the ESS's SoC throughout the race. The flat periods are during nighttime, while the small increases in SoC are from charging outside legal driving hours. The charging happens before 08:00.

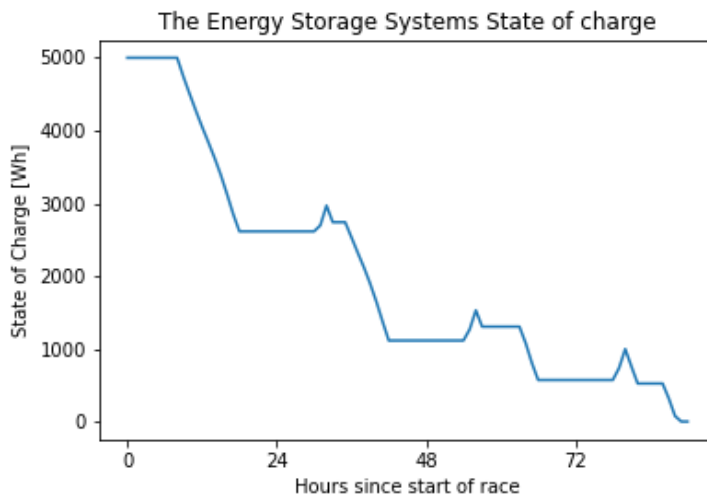


Figure 50: The ESS's SoC throughout the race.

Figure 51 depicts the SC's progress throughout the race. The flats indicate the time between driving sessions, including nighttime.

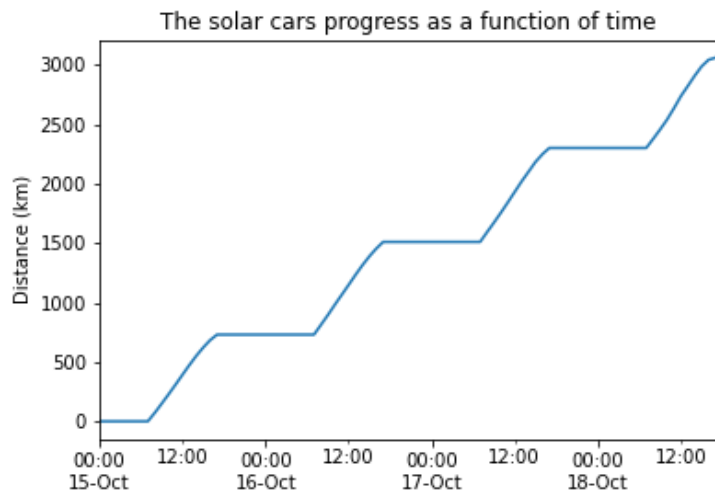


Figure 51: The progress of the simulated SC as a function of time. The race ends at the end of the fourth day.

7 Discussion

This chapter will discuss the results presented in Chapter 6. It will also discuss the impact of the decisions made, which were presented in Chapter 4 and partly in Chapter 5.

7.1 Weather data

7.1.1 Solar Irradiance Data

The SI data can be retrieved in the TMY format or for a specific time period. However, the only data used for the simulation was the TMY data. This presents the weakness of non-standardized values. By looking at SubFigure 35a, we see that the SI has a very stable value due to that year's weather and cloud coverage. Subfigure 35b, in contrast, is uneven. It has several dips in SI. This is especially visible between the fifth sixth days, where the SI for the sixth day is less than half that of the previous day's SI. This discrepancy is more visible when looking at the graph in Figure 44.

Figure 11 implies that the average SI along the route should be highest just before reaching Alice Springs and slowly decline the further away from the Equator one travels. The graph depicts an SI slump around Tennant Creek instead. This discrepancy could result from the Figure being based on another weather database than the one PVGIS utilizes. It might also be due to the SI data for October diverging from the long-term averages. Future comparison between TMY data and average values from different sources is suggested.

Due to the data's location specificity, the solar profile's consistency suffers. TMY SI data retrieved from PVGIS for a location is represented with measurements from a previous year. Two locations may have data from differing years in a TMY data file. This can cause holes in the continuity of the simulation. As the SC would arrive at a new location, the data for the two neighbouring locations may not correspond for the particular hour that the race simulation retrieves data from, resulting in unrealistic changes in weather conditions.

7.1.2 Wind

Wind data is retrieved similarly to SI data and can be properly utilized. An attempt to visually present the average wind speed, maximum wind speed, and wind direction was made, and some comparisons to the load model results can be made. The consistency issue discussed in the previous paragraph is more relevant to the wind data. PVGIS is a PV-focused tool. Thus SI data has a higher priority than wind data when selecting the TMY standard.

None of the TMY data sets include extreme weather. The strongest winds for the TMY data used are just above 12.0m/s in Coober Pedy. On the Beaufort wind scale, that is categorized as a strong breeze. However, if winds are strong enough to pose a danger to a driver and their SC, the event organizers possess the power to cancel the event. This validates the simulation's weather data uses, as it would be meaningless to simulate SC performance under extreme driving conditions.

Another fact that has yet to be considered is the effects of side winds. The wind data is utilized purely to calculate the SC's load based on its speed along a single axis. The effects of side winds on air drag due to the SC's shape have not been explored. A more detailed study side winds' effects has on SC racing should be considered.

7.2 Photovoltaic generation

The generation data depicted can be seen as directly correlated to the SI data. This is most visible in the graphs depicting the average values for each location. The way the generation is calculated is simplified. The generation does not account for tilt, azimuth, temperature, or electrical dynamics.

7.2.1 Array orientation

As explained in Chapter 3, the PV's facing the sun will result in the highest power output. The general direction of the race is south, meaning the optimal azimuth for the SC's PV cells would be closer to the opposite of the bearing. This supports arguments for an MH-shaped SC since most of its PVs face backward. The cockpit's frontal position would also minimize potential shading. It should also be noted that the expected tilt of an MH SC is around 10° , which would barely affect the expected output. However, the effect of the SC's PV's tilt would be amplified, affecting energy production during inclines like Hayes Creek Hill's 11.5.

One should also note that legal driving hours are about three to four hours shorter than the time between sunrise to sunset in Australia in October. This is also evident in how the curve shown for the SC's speed starts at a relatively high speed. As the PV output calculations are based on SI on a horizontal surface, ESS charging can be improved in simulations and with realistic strategies. The top of most SCs can be flipped into a vertical position. This allows for a more effective solar collector than a horizontal one while the sun is in a low position in the sky.

7.2.2 Temperature

As stated in 3, the temperature will negatively affect the power output of PVs in a realistic scenario. However, the simulation model does not account for ambient temperature, affecting the realism of the output. A temperature-based power production reduction function could be implemented with little difficulty, depending on how one would define the loss of efficiency. It is also a fact that the round-trip efficiency, life expectancy, and safety of the ESS would be affected by high temperatures.

The peak temperature reaches 40° at several locations throughout the route. This would not only pose a threat to the ESS but to the driver also. Air cooling will still be viable due to the SC's high cruising speeds. However, such high ambient temperatures might strain the ESS during incline-induced high loads and acceleration events. A future investigation of effective cooling systems is therefore highly encouraged.

7.2.3 Electrical dynamics

The electrical analysis of the system was, for the most part, disregarded, as stated in Chapter 4. The PV's voltage will drop as the available SI drops. The PV's voltage would also drop as the cell temperature increases. This would likely cause a higher loss in the DC-DC converter. The same would also be true for the ESS. The main bus voltage would drop as the ESS is depleted, leading to changes in the total system efficiency. A total system efficiency of 90% and above is expected, so the assumed efficiency is still realistic.

7.3 The Solar Car's energy consumption

The dynamic model presented in Equation 32 responds as predicted, as shown in Figures 45, 46, and 48. It increases exponentially as a function of the SC's velocity. We can also see that the incline impacts the SC's energy consumption the most.

As shown in Figure 47, the wind coming from behind affects the load unrealistically at low speeds. This is due to how the load equation is being solved. However, this is irrelevant if the SC travels

at a higher relative speed. The average wind speed is less than half the cruising speeds, and the maximum only surpasses vehicle speed during a single hour of the main simulation. Thus the way the equation is solved works for the simulations as is. A simple if statement might solve this bug by expanding "def equation();" shown at the end of Chapter 5. However, the secant method might not behave favorably in response to this proposed change. Alternative ways of solving third-order equations through Python should be explored.

Another flaw of the simulation is how incline is treated. Stanford Solar Car Team's map shows a maximum incline of 11.5° in the first half of the climb. The elevation profile depicted in Figure 24 also shows us that there are several small inclines and declines along the route. However, the map used for the simulations has incline values closer to the average incline value. As the SC will do approximately the same total amount of work for the total rise in elevation, the simulation results still stand as a viable performance analysis tool. This will change if a model for the electrical system is developed. Electrical efficiencies will be affected by the magnitude of the drawn current due to the increased maximum load, which again emphasizes the need for a detailed electrical analysis.

7.4 Choice of Components

The history of previous contestants indicates that the optimal SC **shape** is an MH one. The list of the top three contestants in Table 9, and the full list of contestants in Table 13, show how MH-shaped SCs have become the overall top performers. Nevertheless, Michigan's win with an AC-shaped SC does prove that the shape is just a single factor in predicting SC performance.

The best **PV material** needs clarification. Monocrystalline silicon is still a great option, as it has always been in the WSC. Progress within its efficiencies can be seen throughout the history of Tokai University's SCs, which always finished among the top 5, with their stated PV efficiencies steadily increasing over the past decade. Most of the top performers in 2017 and 2019 had a form of GaAs-based PV system. Be it thin film- or MJ technologies. The potential for MJ perovskite-based PV-powered SCs exists. Their efficiencies have improved dramatically over the past decade, and new fabrication methods may be beneficial for SC manufacturing. The rules do not specify a specific size for perovskite-based PVs, which would lead to $4.0m^2$ of potentially higher than monocrystalline silicon efficiency is likely legal. The rules surrounding PV materials are vague, however. The rules specify that the organizers must be contacted if a non-standard solar collector (silicon) is to be used. The effects of high ambient temperatures on perovskite-based PV cells remain to be determined. A comparison between the two types of cells for high-temperature applications is suggested for future work.

The **microgrid topology** in Chapter 3's Figure 8 is likely best. The rules specify that the ESS can be split into a maximum of two separate battery packs. There are no restrictions on the wiring of the PV cells, allowing for experimentation. A series wiring would yield the highest voltage due to all the individual modules' voltages being added up. However, wiring all the modules in a series would leave the grid susceptible to failure, as a single fault would likely cut off the SC's entire generation. The impact of the PV system's wiring must be investigated to determine the optimal voltage yield and the risk factor.

No matter if the PVs are wired in a parallel or a series or if the **ESS** is split in two, the ESS will serve as the main bus voltage basis. Its predictable voltage changes due to SoC would provide much-needed stability to a system that might experience large steps in load. Keeping the number of power electronic components to a minimum would also minimize switching losses and heat losses, as it is favorable to keep the number of transistors between the power source and the load to a minimum. This will be especially true if the acceleration phase is accounted for. The acceleration would likely demand a higher current than the PV generators are capable of delivering, thus leading to the ESS being the main source of power during it.

By looking at previous contestants, it is safe to assume **Li-ion** batteries are the most viable option for the ESS. **Li-S** batteries have a higher realized- and a much higher theoretical maximum energy density. However, they have yet to be made commercially available. They are listed in the rules,

indicating that the organizers predict their presence in the WSC future events.

The **power electronics** for the system are undetermined at the time of this thesis. The research and advice from earlier contestants advise the inclusion of an MPP tracker for the PVs. The optimal inverter is also undecided. One of the requirements is that it needs to be a three-phase inverter, as the chosen motor type requires a three-phase current to function. By its description, a three-level three-phase inverter is likely the most efficient. As the switching losses are a dominant part of the inverter's losses, halving the switching time should limit these losses. The increased switching frequency and speed will be detrimental to the system's lifespan, however. The strengths and weaknesses of the components need more consideration before a decision should be made, and the losses from heat development and switching are proposed as future work.

7.5 Codebase

The method in which most of the results were produced was through programming in Python. Python was chosen because this thesis's author is the most familiar with it compared to other languages. It is also most students' introduction to programming, which makes the library more comprehensible to eventual new members of Nordlys NTNU. The library `pvlb` also provides a convenient way of accessing location-based SI data through code.

By comparing the average finishing speed of the simulations and previous competitors, we can determine that the results from the simulations are realistic. The weight chosen is heavier than most of the competitors. However, other simplifications, such as disregarding the system's thermal sensitivity, might compensate for the extra weight's negative effect. Further testing with more data sets is required to confirm its realism.

How the code is structured works for the tests run for this thesis's goals. A restructuring might be necessary for a more detailed simulation with more realistic results. The main simulation file `Race_simulation.Py` depends on SI data being processed into PV output files before simulation. This simplifies the bug-fixing progress and lowers the code's dependency on an internet connection for simulation. The retrieval of SI data is the most time-consuming part of the simulation, and keeping the process separate from the race simulation saves time.

The code uses a relatively small Excel file filled with location names, which expands into including coordinates, elevation, the distance between locations, general incline, and bearing. The map functions will allow for simulations in other races or routes and not just the WSC route. However, as mentioned in section 4, the Stanford Solar Car Team's map file contains a very detailed route map. How SI data is retrieved and processed precludes its use without slicing, and how the race simulation calculates the distance traveled is also incompatible with Stanford's map. The main while loop of `Race_simulation.Py` iterates every hour and switches location once per loop, which would not be compatible with Stanford's map's 204'878 locations, as the simulated SC would pass several locations in an hour.

A proposed fix to the issue of overshooting locations would be to decrease the time jumps for each loop. The same overall structure could be used. However, a fraction of the same values could be used instead of calculating the distance traveled with a 1:1 ratio to the SC's speed given in km/h. This should only affect the number of loops per simulation, not the result.

Another proposed rework of the code would be a procedural retrieval of SI data. The data could be stored similarly but overwritten as the new data is retrieved. This would solve the data storage problem mentioned in Chapter 4. Stanford's map file does not contain incline data, but that can be calculated with a simple function. Another map file based on Stanford's can also be created. The new file would then be the same route but with fewer locations. The procedural data retrieval would rid `scpylib` of its storage problem, and the new map file would make the amount of data retrieved more manageable. However, this will increase simulation time drastically as the SI data retrieval is `scpylib`'s most time-consuming process.

7.5.1 Energy Storage System Utilization Strategy

Another area that can be improved is the ESS utilization strategy. The implemented function works and ensures the discharge is consistent throughout the race. It also accounts for the fact that discharging at higher SC speeds will result in a lower return compared to an equal discharge at a lower speed. Consistent power output from the ESS through the race is also the ideal way to use it. From what we can observe in Table 12, it would be correct to assume that depleting the battery just as the SC crosses the finish line would be the ideal scenario.

The problem with how the ESS is utilized in the simulation as it stands at the moment this thesis is written is inflexibility. The code cannot plan ahead and make decisions regarding expected power output at later stages in the route. The WSC organizers have said themselves that the inclusion of an ESS was to counter bad weather conditions, steep hills, and allow for overtaking of other cars. If the SC were to have close to a fully depleted ESS, then experience full sky coverage, it would result in being stranded until the weather allowed for power generation. This would not only be detrimental in the context of a race but could potentially be dangerous as the race is along a highway.

Another potential improvement would be to charge the ESS during solar peaks. scpylib currently charges the ESS exclusively outside legal driving hours. Figures 45-48 all show how the load increases exponentially. Overall race performance will increase if the SC can drive at lower speeds than its maximum potential and charge its ESS with excess energy. This is due to the diminishing returns per unit of power spent at high speeds. The SC will then hypothetically experience increased overall efficiency as it would spend the excess energy during lower PV output levels and experience a higher speed return on the energy spent. Investigating the strategy's viability and feasibility is proposed as future work.

7.6 Future work

7.6.1 Electric analysis

As stated above, the SC's electrical system's components have been studied. However, the details and calculations lack substance. The author would propose a thorough electrical analysis of the power electronics in such a system. The author would also propose a more detailed study on the effects of high ambient temperatures surrounding the PVs and ESS. This pertains to the ESS especially, as it would be the component with the most severe ramifications if a fault were to occur. A cost-benefit analysis of the converter- and inverter types should also be conducted. Defining battery voltage levels and calculating expected PV voltage levels will allow for a more informed choice of such components

A cooling system for the power electronics and ESS should also be investigated. The effects of air-cooling from the SI's movement might not be enough to meet their needs, and a heating-induced breakdown of the ESS would be catastrophic due to the electrical system's main bus voltage being based on it.

7.6.2 Solar car shape

Investigating previous contestants proves that an MH-shape SC is the best option. The shape allows for a very aerodynamic- and symmetric design, low weight, and possibly more optimal PV positioning. The author proposes a small-scale aerodynamic analysis to find the optimal shape.

7.6.3 Load model

The load model works for its intended purpose. However, it lacks the acceleration component, which would increase the total energy need of the simulated SC. The formula for acceleration is widely known, and including the calculation shouldn't be a problem. However, the problem lies in

how to define the acceleration phase. This problem must be solved if a more realistic simulation is to be made. How the model calculates the load at lower speeds should also be improved by updating the equation-defining function and possibly solving the load equation with another method than the secant method.

7.6.4 Simulation improvements

The author would propose an alternative method of SI data retrieval. This should be possible by incorporating the data retrieval and processing within the main loop of the simulation. The author would advise future users to limit the number of samples made by slicing the Stanford map file into a more manageable size. The author suggests changing the way hourly data is iterated to enable calculations for smaller increments of time.

The author also suggests incorporating sky coverage functions in combination with the restructuring of race simulations and data retrieval. Functions for altering the SI data based on sky coverage also exist within `scpylib`, but still need to be properly implemented within `Race_simulation.Py` yet. The author would propose to experiment with ways of dynamically implementing it into the simulation to enable predictive simulation based on weather forecasts

The author would also suggest improvements within the ESS utilization strategy. A proposed method is to automate the process of determining the optimal C-rate. This would also allow for optimization algorithms to be implemented. Several alternatives exist in which constraints for set parameters can be set, and the code would automatically find the ideal ESS usage. This would be more relevant for actual racing strategy in an actual race, where the team would plan based on distance traveled, ESS SoC, and weather forecast.

The author also suggests investigating the possibility of charging the SC's ESS during driving sessions. This would increase the SC's overall performance. The optimal charging strategy should also be investigated if this is possible.

A new model for the effects of the sun's position should also be considered. This would require a proper way to calculate the PV output based on its relative orientation based on the map values for incline, bearing, and time of day. This also requires more data to be retrieved, increasing the total time requirements for simulations.

The author also suggests attempting to implement optimization algorithms. This should be feasible by setting C-rate and ESS maximum capacity as constraints, and optimizing for maximum average cruising speeds. One could incorporate weather forecasts, ESS SoC, and current location as input variables, making real-time racing strategy possible.

7.6.5 Data Processing and Standardization

The data processing process could be shortened to ease simulations with larger data sets. The way the data is currently processed is satisfactory for the code, as is with tests run during the making of this thesis. However, it is likely insufficient for future testing and optimizing algorithms. It is therefore proposed to improve the way data is processed.

SI data for a TMY from PVGIS has some irregularities that could affect the simulations' reliability. The tests made were all done with TMY data. The author would therefore propose future simulations to use SI data for specific years. The author also proposes to standardize the SI for a given location if data is to be used in the same manner it is currently being used. This way, the data could be altered using the functions for sky coverage within `scpylib`, which again would be ideal for optimizing based on weather forecast. This would also aid future users of `scpylib` in creating a real-time race-strategizing tool.

The author also suggests investigating the use of other solar data retrieval software. PVGIS provides a free and accessible tool since a future SC racing team might benefit from more sources of information.

8 Conclusion

This thesis sought to establish a well-rounded foundational understanding of the aspects of energy management for an SC participating in the WSC. This includes:

- creating a solar profile for the route
- calculating the energy production of the PV-system
- calculate the energy consumption
- choose suitable components

The chosen approach to these tasks was to simulate the system using Python programming.

The library created to address these aspects, `scpylib`, works satisfyingly as a viability analysis tool. It manages to retrieve SI and weather data for locations specified in a map file, process it, and store it in readily available csv files. `scpylib` can also calculate the expected power output of the SC's PV generators based on its location. The SI data can also be modified based on sky coverage, but this feature was not utilized during simulations.

`scpylib` also has a module for the SC's ESS, based on a simple energy balance equation, with a non-optimized utilization strategy. The strategy ensures an even depletion rate of the ESS, which lowers the faster the SC travels.

The created library can then run simulations based on the PV output data and a mathematical load model of the SC's cruising speed energy demand. These simulations allow changes in the SC's parameters, such as its physical dimensions, PV specifications, and ESS C-rate. The model works satisfyingly and produces a realistic average cruising speed.

Through running simulations while manually adjusting the ESS's C-rate, a C-rate between 0.0525 and 0.05 was found to be the best for the given utilization strategy. It was also determined that a utilization strategy that would ensure an even depletion through the race, which results in a fully depleted ESS just before the finish line, would be ideal.

Some things were determined through an extensive literature review and investigating previous contestants. The ideal shape with the most recent rule set would be an MH. It has become the overall highest-performing SC shape through 2017 and 2019. And for the grid topology, basing the main bus on the ESS is best. The predictable voltage would provide a system that experiences much variance in its power generation with some much-needed stability. It would also minimize the number of transistors between the power source and load. The best ESS chemical makeup would be Li-ion. It is the most used chemistry and has the highest energy density of all the more available listed legal chemical makeups. Li-S-based ESSs promise a higher energy density but are yet to be commercially available for such an application. Future SC teams will be able to take advantage of Li-S batteries.

A future prospect for SC teams would be alternative MJ PV technologies to the now race illegal GaAs-based technologies. Perovskite-based PV's has seen promising developments in the past years, and new ways of manufacturing them might make them a good fit for constructing an SC. Silicon-based PV's are still a competitive option as proven by Tokai University, with their SC Tokai Challenger always finishing among the five fastest while always using monocrystalline silicon PV cells. The optimal wiring of the PV modules needs to be investigated in future work.

The power electronics, the converter, and the inverter are connected to both the PV cells and the ESS. The ideal DC-DC converter between the PVs and the ESS should be equipped with an MPP tracker, ensuring optimal power production at all times. Further, a three-level three-phase inverter is recommended. The added neutral point to its DC-link allows faster switching times and better frequency regulation. This would minimize its losses, resulting in a higher system efficiency at the cost of the inverter's total lifetime.

A detailed electrical analysis has yet to be made. This includes anything pertaining to specific voltages, current levels, heat development or switching losses. The analysis's most important aspect would be determining the efficiency drop in the PVs and the ESS due to heat development. This would be especially important regarding the ESS as it would pose a risk to the driver and the SC. This is proposed as future work.

The author would suggest scpylib to be improved in several aspects. The load model is inaccurate at low cruising speeds and does not account for the acceleration of the SC. Methods of solving this have been proposed and should be developed to allow for a more realistic simulation. The way SI data is procured is both positive and negative for its realistic values. The SI data values are measurements from previous years. This allows for realistic simulations but not more general optimization of the ESS utilization. The author would suggest either finding an optimal ESS utilization strategy using data from specific years or standardizing the data. By standardizing the data, future SC teams can perform simulations and strategize by manipulating the standardized data based on weather forecasts. Currently, scpylib's main simulation tool works only if the input data is prepared beforehand. This allows for rapid simulations but limits their accuracy. This is due to the data storage constraints a detailed simulation would face. Suggested further work would incorporate the data-retrieval function within the race simulation which would solve the storage problem at the cost of long simulation times.

This paper has compiled the necessary information and knowledge for anyone who wishes to participate in SC racing, emphasizing the WSC. Accompanying it is scpylib, an in-progress simulation tool that serves as a foundation to simulate an SC. It is flexible in its location application but less so regarding other inputs. It lacks some features and is not quite ready for usage in live race strategizing, but it possesses building blocks for those that may wish to do so.

Bibliography

- [1] “Illustration microgrid,” Dec. 2018. [Online]. Available: <https://www.iamrenew.com/wp-content/uploads/2019/05/Illustration-microgrid.jpg>
- [2] “Fig. 1 World solar radiation map.” [Online]. Available: https://www.researchgate.net/figure/World-solar-radiation-map_fig1_273695628
- [3] “Solar resource maps of Australia.” [Online]. Available: <https://solargis.com/maps-and-gis-data/download/australia>
- [4] D.-I. S. Völler, “Tet4175 design and operation of smart grid power systems,” 2019, last accessed 25. May 2023. [Online]. Available: <https://www.ntnu.no/studier/emner/TET4175/2013#tab=omEmnet>
- [5] G. M. Masters, *Renewable and efficient electric power systems*, 2nd ed., ser. Wiley - IEEE. New York: Wiley, 2013.
- [6] I. F. Corporation, “_USUtility-Scale Solar Photovoltaic Power Plants: A Project Developer’s Guide,” World Bank, Washington, DC, Working Paper, Jun. 2015, accepted: 2015-10-23T20:56:31Z. [Online]. Available: <https://openknowledge.worldbank.org/handle/10986/22797>
- [7] “Voltage at the maximum power point - Vmp | PVEducation.” [Online]. Available: <https://www.pveducation.org/pvcdrom/voltage-at-the-maximum-power-point-vmpp>
- [8] A. B. Sproul, Green, A. B. Sproul, and Green, “Effect of temperature.” [Online]. Available: <https://www.pveducation.org/pvcdrom/solar-cell-operation/effect-of-temperature>
- [9] R. Nilsen, “Tet4120 electric drives compendium,” 2018, last accessed 05 Desember 2022.
- [10] “Friction on an inclined plane.” [Online]. Available: http://www.engineerstudent.co.uk/friction_on_an_inclined_plane.php
- [11] Tony, “2019 World Solar Challenge: the route,” Jun. 2019. [Online]. Available: <https://scientificgems.wordpress.com/2019/06/15/2019-world-solar-challenge-the-route/>
- [12] E. Edge and E. E. LLC, “Viscosity of Air, Dynamic and Kinematic.” [Online]. Available: https://www.engineersedge.com/physics/viscosity_of_air_dynamic_and_kinematic_14483.htm
- [13] O. US EPA, “Greenhouse Gas Emissions from a Typical Passenger Vehicle,” Jan. 2016. [Online]. Available: <https://www.epa.gov/greenvehicles/greenhouse-gas-emissions-typical-passenger-vehicle>
- [14] N. Van Linh, T. Tran-Quoc, B. Seddik, and N. Be, “Charging strategies to minimize the peak load for an electric vehicle fleet,” Oct. 2014.
- [15] H. Ritchie, M. Roser, and P. Rosado, “Energy,” *Our World in Data*, Oct. 2022. [Online]. Available: <https://ourworldindata.org/electricity-mix>
- [16] “Peaking power - Energy Education.” [Online]. Available: https://energyeducation.ca/encyclopedia/Peaking_power
- [17] “THE 17 GOALS | Sustainable Development.” [Online]. Available: <https://sdgs.un.org/goals>
- [18] W. Bergesen, “Energy management of a solar car,” 2022, specialization project for this thesis.
- [19] B. W. S. C. Challenge, “2023 bridgestone world solar challenge website,” 2022, 21.11.2022. [Online]. Available: <https://www.worldsolarchallenge.org/>
- [20] “1987 World Solar Challenge – primotipo...” [Online]. Available: <https://primotipo.com/tag/1987-world-solar-challenge/>

-
- [21] P. M. P. LIBRARY, "Solar car entrant for World Solar Challenge '87 - Stock Image - T152/0250." [Online]. Available: <https://www.sciencephoto.com/media/341165/view/solar-car-entrant-for-world-solar-challenge-87>
- [22] "Solar car racing," Oct. 2022, page Version ID: 1113945217. [Online]. Available: https://en.wikipedia.org/w/index.php?title=Solar_car_racing&oldid=1113945217
- [23] B. W. S. C. Challenge, "2023 bridgestone world solar challenge regulations," 2023, 25.05.2023. [Online]. Available: https://worldsolarchallenge.org/files/2268_2023_bwsc_regulations_release-version_2_published_24_02_2023_final.pdf
- [24] "18650 Li-Ion Battery Guide | Battery Specialists | SIMPOWER," Aug. 2020. [Online]. Available: <https://www.simpower.co.nz/li-ion-18650-battery-guide/>
- [25] Chris-WSC, "Personal communication," Desember 2022.
- [26] M. Karlsen, "Energioptimalisering og mikrogrid, Granåsen skisenter," Master's thesis, NTNU, 2019, accepted: 2019-10-31T15:05:58Z ISSN: 2283-6624. [Online]. Available: <https://ntnuopen.ntnu.no/ntnu-xmlui/handle/11250/2625687>
- [27] Irena, "Innovation outlook: Renewable mini-grids," Abu Dhabi, 2016.
- [28] M. K. Jayaraj, A. Antony, and P. P. Subha, Eds., *Energy Harvesting and Storage: Fundamentals and Materials*, ser. Energy Systems in Electrical Engineering. Singapore: Springer Nature, 2022. [Online]. Available: <https://link.springer.com/10.1007/978-981-19-4526-7>
- [29] R. Garner, "Solar Irradiance," Apr. 2015. [Online]. Available: http://www.nasa.gov/mission_pages/sdo/science/solar-irradiance.html
- [30] C. S. a. S. T.-A.-C. Ltd, "Sunrise and Sunset Time." [Online]. Available: <https://www.sunrisesunsettime.org/>
- [31] "Solar Photovoltaic Cell Basics." [Online]. Available: <https://www.energy.gov/eere/solar/solar-photovoltaic-cell-basics>
- [32] S. Hårklau, "Elektrisk energiproduksjon fra et delvis skyggelagt solcelleanlegg i Trondheim."
- [33] "Perovskite Solar Cells." [Online]. Available: <https://www.energy.gov/eere/solar/perovskite-solar-cells>
- [34] M. Ren, X. Qian, Y. Chen, T. Wang, and Y. Zhao, "Potential lead toxicity and leakage issues on lead halide perovskite photovoltaics," *Journal of Hazardous Materials*, vol. 426, p. 127848, Mar. 2022. [Online]. Available: <https://www.sciencedirect.com/science/article/pii/S030438942102817X>
- [35] K. W. Torrance, H. E. Keenan, A. S. Hursthouse, and D. Stirling, "Measurement of arsenic and gallium content of gallium arsenide semiconductor waste streams by ICP-MS," *Journal of Environmental Science and Health, Part A*, vol. 45, no. 4, pp. 471–475, Feb. 2010, publisher: Taylor & Francis _eprint: <https://doi.org/10.1080/10934520903540133>. [Online]. Available: <https://doi.org/10.1080/10934520903540133>
- [36] F.-W. Liu, G. Biesold, M. Zhang, R. Lawless, J.-P. Correa-Baena, Y.-L. Chueh, and Z. Lin, "Recycling and recovery of perovskite solar cells," *Materials Today*, vol. 43, pp. 185–197, Mar. 2021. [Online]. Available: <https://www.sciencedirect.com/science/article/pii/S1369702120304533>
- [37] "Crystalline Silicon Photovoltaics Research." [Online]. Available: <https://www.energy.gov/eere/solar/crystalline-silicon-photovoltaics-research>
- [38] W. Qarony, M. I. Hossain, M. K. Hossain, M. J. Uddin, A. Haque, A. R. Saad, and Y. H. Tsang, "Efficient amorphous silicon solar cells: characterization, optimization, and optical loss analysis," *Results in Physics*, vol. 7, pp. 4287–4293, Jan. 2017. [Online]. Available: <https://www.sciencedirect.com/science/article/pii/S2211379717312123>
-

-
- [39] A. Romeo and E. Artigiani, “CdTe-Based Thin Film Solar Cells: Past, Present and Future,” *Energies*, vol. 14, no. 6, p. 1684, Jan. 2021, number: 6 Publisher: Multidisciplinary Digital Publishing Institute. [Online]. Available: <https://www.mdpi.com/1996-1073/14/6/1684>
- [40] T. Feurer, R. Carron, G. Torres Sevilla, F. Fu, S. Pisoni, Y. E. Romanyuk, S. Buecheler, and A. N. Tiwari, “Efficiency Improvement of Near-Stoichiometric CuInSe₂ Solar Cells for Application in Tandem Devices,” *Advanced Energy Materials*, vol. 9, no. 35, p. 1901428, 2019, eprint: <https://onlinelibrary.wiley.com/doi/pdf/10.1002/aenm.201901428>. [Online]. Available: <https://onlinelibrary.wiley.com/doi/abs/10.1002/aenm.201901428>
- [41] S. Ishizuka, “CuGaSe₂ Thin Film Solar Cells: Challenges for Developing Highly Efficient Wide-Gap Chalcopyrite Photovoltaics,” *physica status solidi (a)*, vol. 216, no. 15, p. 1800873, 2019, eprint: <https://onlinelibrary.wiley.com/doi/pdf/10.1002/pssa.201800873>. [Online]. Available: <https://onlinelibrary.wiley.com/doi/abs/10.1002/pssa.201800873>
- [42] M. M. Rahman, A. M. Asiri, T. A. Tabbakh, A. Khan, and Inamuddin, *Post-Transition Metals*. BoD – Books on Demand, Apr. 2021, google-Books-ID: hpQtEAAAQBAJ.
- [43] X. Wu, B. Li, Z. Zhu, C.-C. Chueh, and A. K.-Y. Jen, “Designs from single junctions, heterojunctions to multijunctions for high-performance perovskite solar cells,” *Chemical Society Reviews*, vol. 50, no. 23, pp. 13 090–13 128, 2021, publisher: Royal Society of Chemistry. [Online]. Available: <https://pubs.rsc.org/en/content/articlelanding/2021/cs/d1cs00841b>
- [44] A. Kowsar and S. Farhad, “High Efficiency Four Junction III-V Bismide Concentrator Solar Cell: Design, Theory, and Simulation,” *International Journal of Renewable Energy Research*, vol. 8, pp. 1762–1769, Sep. 2018.
- [45] “Solar cell materials : developing technologies,” 2014, iISBN: 1-118-69583-6 Place: Chichester, England Series: Wiley series in materials for electronic and optoelectronic applications.
- [46] S. Gharibzadeh, B. Abdollahi Nejang, M. Jakoby, T. Abzieher, D. Hauschild, S. Moghadamzadeh, J. A. Schwenzler, P. Brenner, R. Schmager, A. A. Haghghirad, L. Weinhardt, U. Lemmer, B. S. Richards, I. A. Howard, and U. W. Paetzold, “Record Open-Circuit Voltage Wide-Bandgap Perovskite Solar Cells Utilizing 2D/3D Perovskite Heterostructure,” *Advanced Energy Materials*, vol. 9, no. 21, p. 1803699, 2019, eprint: <https://onlinelibrary.wiley.com/doi/pdf/10.1002/aenm.201803699>. [Online]. Available: <https://onlinelibrary.wiley.com/doi/abs/10.1002/aenm.201803699>
- [47] M. P. U. Haris, S. Kazim, and S. Ahmad, “Low-Temperature-Processed Perovskite Solar Cells Fabricated from Presynthesized CsFAPbI₃ Powder,” *ACS Applied Energy Materials*, vol. 4, no. 3, pp. 2600–2606, Mar. 2021, publisher: American Chemical Society. [Online]. Available: <https://doi.org/10.1021/acsam.0c03160>
- [48] M. T. Hörantner, T. Leijtens, M. E. Ziffer, G. E. Eperon, M. G. Christoforo, M. D. McGehee, and H. J. Snaith, “The Potential of Multijunction Perovskite Solar Cells,” *ACS Energy Letters*, vol. 2, no. 10, pp. 2506–2513, Oct. 2017, publisher: American Chemical Society. [Online]. Available: <https://doi.org/10.1021/acsenergylett.7b00647>
- [49] “How to calculate output energy of PV solar systems?” [Online]. Available: <https://photovoltaic-software.com/principle-ressources/how-calculate-solar-energy-power-pv-systems>
- [50] J. M. Hansen and G. A. Xydis, “Rural electrification in Kenya: a useful case for remote areas in sub-Saharan Africa,” *Energy Efficiency*, vol. 13, no. 2, pp. 257–272, Feb. 2020. [Online]. Available: <https://doi.org/10.1007/s12053-018-9756-z>
- [51] “Electric vehicles | Battery | Capacity and Lifespan.” [Online]. Available: <https://www.eonenergy.com/electric-vehicle-charging/costs-and-benefits/battery-capacity-and-lifespan.html>
- [52] J. Van Mierlo, M. Bercibar, M. El Baghdadi, C. De Cauwer, M. Messagie, T. Coosemans, V. Jacobs, and O. Hegazy, “Beyond the State of the Art of Electric Vehicles:
-

A Fact-Based Paper of the Current and Prospective Electric Vehicle Technologies,” *World Electric Vehicle Journal*, vol. 12, no. 1, p. 20, Feb. 2021. [Online]. Available: <https://www.mdpi.com/2032-6653/12/1/20>

- [53] G. Zhou, H. Chen, and Y. Cui, “Formulating energy density for designing practical lithium–sulfur batteries,” *Nature Energy*, vol. 7, no. 4, pp. 312–319, Apr. 2022, number: 4 Publisher: Nature Publishing Group. [Online]. Available: <https://www.nature.com/articles/s41560-022-01001-0>
- [54] Y. Feng, G. Wang, J. Ju, Y. Zhao, W. Kang, N. Deng, and B. Cheng, “Towards high energy density Li–S batteries with high sulfur loading: From key issues to advanced strategies,” *Energy Storage Materials*, vol. 32, pp. 320–355, Nov. 2020. [Online]. Available: <https://www.sciencedirect.com/science/article/pii/S2405829720302658>
- [55] A. Zobia, Ed., *Energy Storage - Technologies and Applications*. InTech, Jan. 2013. [Online]. Available: <http://www.intechopen.com/books/energy-storage-technologies-and-applications>
- [56] D. R. Daan de Rooij, “Personal communication,” January 2023.
- [57] “Battery Roundtrip Efficiency.” [Online]. Available: https://www.homerenergy.com/products/pro/docs/latest/battery_roundtrip_efficiency.html
- [58] “Glendambo Weather | Elders Weather.” [Online]. Available: <https://www.eldersweather.com.au/climate-history/sa/glendambo>
- [59] J. Lindgren and P. D. Lund, “Effect of extreme temperatures on battery charging and performance of electric vehicles,” *Journal of Power Sources*, vol. 328, pp. 37–45, Oct. 2016. [Online]. Available: <https://www.sciencedirect.com/science/article/pii/S0378775316308941>
- [60] “Depth of Discharge - an overview | ScienceDirect Topics.” [Online]. Available: <https://www.sciencedirect.com/topics/engineering/depth-of-discharge>
- [61] X. Han, L. Lu, Y. Zheng, X. Feng, Z. Li, J. Li, and M. Ouyang, “A review on the key issues of the lithium ion battery degradation among the whole life cycle,” *eTransportation*, vol. 1, p. 100005, Aug. 2019. [Online]. Available: <https://www.sciencedirect.com/science/article/pii/S2590116819300050>
- [62] QuantumScape, “Charge Rates for Next-Generation Batteries,” Nov. 2021. [Online]. Available: <https://www.quantumscape.com/resources/blog/distinguishing-charge-rates-for-next-generation-batteries/>
- [63] G. Liu, M. Ouyang, L. Lu, J. Li, and X. Han, “Analysis of the heat generation of lithium-ion battery during charging and discharging considering different influencing factors,” *Journal of Thermal Analysis and Calorimetry*, vol. 116, no. 2, pp. 1001–1010, May 2014. [Online]. Available: <https://doi.org/10.1007/s10973-013-3599-9>
- [64] D.-I. P. K. Olsen, “Tele2007 kraftelektronikk og motordrifter,” 2020, last accessed 10. Desember 2022. [Online]. Available: <https://www.ntnu.no/studier/emner/TELE2007/2019/A#tab=omEmnet>
- [65] K. V. G. Raghavendra, K. Zeb, A. Muthusamy, T. N. V. Krishna, S. V. S. V. P. Kumar, D.-H. Kim, M.-S. Kim, H.-G. Cho, and H.-J. Kim, “A Comprehensive Review of DC–DC Converter Topologies and Modulation Strategies with Recent Advances in Solar Photovoltaic Systems,” *Electronics*, vol. 9, no. 1, p. 31, Jan. 2020, number: 1 Publisher: Multidisciplinary Digital Publishing Institute. [Online]. Available: <https://www.mdpi.com/2079-9292/9/1/31>
- [66] J. L. Santos, F. Antunes, A. Chehab, and C. Cruz, “A maximum power point tracker for PV systems using a high performance boost converter,” *Solar Energy*, vol. 80, no. 7, pp. 772–778, Jul. 2006. [Online]. Available: <https://www.sciencedirect.com/science/article/pii/S0038092X05002355>
- [67] R. Nilsen, “Personal communication,” Desember 2022.

-
- [68] Y. Yang, Q. He, C. Fu, S. Liao, and P. Tan, "Efficiency improvement of permanent magnet synchronous motor for electric vehicles," *Energy*, vol. 213, p. 118859, Dec. 2020. [Online]. Available: <https://www.sciencedirect.com/science/article/pii/S0360544220319666>
- [69] S. C. Frautschi, R. P. Olenick, T. M. Apostol, and D. L. Goodstein, *The Mechanical Universe: Mechanics and Heat, Advanced Edition*. Cambridge University Press, 2007, google-Books-ID: ZTnxQGJ1fHMC.
- [70] A. L. F. Hugh D. Young, Roger A. Freedman, *University Physics with Modern Physics, 14th edition*. Pearson, 2012.
- [71] S. T. Kaluva, A. Pathak, and A. Ongel, "Aerodynamic drag analysis of autonomous electric vehicle platoons," *Energies*, vol. 13, no. 15, p. 4028, Aug 2020. [Online]. Available: <http://dx.doi.org/10.3390/en13154028>
- [72] "Shape Effects on Drag." [Online]. Available: <https://www.grc.nasa.gov/www/k-12/rocket/shaped.html>
- [73] "How Tires Work," Sep. 2000. [Online]. Available: <https://auto.howstuffworks.com/tire.htm>
- [74] "About Anaconda." [Online]. Available: <https://www.anaconda.com/about-us>
- [75] "Home — Spyder IDE." [Online]. Available: <https://www.spyder-ide.org/>
- [76] C. W. H. William F. Holmgren and M. A. Mikofski, "Pvlib python: a python package for modeling solar energy systems." *Journal of Open Source Software*, 2018.
- [77] "Innoptus Solar Team | BluePoint." [Online]. Available: <https://www.solarteam.be/en/cars/bluepoint>
- [78] "Azur Space Building Latest Technology Based Solar Cell With 50+ Years of Experience." [Online]. Available: <https://www.satnow.com/news/details/657-azur-space-building-latest-technology-based-solar-cell-with-50-years-of-experience>
- [79] "Tokai challenger," Jan. 2023, page Version ID: 93609388. [Online]. Available: <https://ja.wikipedia.org/w/index.php?title=%E6%9D%B1%E6%B5%B7%E3%83%81%E3%83%A3%E3%83%AC%E3%83%B3%E3%82%B8%E3%83%A3%E3%83%BC&oldid=93609388>
- [80] Z. Robertson, "Under the hood of Michigan Solar Car Team's "Electrum"," Jul. 2019. [Online]. Available: <https://news.engin.umich.edu/2019/07/under-the-hood-of-michigan-solar-car-teams-electrum/>
- [81] "Nuna (wagen)," May 2023, page Version ID: 64341194. [Online]. Available: [https://nl.wikipedia.org/w/index.php?title=Nuna_\(wagen\)&oldid=64341194](https://nl.wikipedia.org/w/index.php?title=Nuna_(wagen)&oldid=64341194)
- [82] "Sun-Day Driver: We Test The University of Michigan's Solar Car!" Feb. 2018, section: Reviews. [Online]. Available: <https://www.caranddriver.com/reviews/a18368950/we-test-the-university-of-michigans-novum-solar-car-review/>
- [83] "Innoptus Solar Team | Punch 2." [Online]. Available: <https://www.solarteam.be/en/cars/punch-2>
- [84] "Punch Powertrain Solar Team introduces new Solar Car." [Online]. Available: <https://punchpowertrain.com/news/punch-powertrain-solar-team-introduces-new-solar-car/>
- [85] "RED One (2015) | Solar Team Twente." [Online]. Available: <https://www.solarteam.nl/project/red-one/>
- [86] "The RED Engine (2013) | Solar Team Twente." [Online]. Available: <https://www.solarteam.nl/project/the-red-engine/>
- [87] "Top Dutch Solar Racing." [Online]. Available: <http://www.solarracing.nl/cars>
- [88] "CARS [vehicle information]." [Online]. Available: <https://www.kogakuin.ac.jp/solar/cars.html>
-

-
- [89] “Covestro Sonnenwagen.” [Online]. Available: <https://www.sonnenwagen.org/covestro-sonnenwagen>
- [90] “Home - Antakari Solar Team.” [Online]. Available: <http://www.intikallpachile.cl/>
- [91] “Nagoya institute of technology solar car club |.” [Online]. Available: <https://solar-car.club.nitech.ac.jp/>
- [92] “About.” [Online]. Available: <https://www.eclipseets.ca/en/a-propos>
- [93] “Cars.” [Online]. Available: <https://www.jusolarteam.se/cars>
- [94] “Car Models.” [Online]. Available: <https://www.blueskysolar.org/solar-cars>
- [95] “RED Shift | Solar Team Twente.” [Online]. Available: <https://www.solarteam.nl/red-shift/>
- [96] “UNLIMITED 2.0.” [Online]. Available: <https://solarcar.scem.westernsydney.edu.au/unlimited-2>

Appendix

A Previous contestants

2019											
Placement	Team	Car name	Average speed [km/h]	Weight [kg]	Shape	PV-cell type [m ²]	PV-cell area [%]	PV-cell efficiency [kWh]	ESS capacity	ESS-chemistry	References
1	Agoria Solar Team	Bluepoint	86.6	141	AC	MJ-GaAs	2.64	30.0	5.3	Li-ion	[77]
2	Tokai University Solar Car Team	Tokai Challenger	86.1	142	MH	Si	4.00	23.7	5.0	Li-Polymer	[79]
3	University of Michigan Solar Car Team	Electrum	79.6		MH						[80]
4	Top Dutch Solar Racing	Green Lightning	78.4	150	MH	GaAs	3.56				[87]
5	Kogakuin University Solar Team	Kute Eagle	72.1	150	MH	MJ-GaAs					[88]
6	Team Sonnenwagen Aachen e.V.	Covestro Sonnenwagen	71.8	164	MH	MJ-GaAs	2.64	34.0			[89]
7	Antakari Solar Team	INTIKALLPA V	66.9	186	MH	Si	4.00	27	5.0	Li-Polymer	[90]
8	Nagoya Institute of Technology Solar Racing	Horizon Ace	66.5	160	MH	Si	4.00	25.0			[91]
9	Eclipse	Eclipse X	65.1	190	AC	Si	4.00	24.3	5.0	Li-ion	[92]
10	JU Solar Team	Axelent	64.6	200	AC	Si	4.00	25.1	5.3	Li-ion	[93]
11	Blue Sky Solar Racing	Viridian	63.2		MH						[94]

2017											
Placement	Team	Car name	Average speed [km/h]	Weight [kg]	Shape	PV-cell type	PV-cell area [m ²]	PV-cell efficiency [%]	ESS capacity [kWh]	ESS-chemistry	References
1	Nuon Solar Team	Nuna9	81.2	141	AC	MJ-GaAs	2.64				[81]
2	University of Michigan Solar Car Team	Novum	77.1	191	MH	MJ-GaAs			5.0	Li-ion	[82]
3	Punch Powertrain Solar Car Team	Punch Two	76.2	145	AC	MJ-GaAs	2.64		5.0		[83, 84]
4	Tokai University Solar Car Team	Tokai Challenger	75.9	170	MH	Si	4.00	24.1	5.0	Li-ion	[79]
5	Solar Team Twente	RED Shift	75.6	144	AC	Si	4.00	24.0	5.0	Li-ion	[95]
6	Western Sydney Solar Team	Unlimited 2.0	65.5	158	AC	Si	4.00			Li-ion	[96]
7	Kogakuin University Solar Team	Wing	63.8	170	OS			24.8			[88]
8	JU Solar Team	Solveig	59.7	186	AC	Si	4.00	24.3	5.3	Li-ion	[93]
9	Stanford Solar Car Project	Sundae	59.5		AC						
10	Antakari Solar Team	INTIKALLPA IV	59.1	167	AC	Si	4.00	24.0	5.0	Li-Polymer	[90]
11	Blue Sky Solar Racing	Polaris	58.6	300	AC	Si		24.3			[94]
12	Nagoya Institute of Technology Solar Racing	Horizon 17	58.0	190	AC	Si	4.00	24.3			[91]

Table 13: SC-data for all the finishing contestants for the WSC 2019 and 2017. It should be noted that this list only includes finishing teams. The total number of entries into the challenger class would be approximately 30 each year.

B Plots

B.1 Hourly Solar Irradiation Data

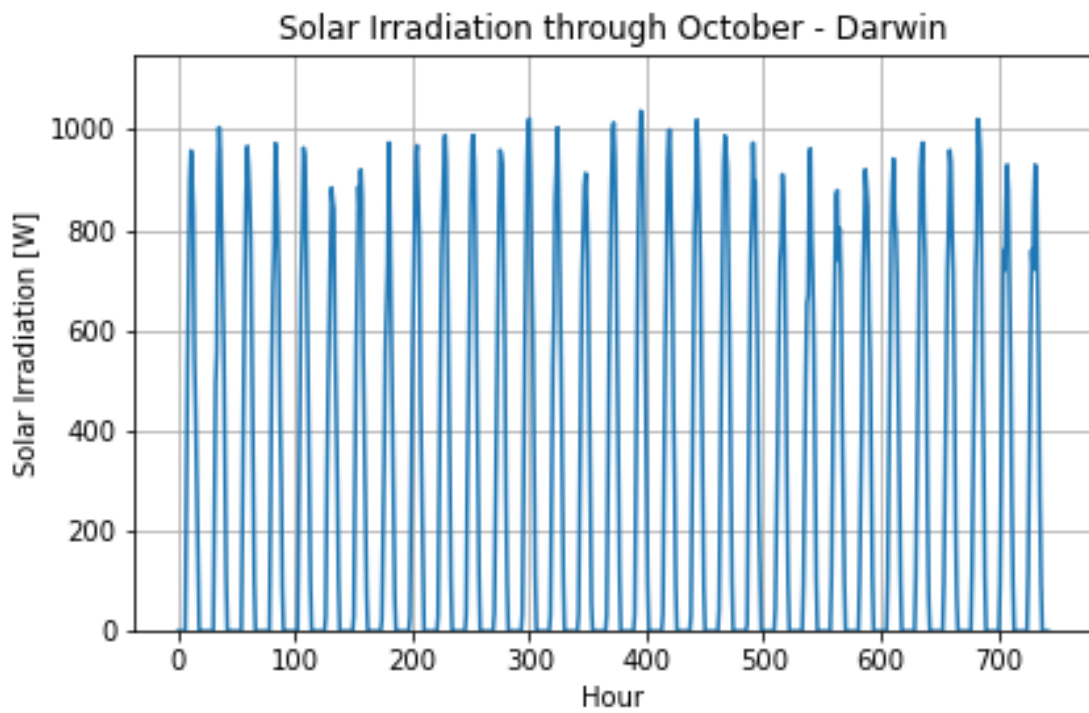


Figure 52: Hourly SI-data for Darwin during October. The data is from a TMY.

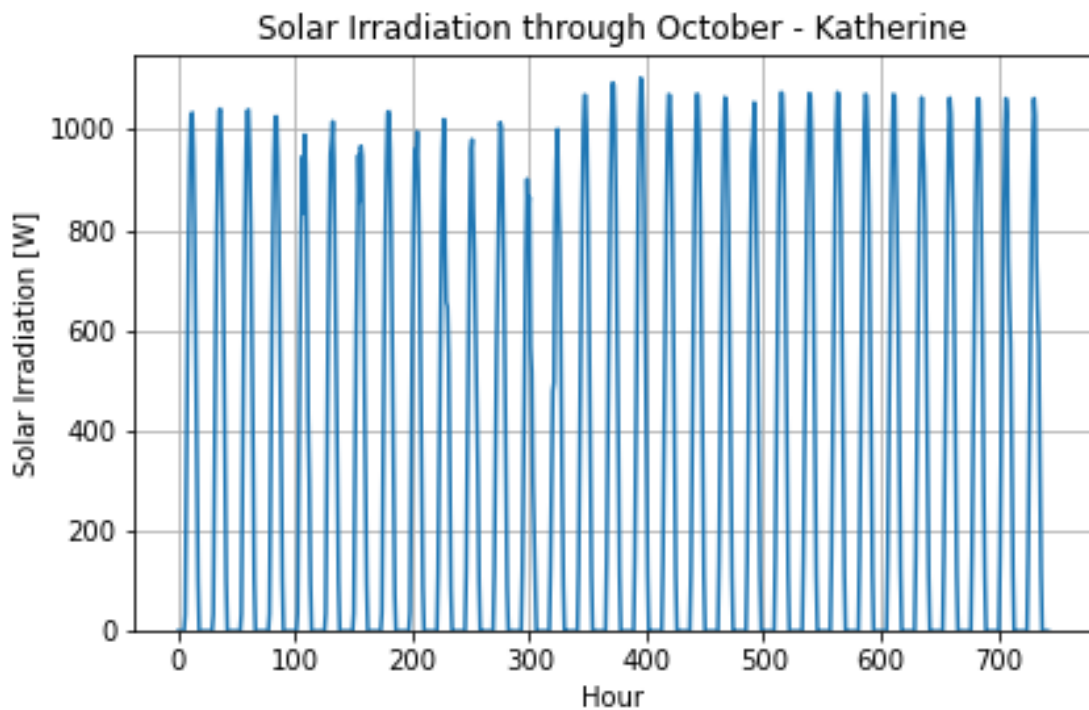


Figure 53: Hourly SI-data for Katherine during October. The data is from a TMY.

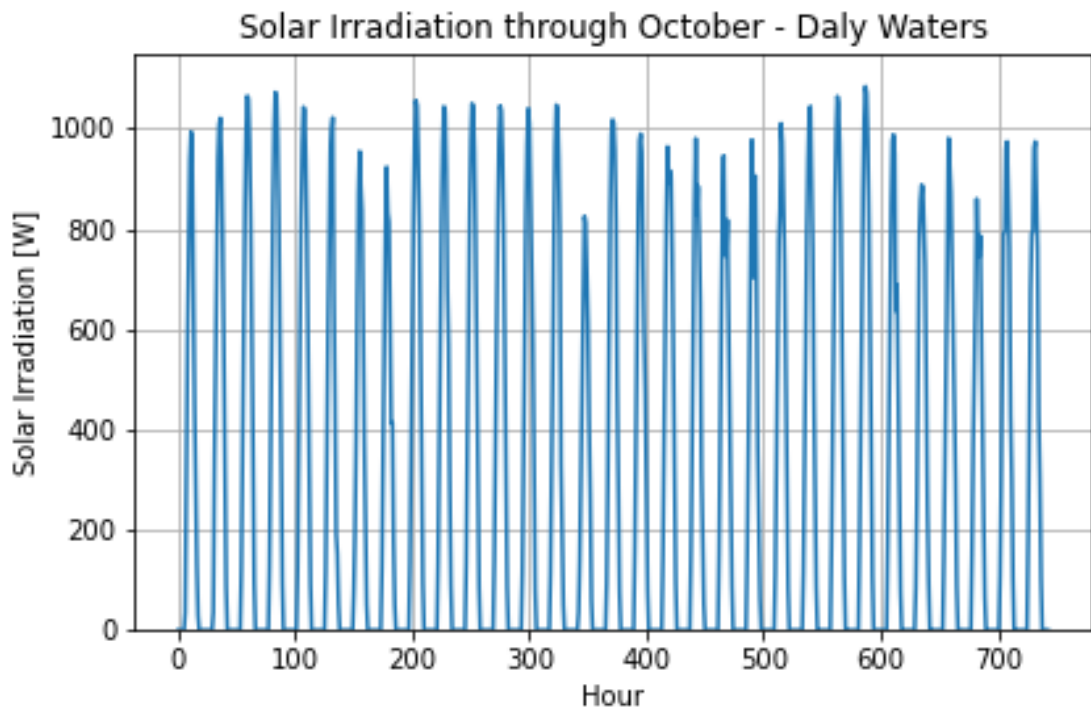


Figure 54: Hourly SI-data for Daly Waters during October. The data is from a TMY.

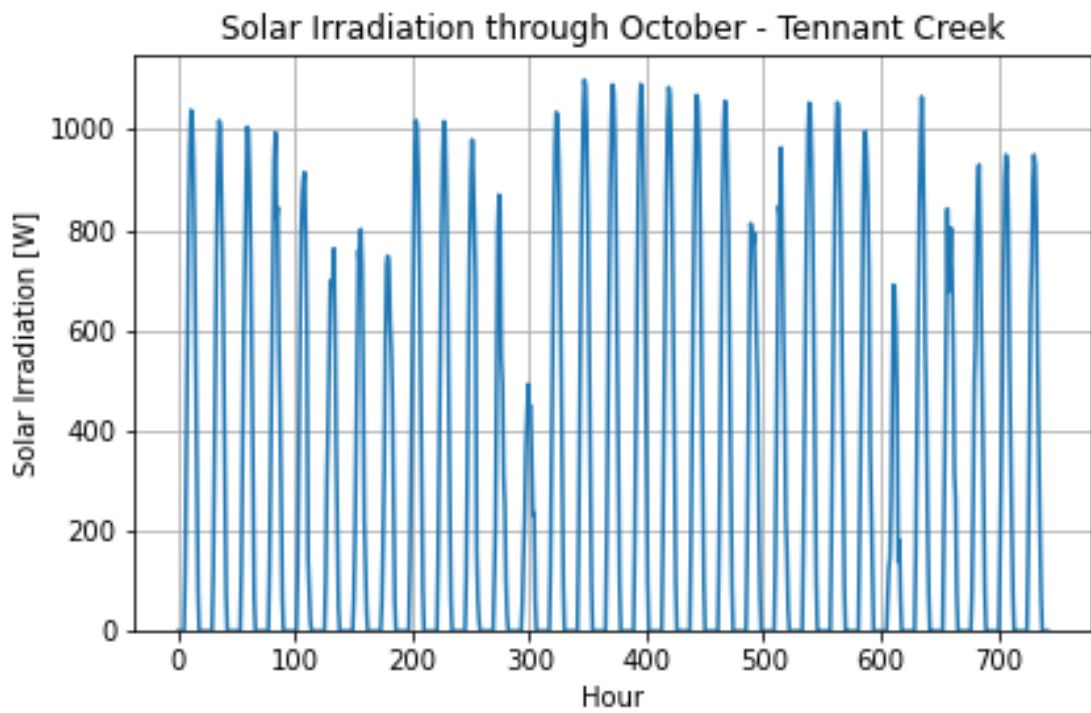


Figure 55: Hourly SI-data for Tennant Creek during October. The data is from a TMY.

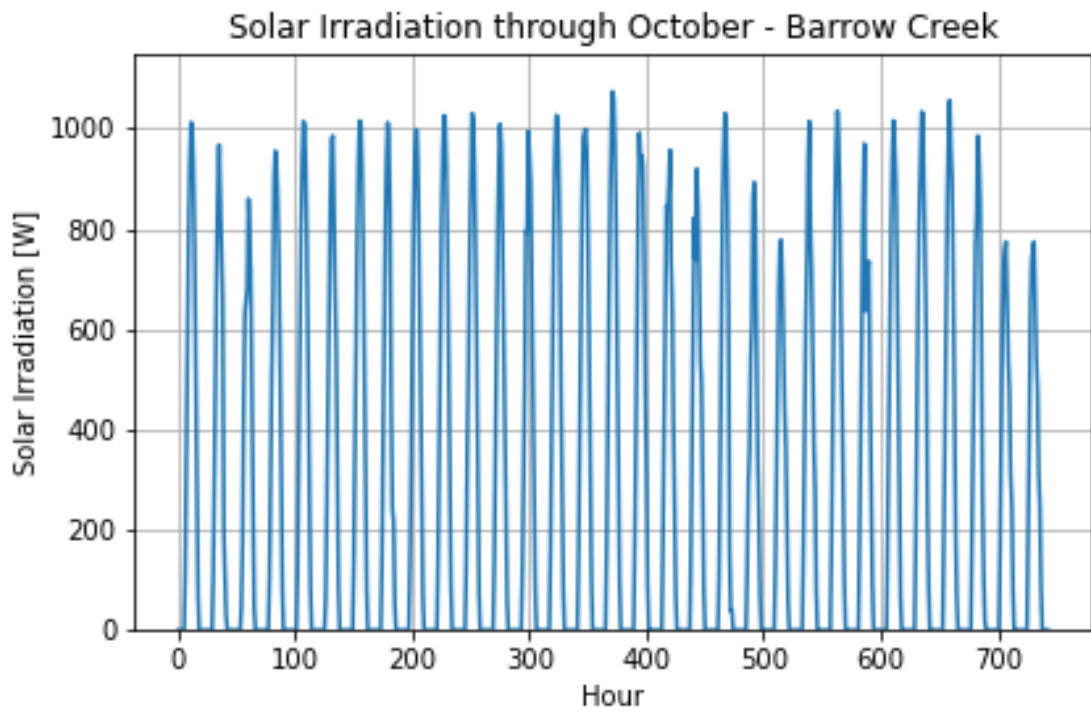


Figure 56: Hourly SI-data for Barrow Creek during October. The data is from a TMY.

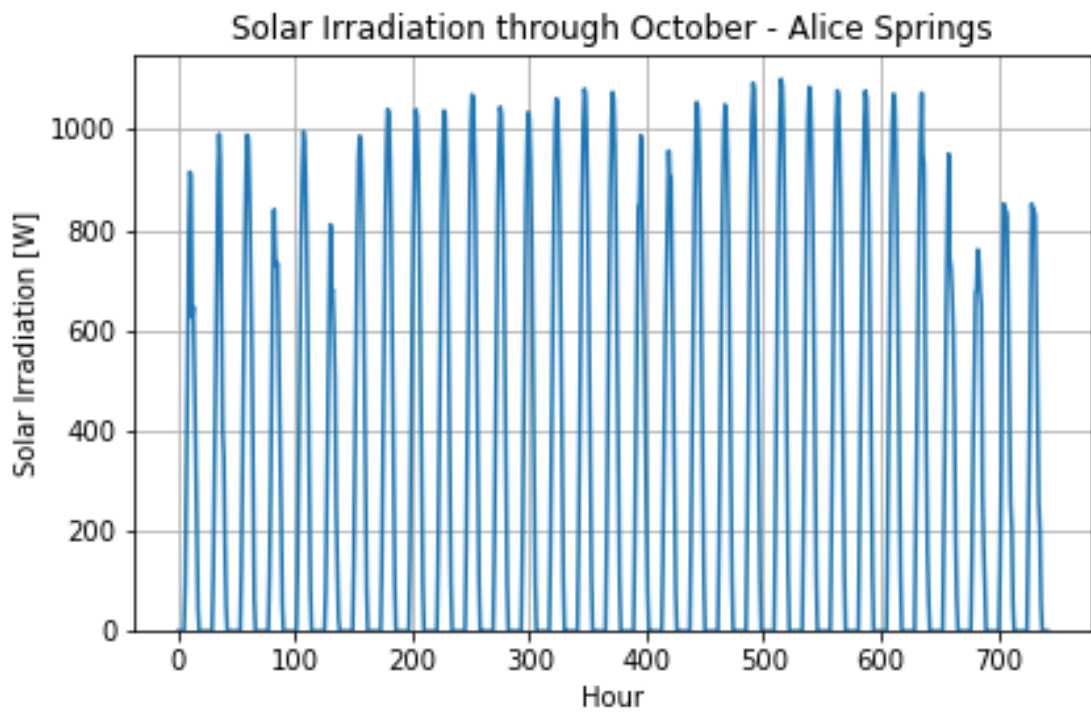


Figure 57: Hourly SI-data for Alice Springs during October. The data is from a TMY.

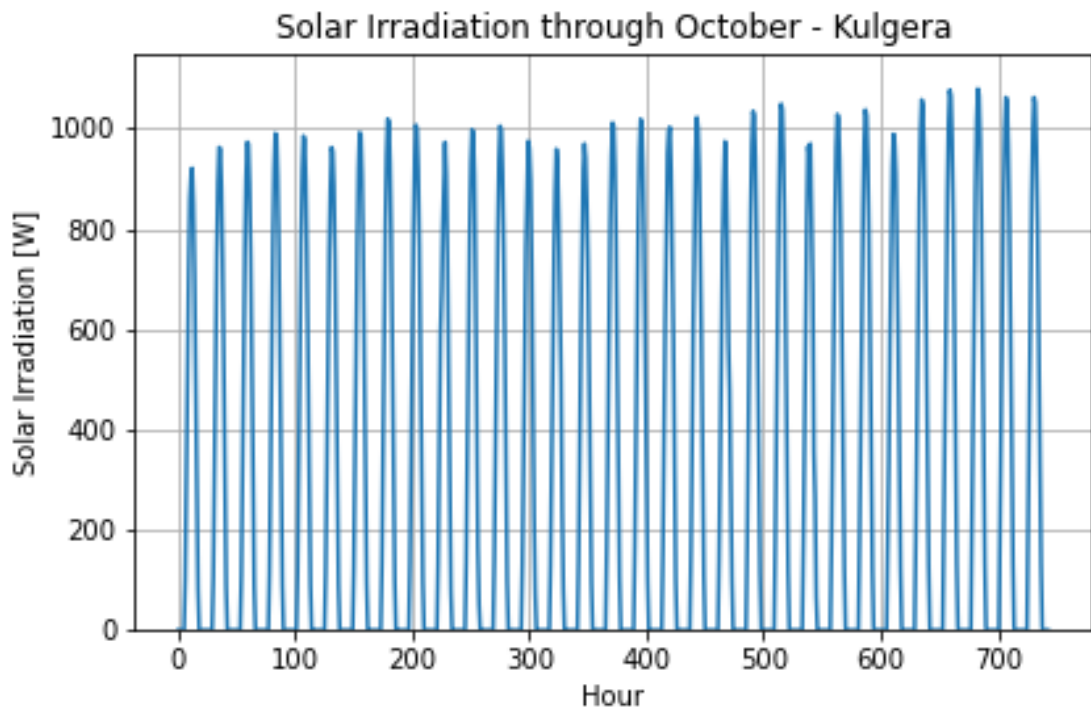


Figure 58: Hourly SI-data for Kulgera during October. The data is from a TMY.

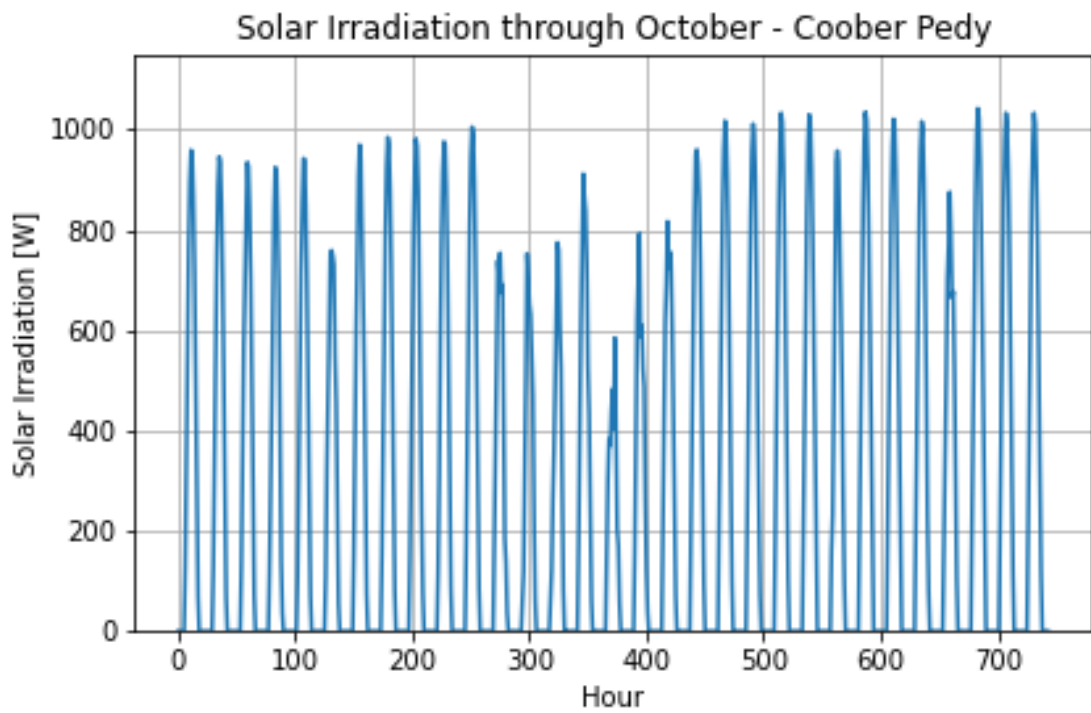


Figure 59: Hourly SI-data for Coober Pedy during October. The data is from a TMY.

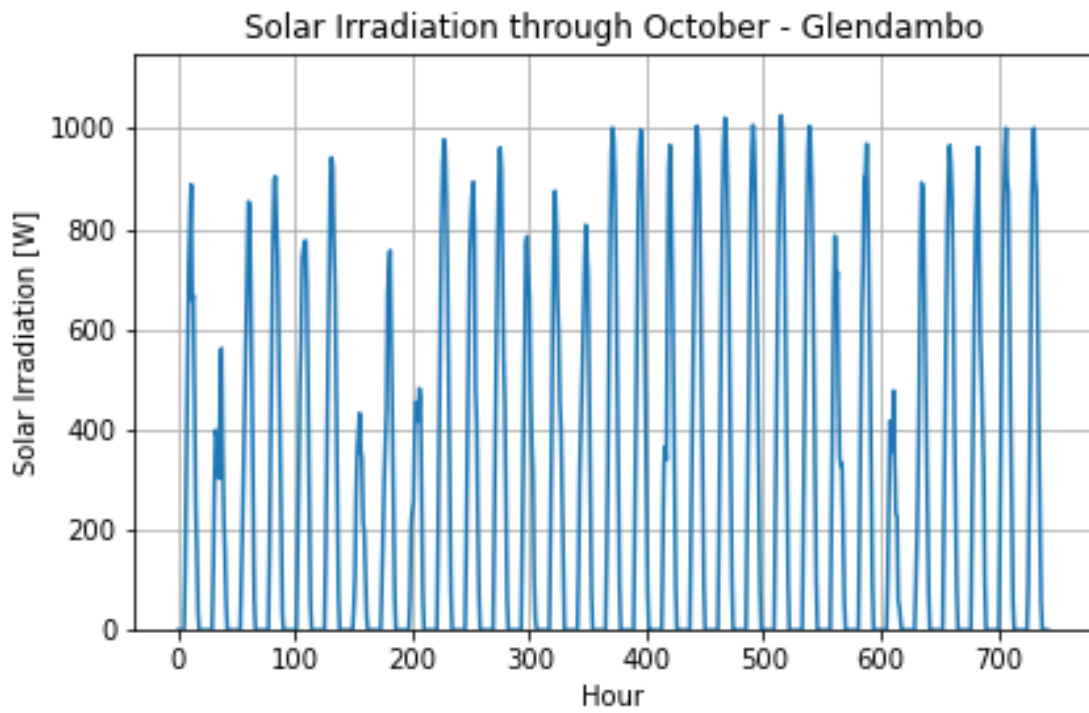


Figure 60: Hourly SI-data for Glendambo during October. The data is from a TMY.

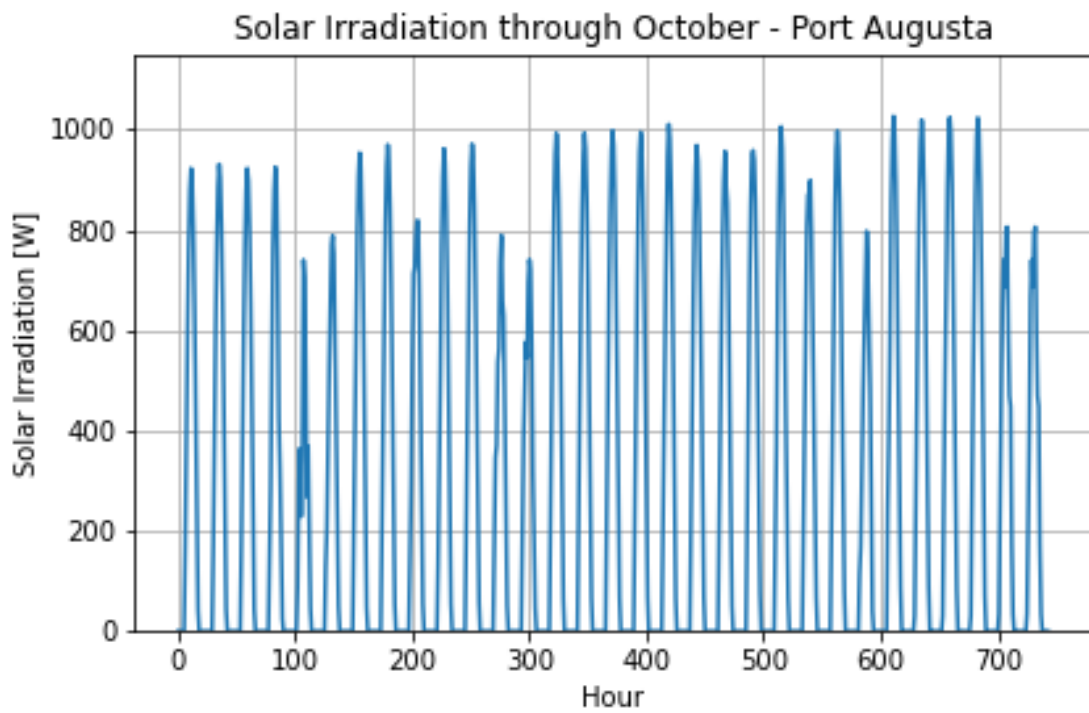


Figure 61: Hourly SI-data for Port Augusta during October. The data is from a TMY.

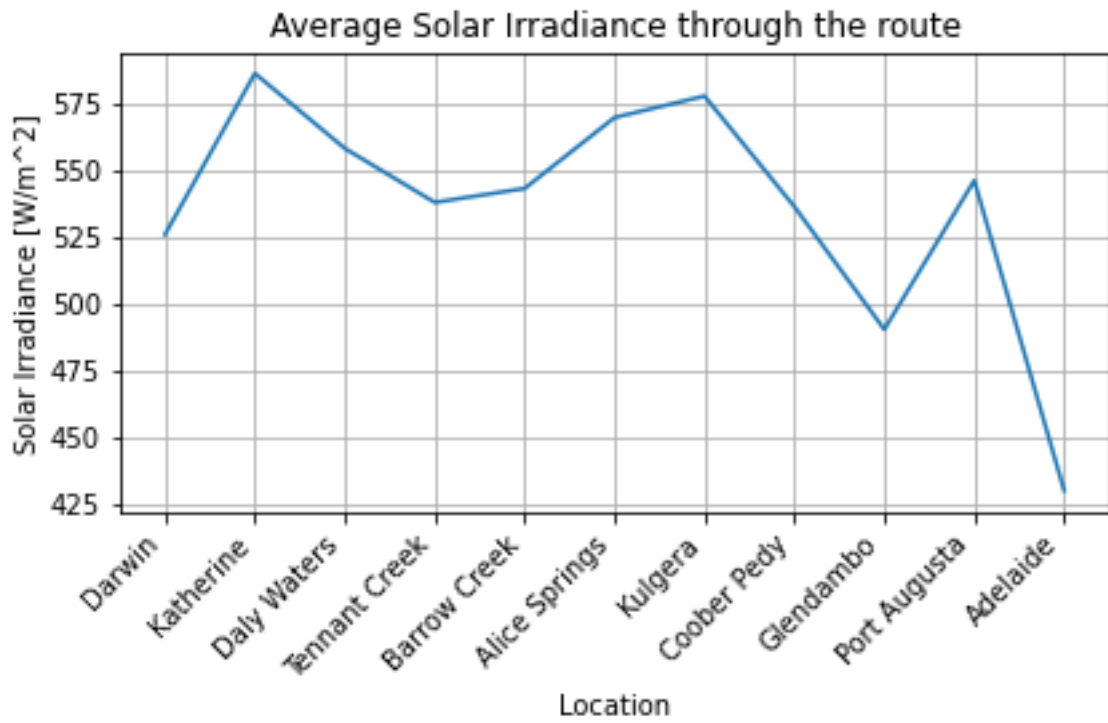


Figure 63: Average SI per day in October throughout the WSC route. The data is from the TMY PVGIS.

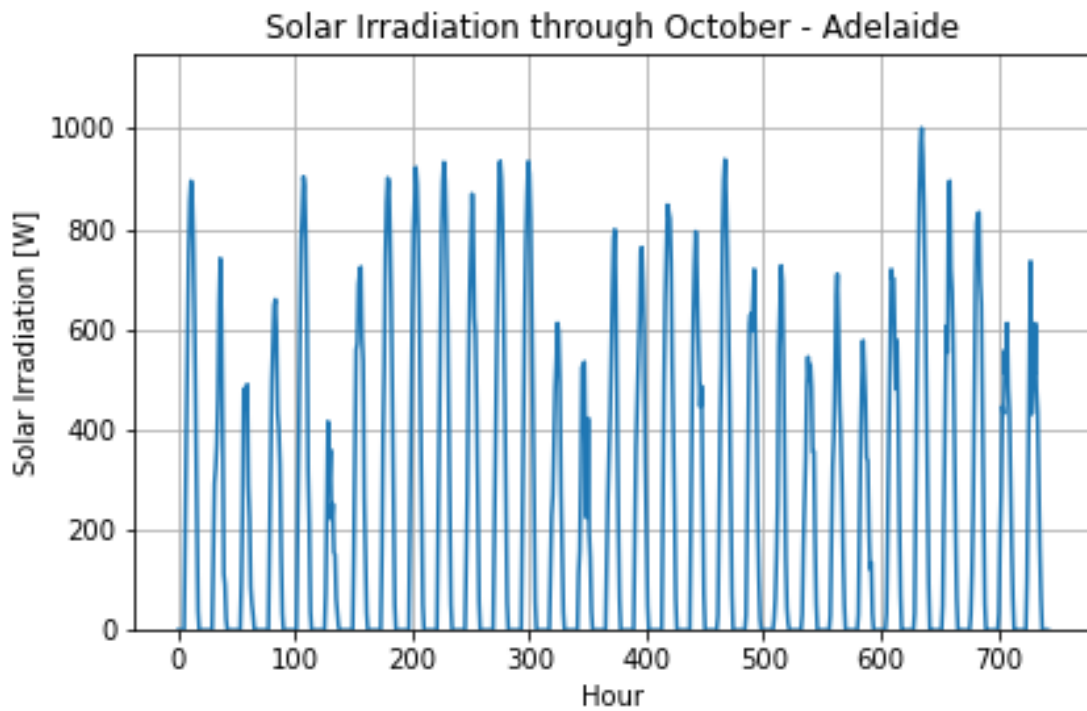


Figure 62: Hourly SI-data for Adelaide during October. The data is from a TMY.

B.2 Average SI value throughout the route

B.3 Hourly Temperature

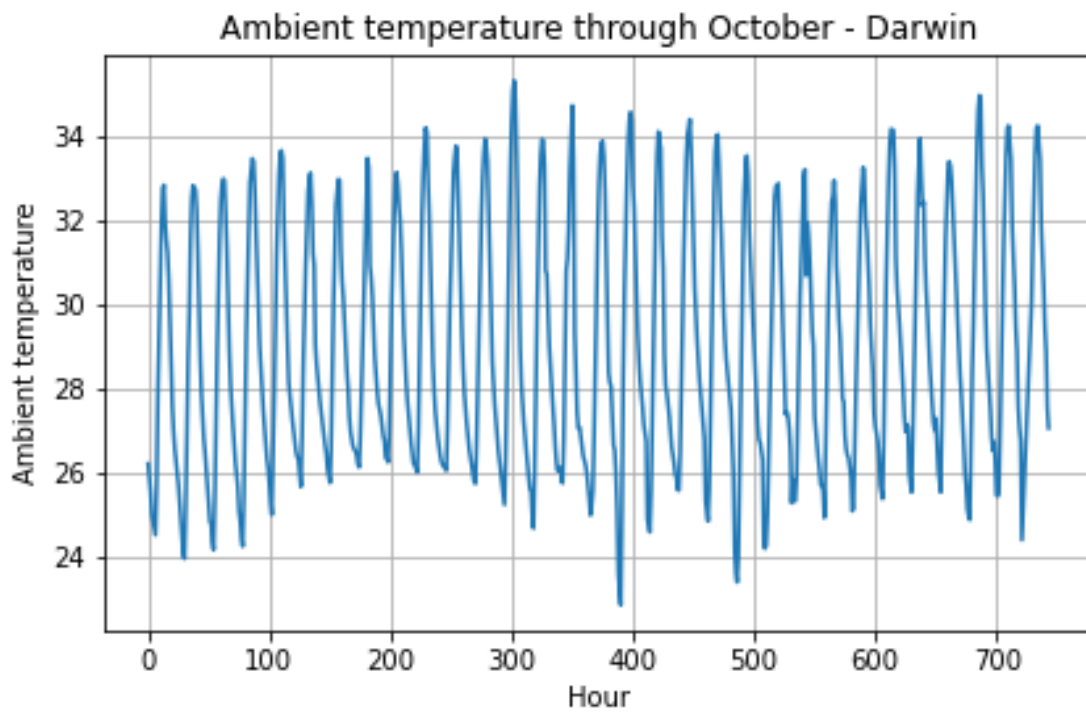


Figure 64: Hourly ambient air temperature for Darwin during October. The data is from a TMY.

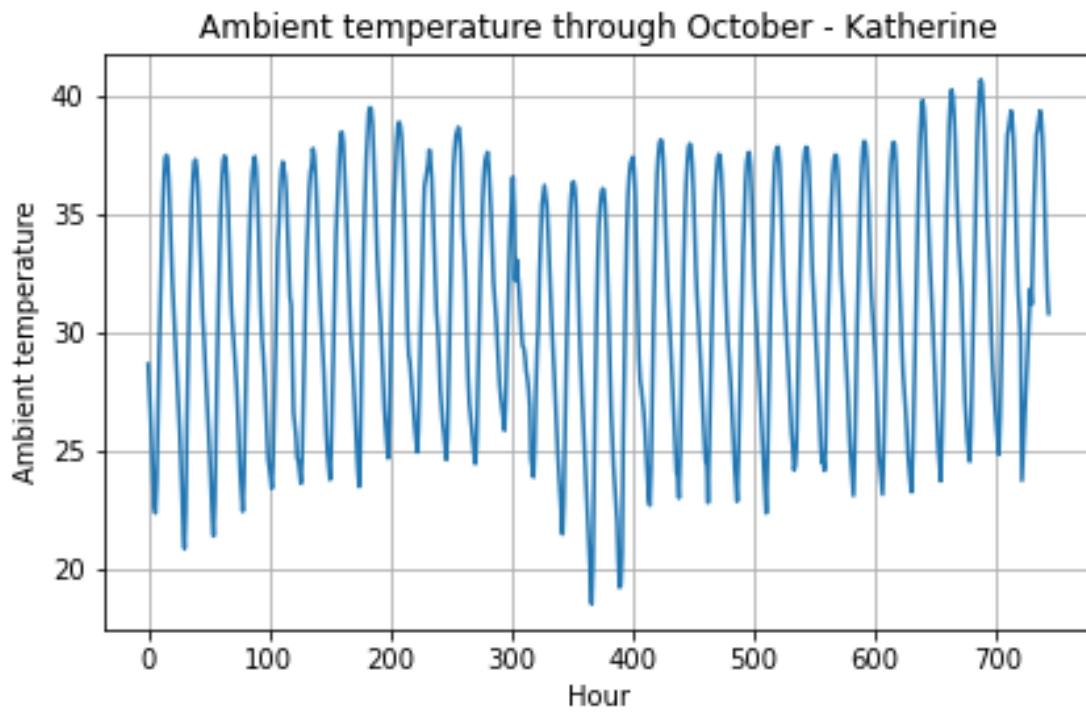


Figure 65: Hourly ambient air temperature for Katherine during October. The data is from a TMY.

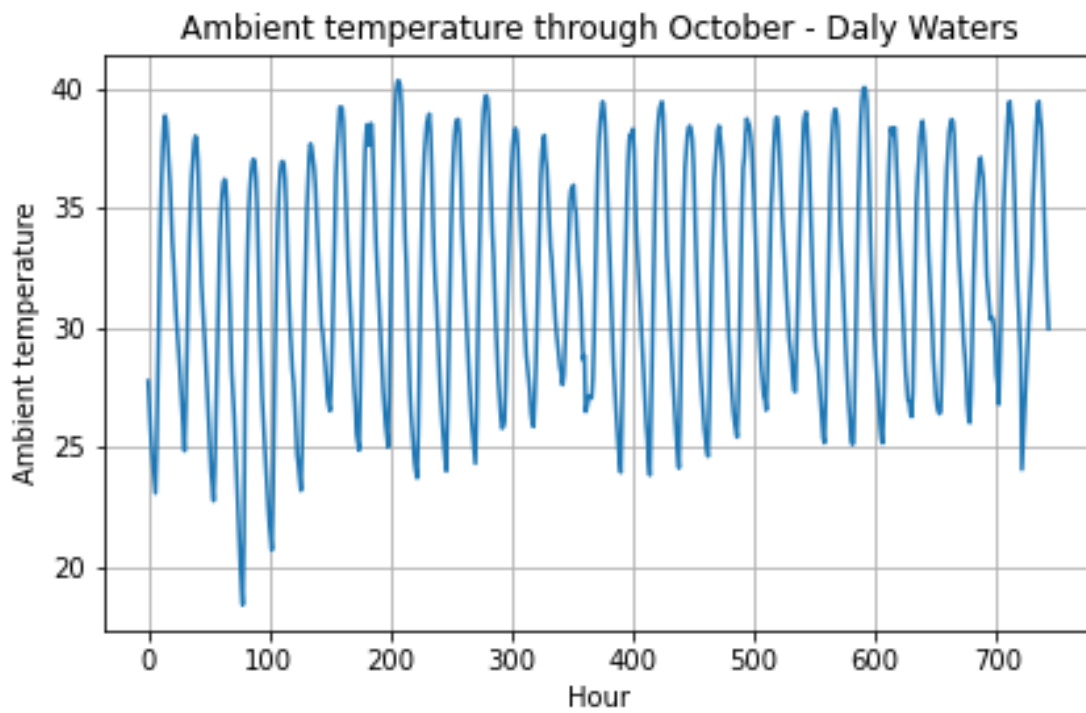


Figure 66: Hourly ambient air temperature for Daly Waters during October. The data is from a TMY.

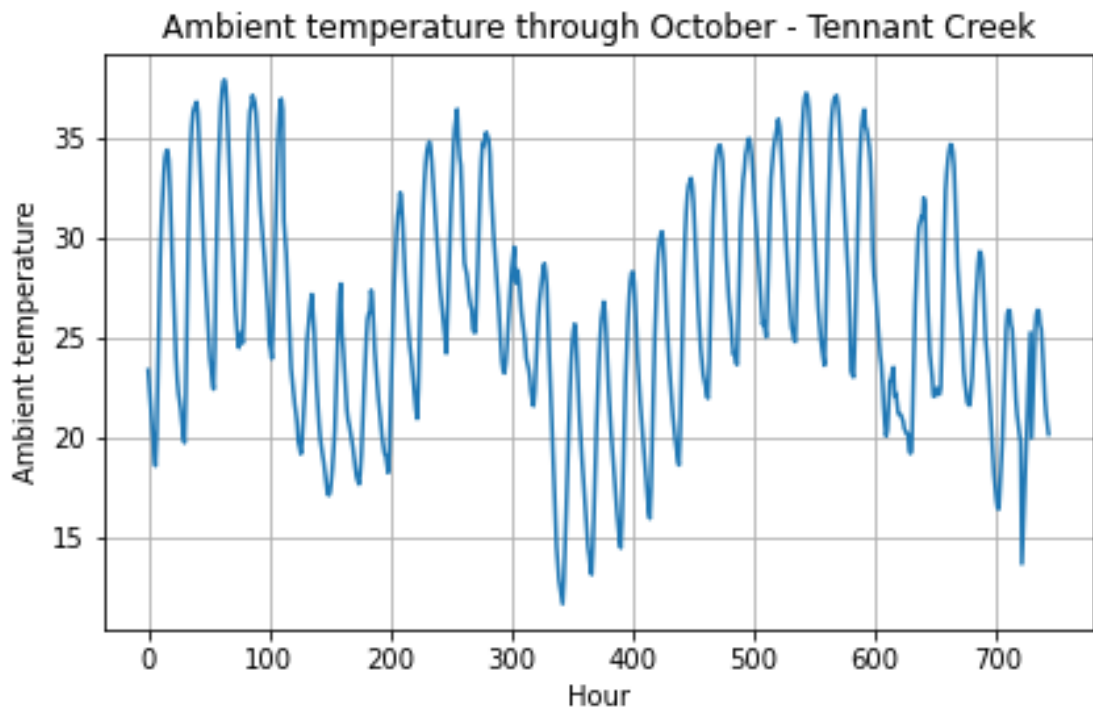


Figure 67: Hourly ambient air temperature for Tennant Creek during October. The data is from a TMY.

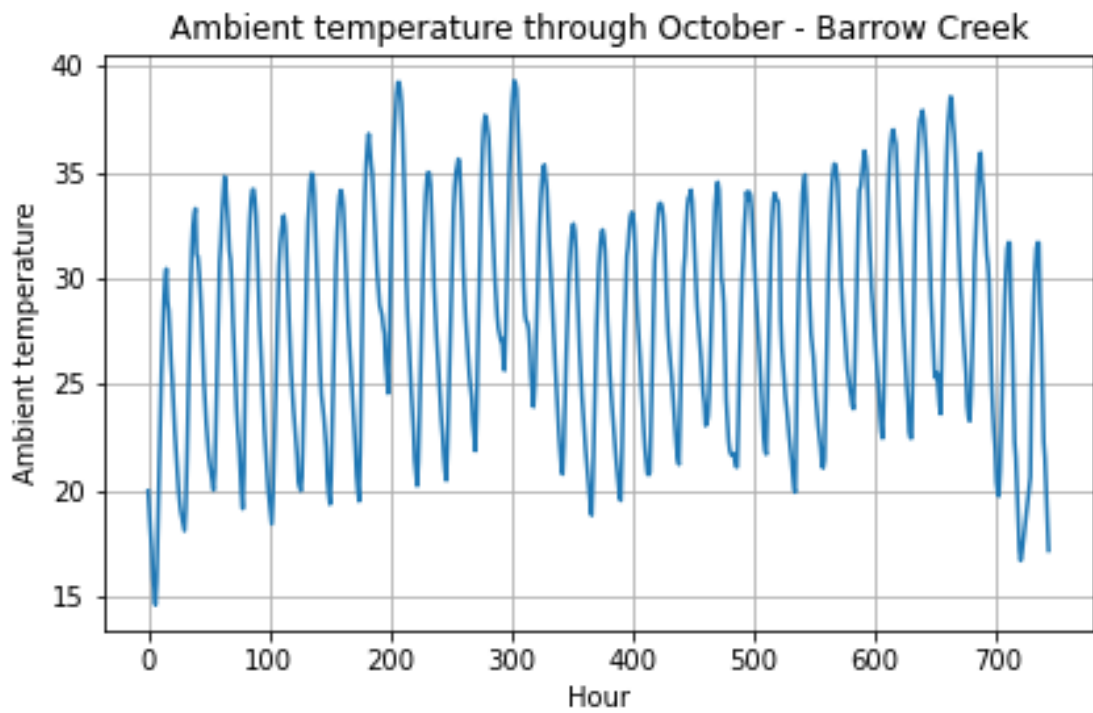


Figure 68: Hourly ambient air temperature for Barrow Creek during October. The data is from a TMY.

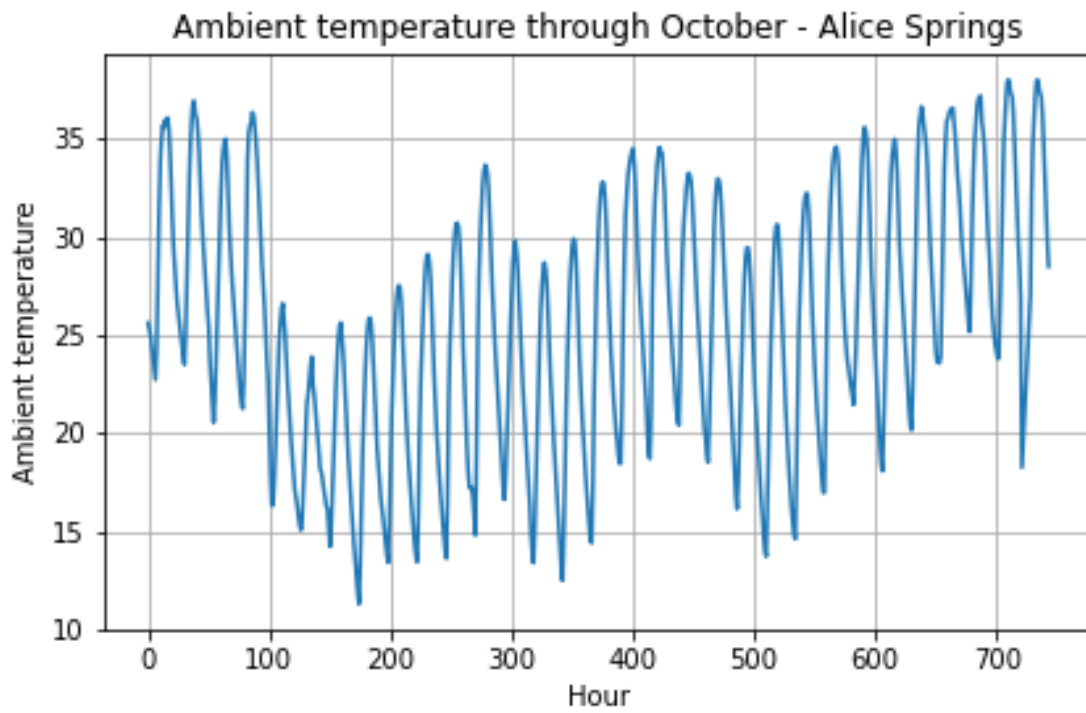


Figure 69: Hourly ambient air temperature for Alice Springs during October. The data is from a TMY.

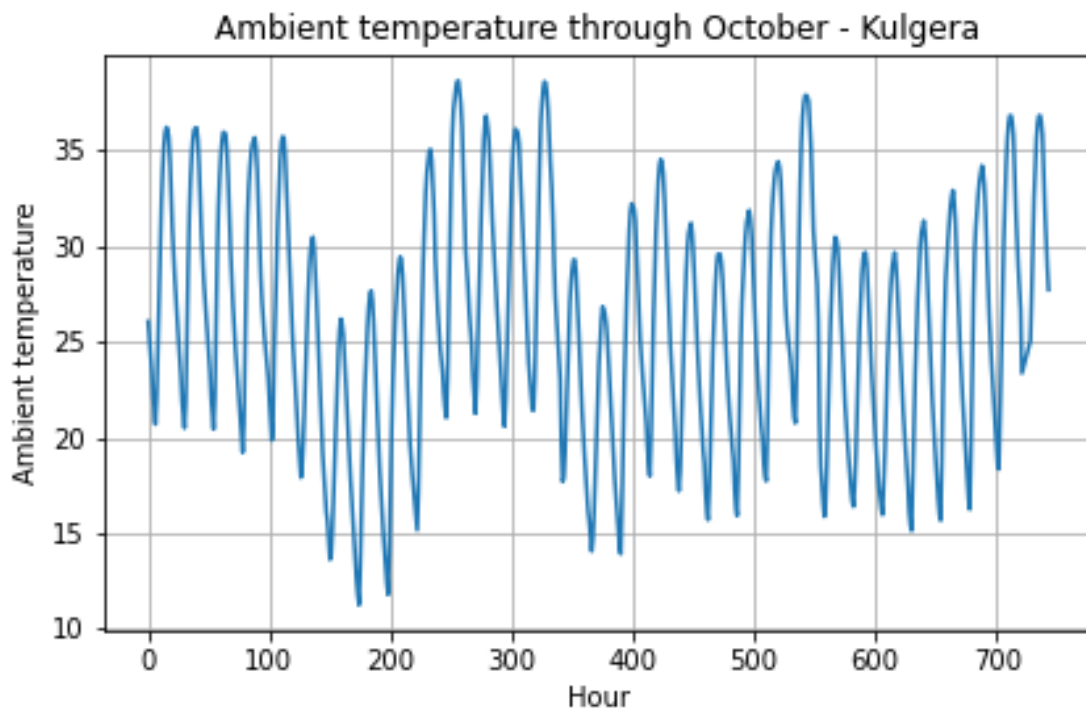


Figure 70: Hourly ambient air temperature for Kulgera during October. The data is from a TMY.

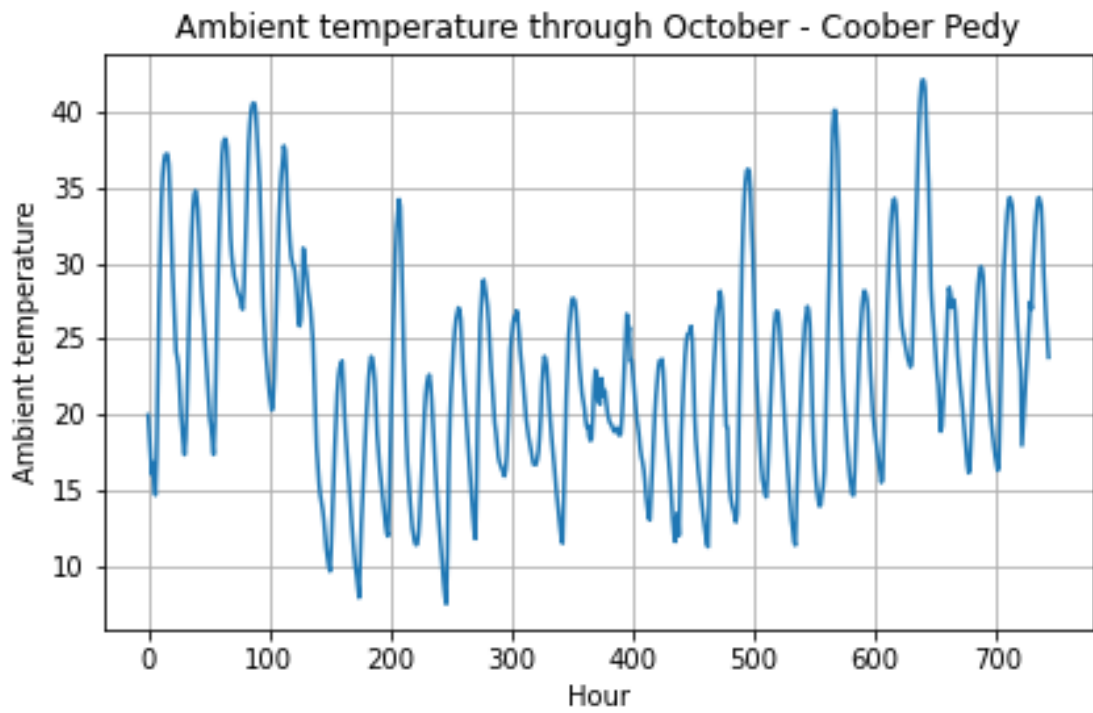


Figure 71: Hourly ambient air temperature for Coober Pedy during October. The data is from a TMY.

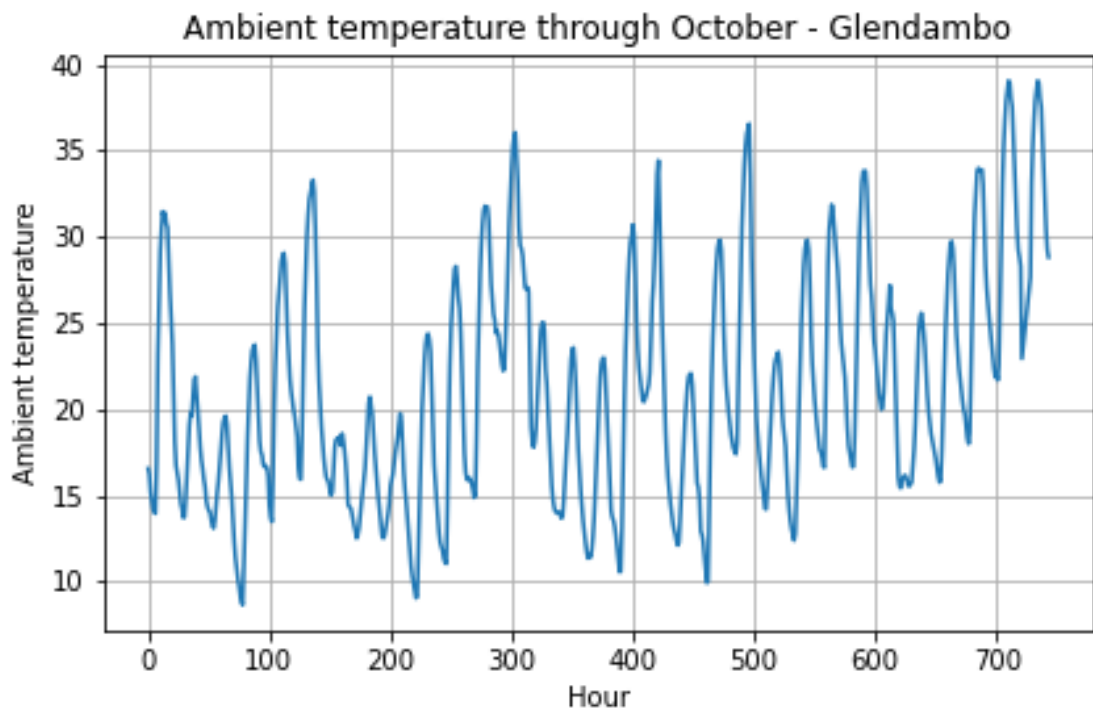


Figure 72: Hourly ambient air temperature for Glendambo during October. The data is from a TMY.

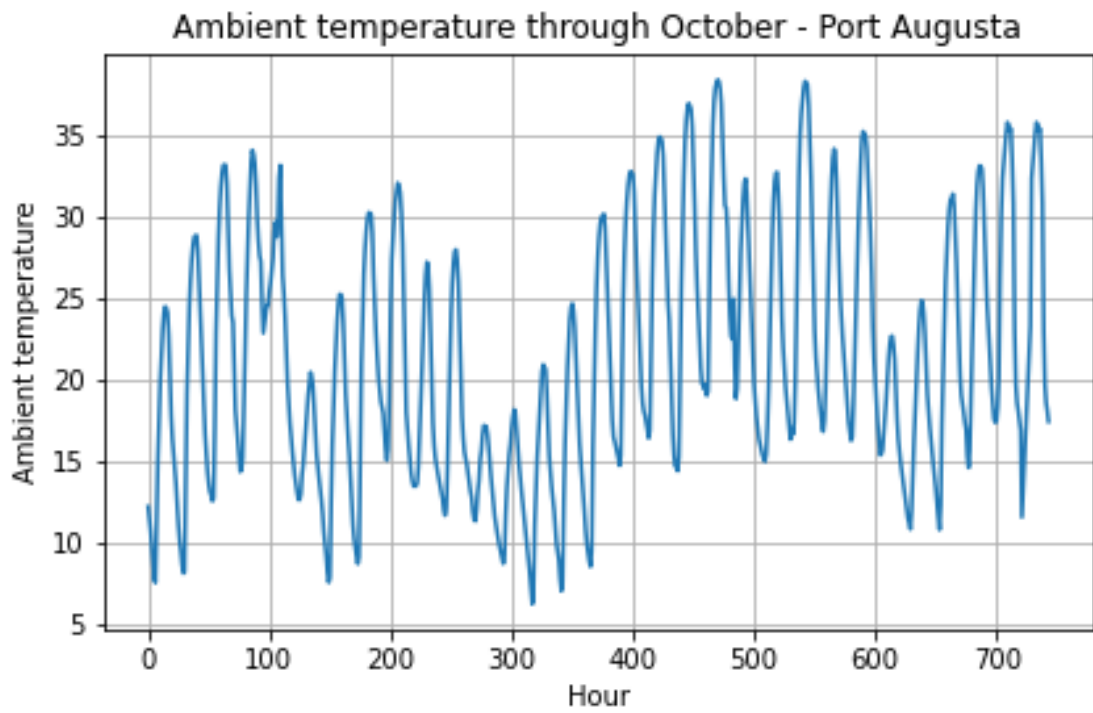


Figure 73: Hourly ambient air temperature for Port Augusta during October. The data is from a TMY.

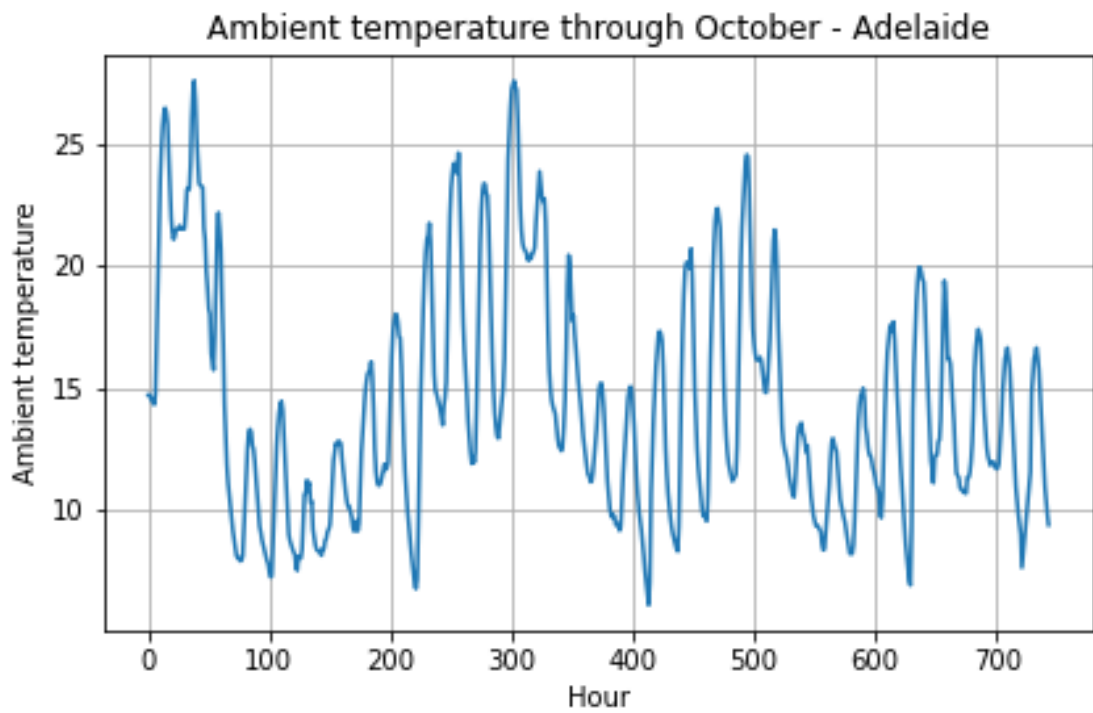


Figure 74: Hourly ambient air temperature for Adelaide during October. The data is from a TMY.

B.4 Average temperature

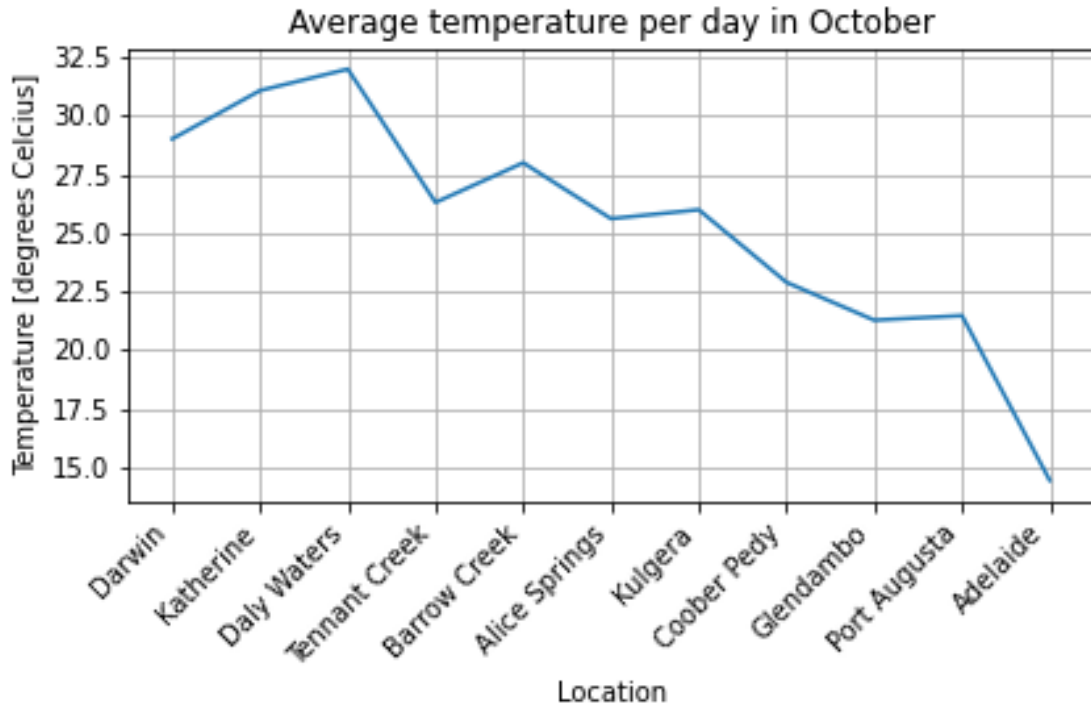


Figure 75: The average temperature for the entire route for the WSC during a TMY.

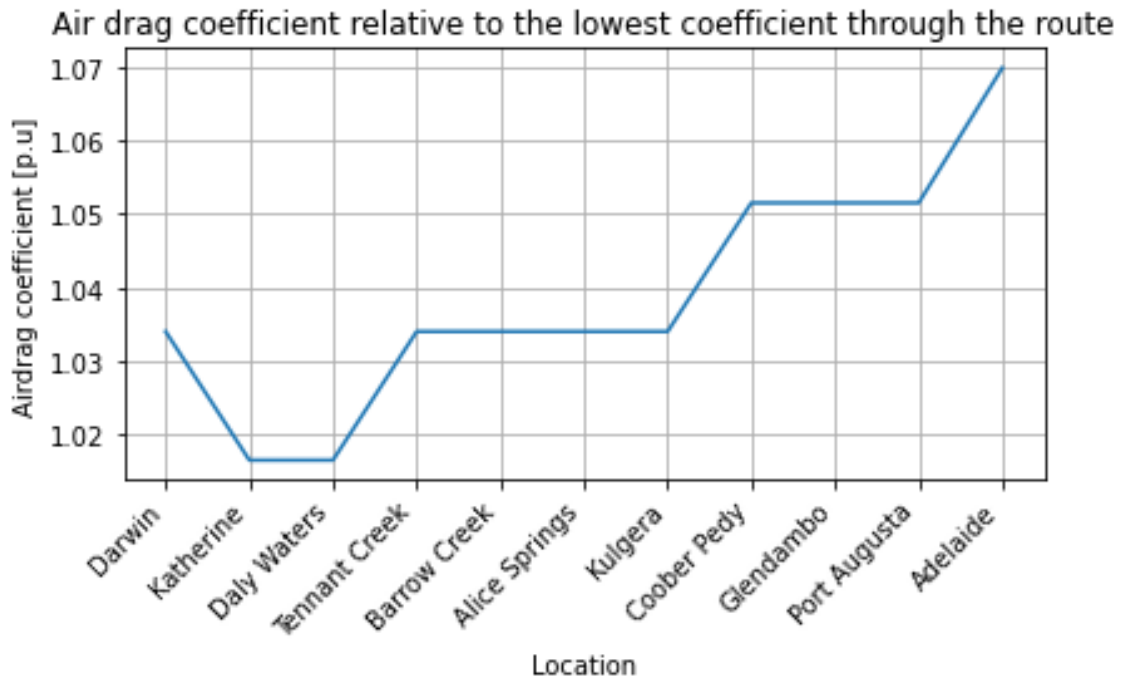


Figure 76: Relative air drag coefficient through the route. 1.0 being the air-drag coefficient for 30°Celsius.

B.5 PV output

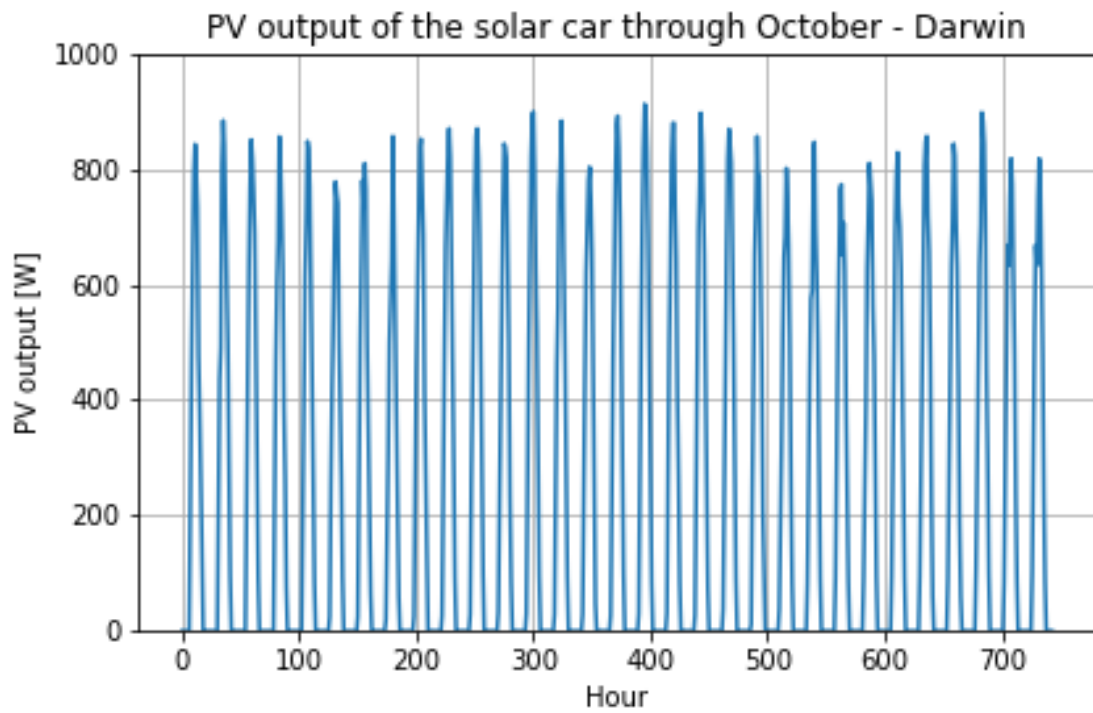


Figure 77: PV output of the SC throughout October in Darwin during a TMY.

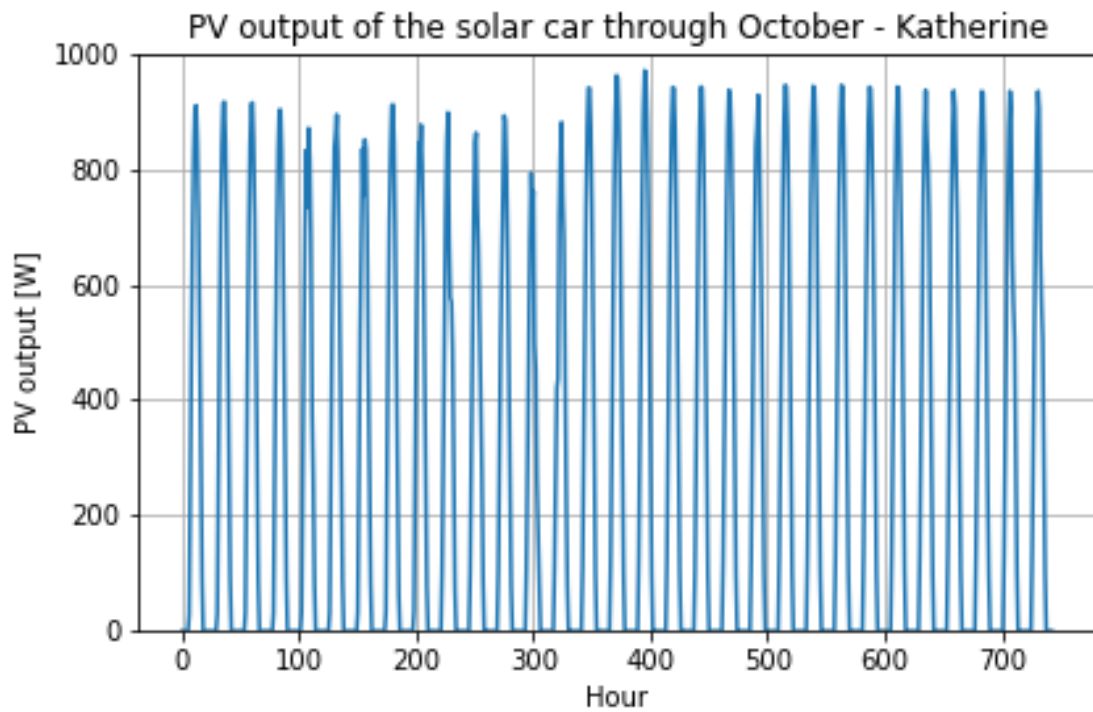


Figure 78: PV output of the SC throughout October in Katherine during a TMY.

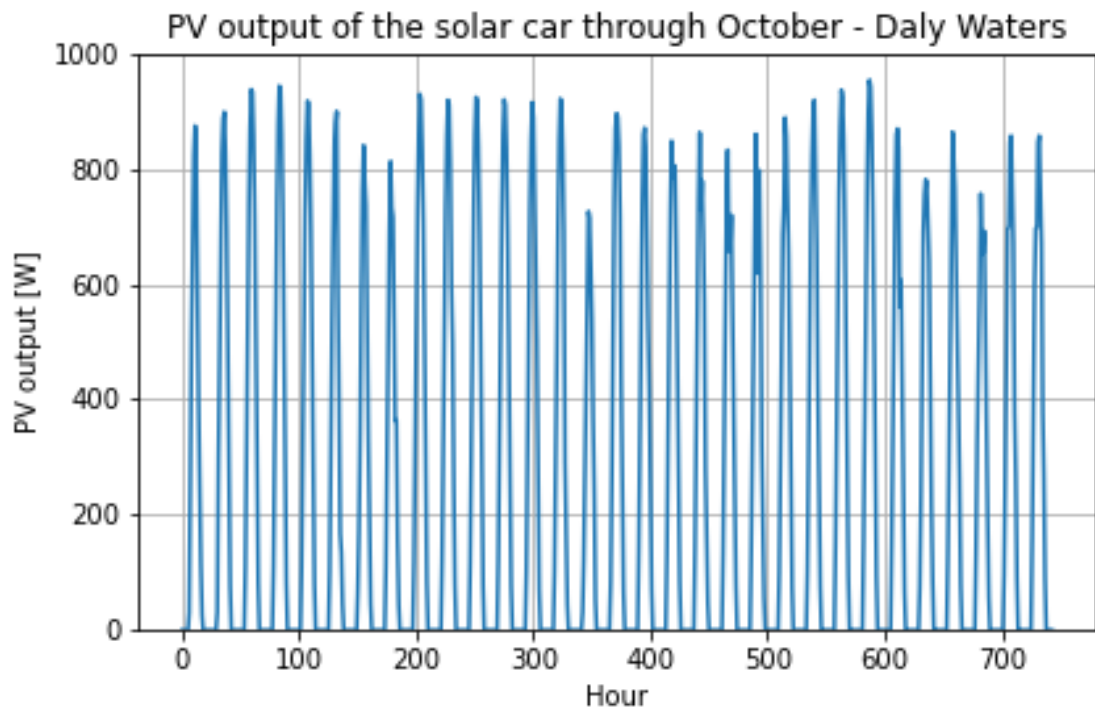


Figure 79: PV output of the SC throughout October in Daly Waters during a TMY.

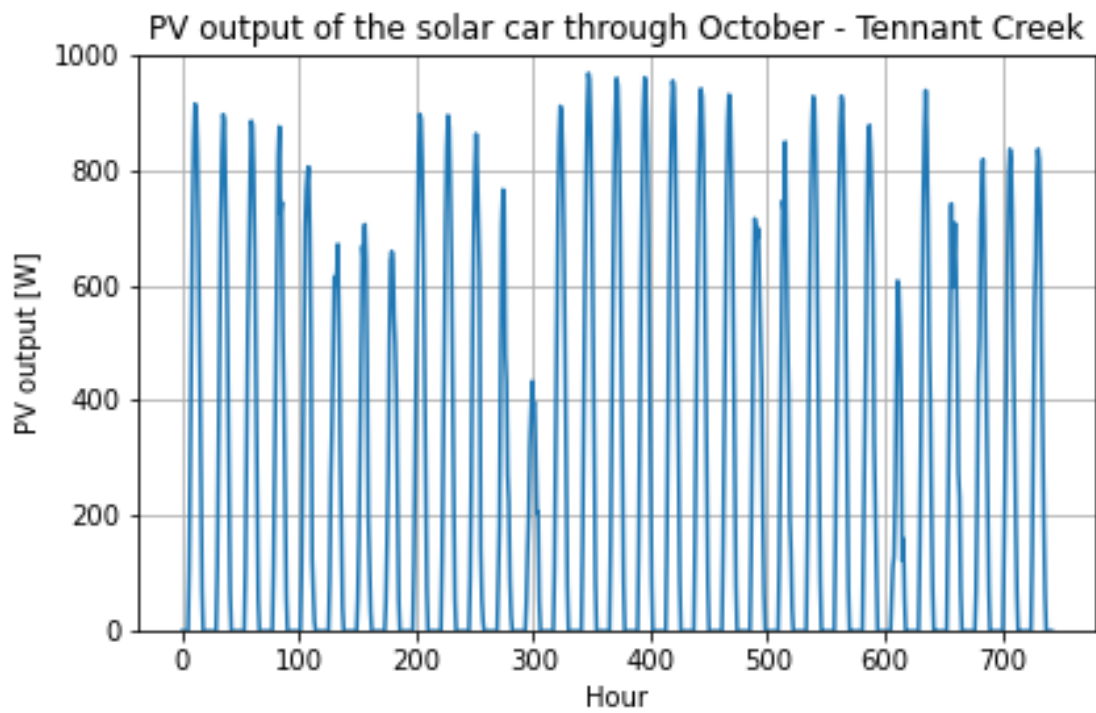


Figure 80: PV output of the SC throughout October in Tennant Creek during a TMY.

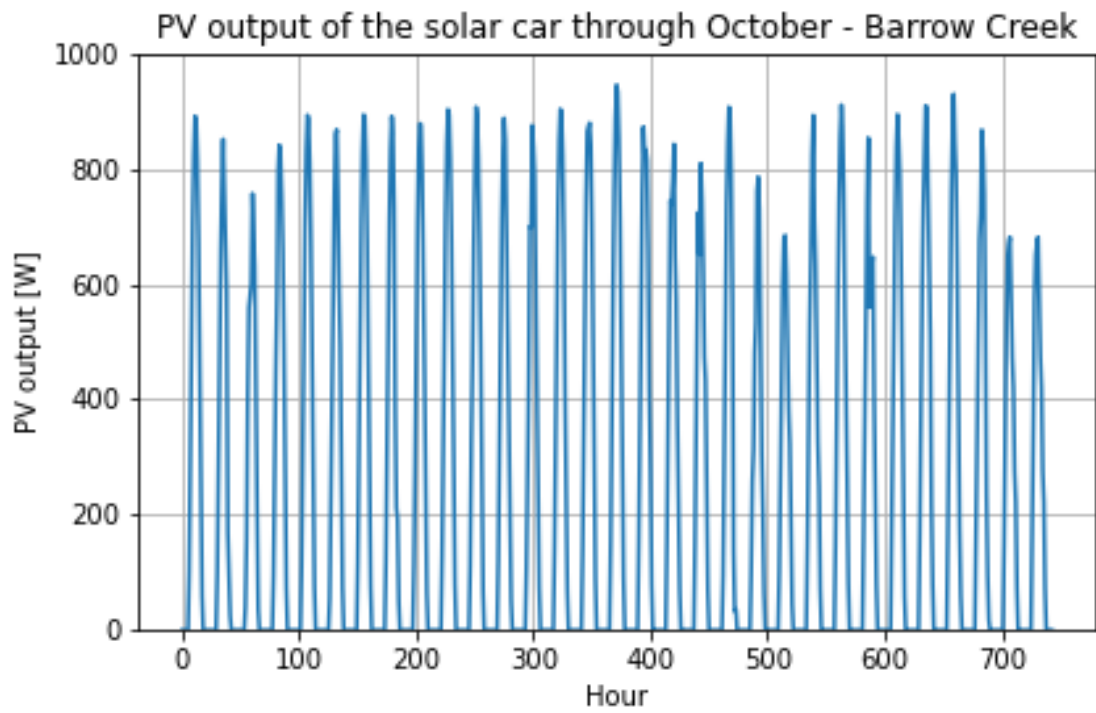


Figure 81: PV output of the SC throughout October in Barrow Creek during a TMY.

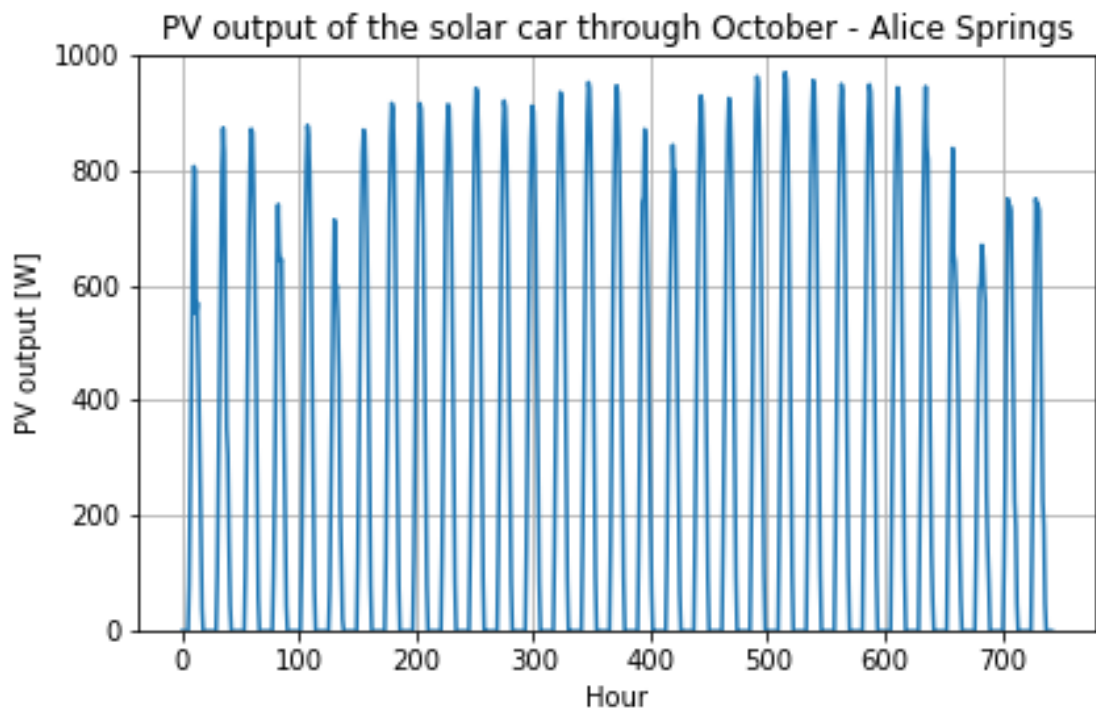


Figure 82: PV output of the SC throughout October in Alice Springs during a TMY.

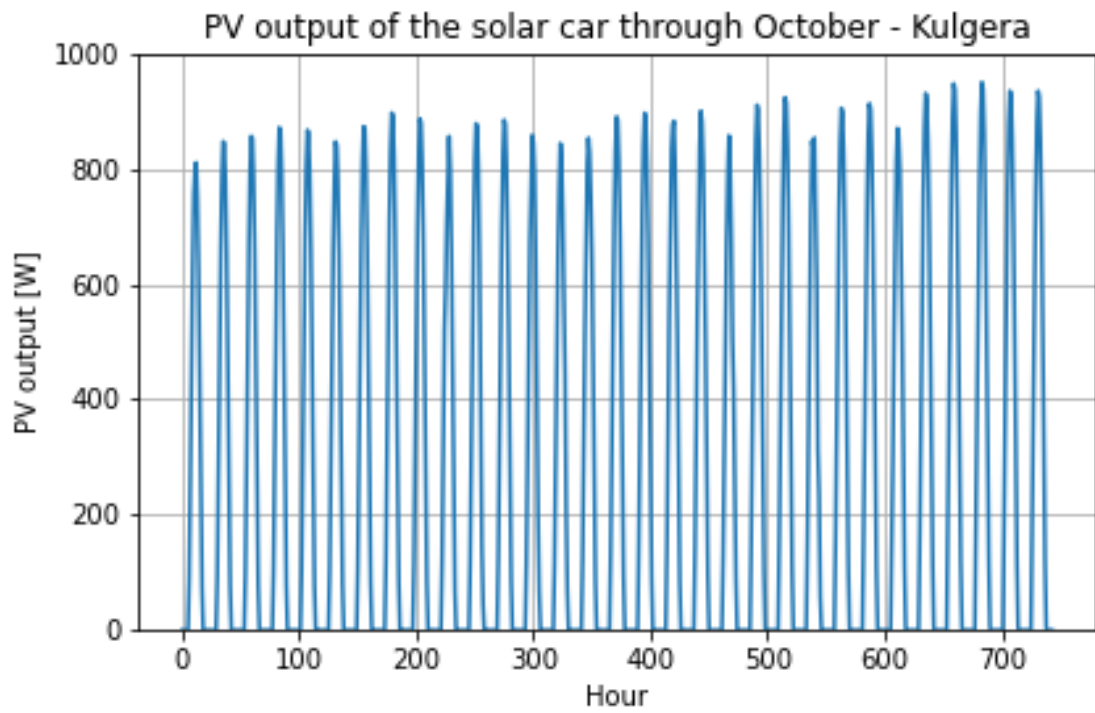


Figure 83: PV output of the SC throughout October in Kulgera during a TMY.

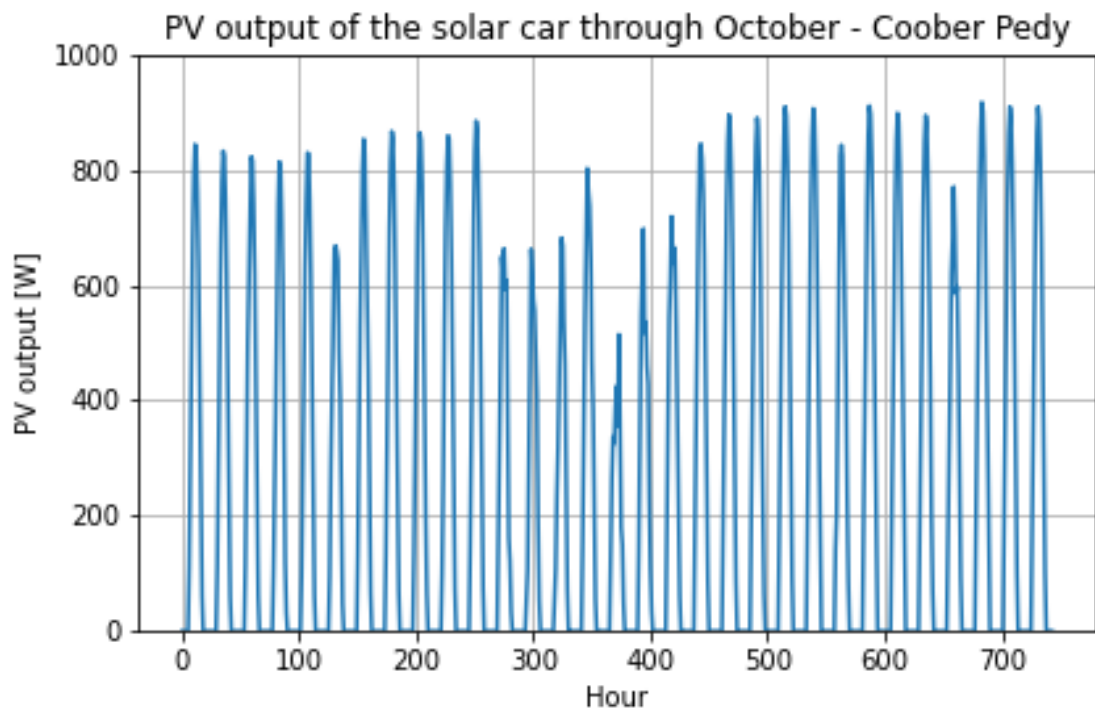


Figure 84: PV output of the SC throughout October in Coober Pedy during a TMY.

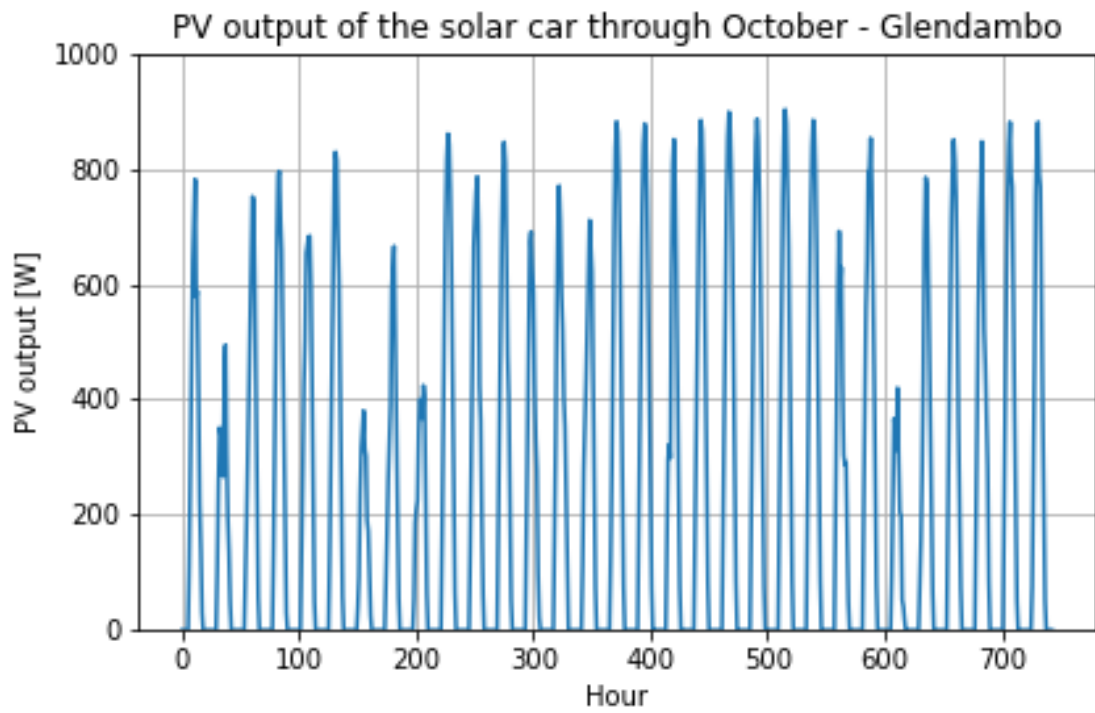


Figure 85: PV output of the SC throughout October in Glendambo during a TMY.

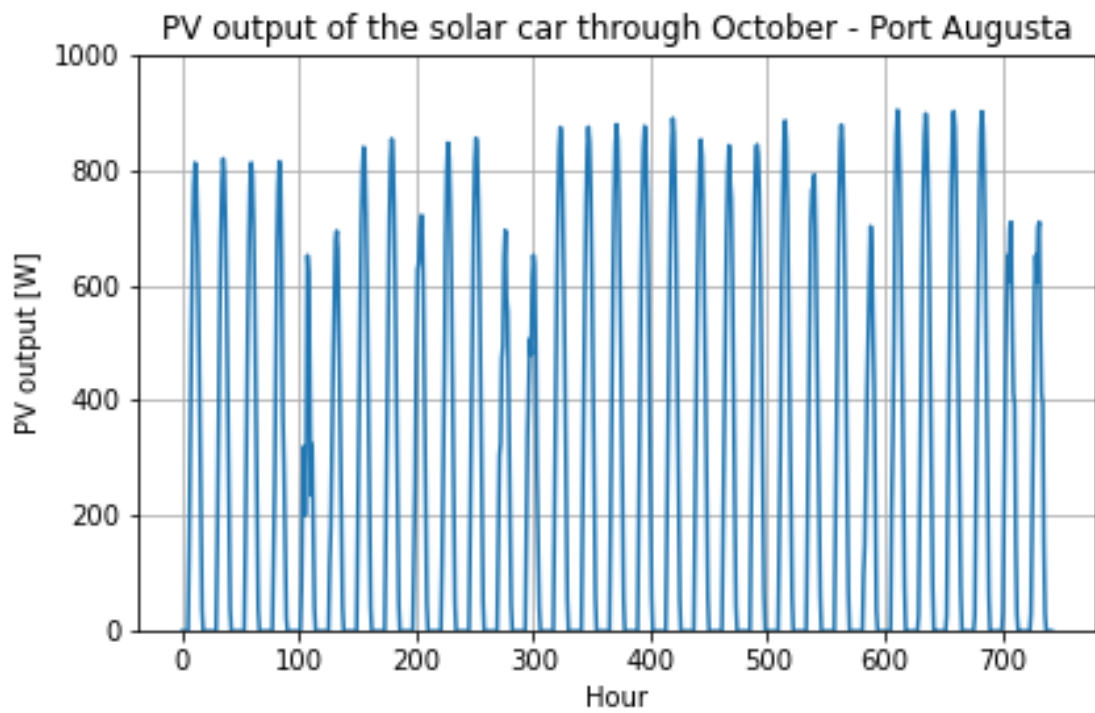


Figure 86: PV output of the SC throughout October in Port Augusta during a TMY.

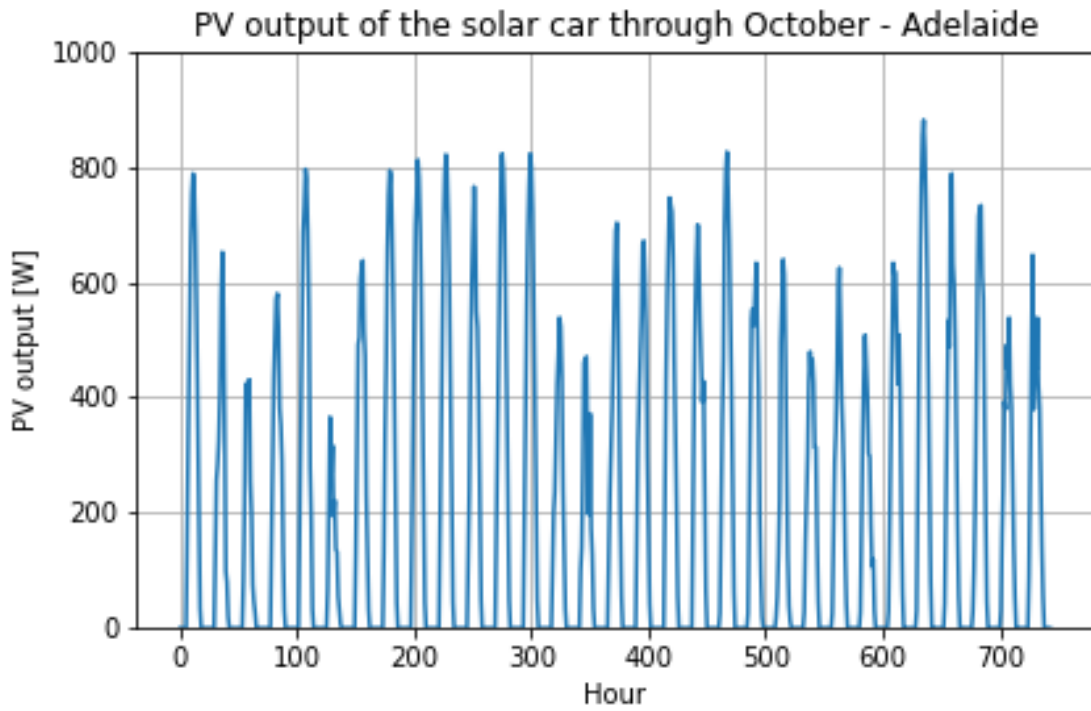


Figure 87: PV output of the SC throughout October in Adelaide during a TMY.

B.6 Average PV output per day throughout the route.

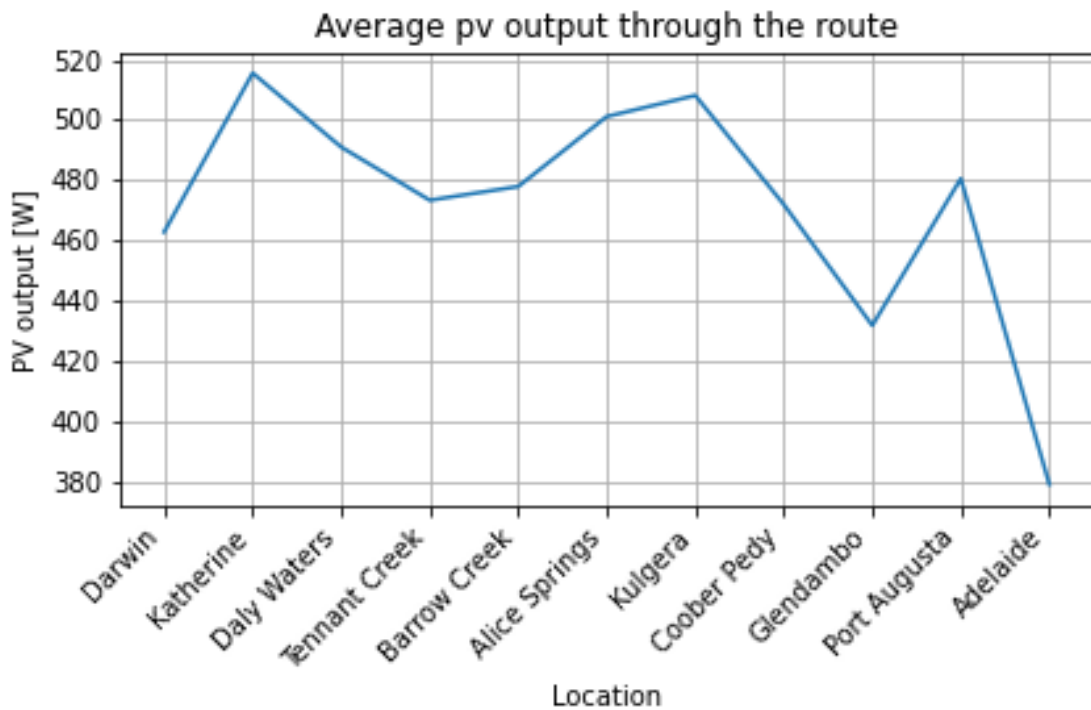


Figure 88: Average PV-output per day throughout the route in october during a TMY.

B.7 Load

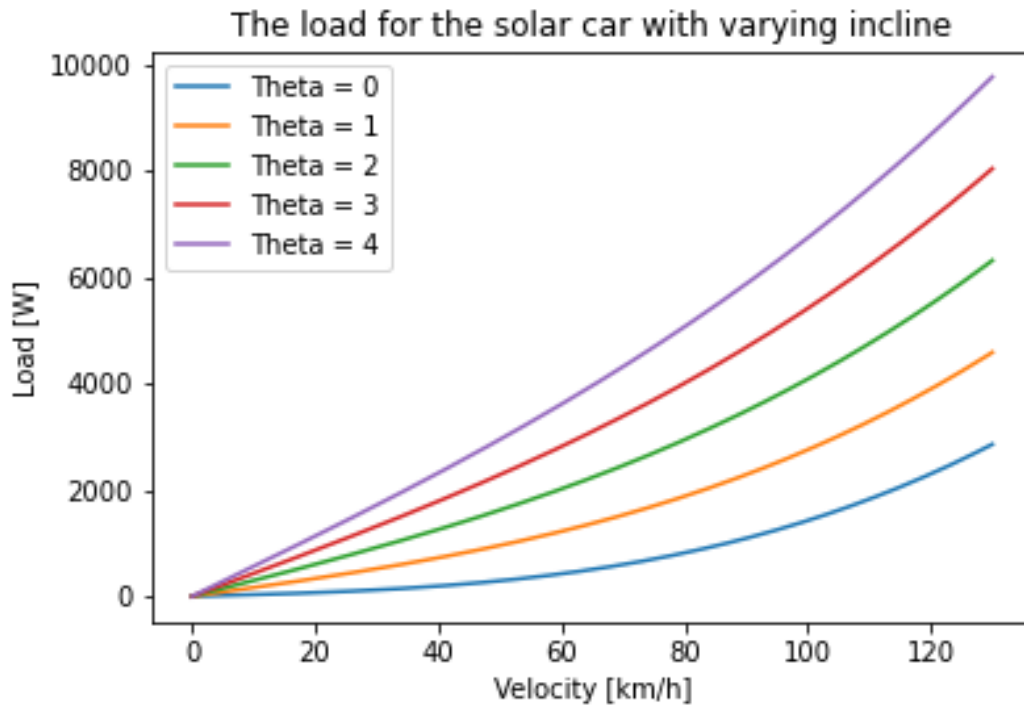


Figure 89: The load for the SC with steps in incline.

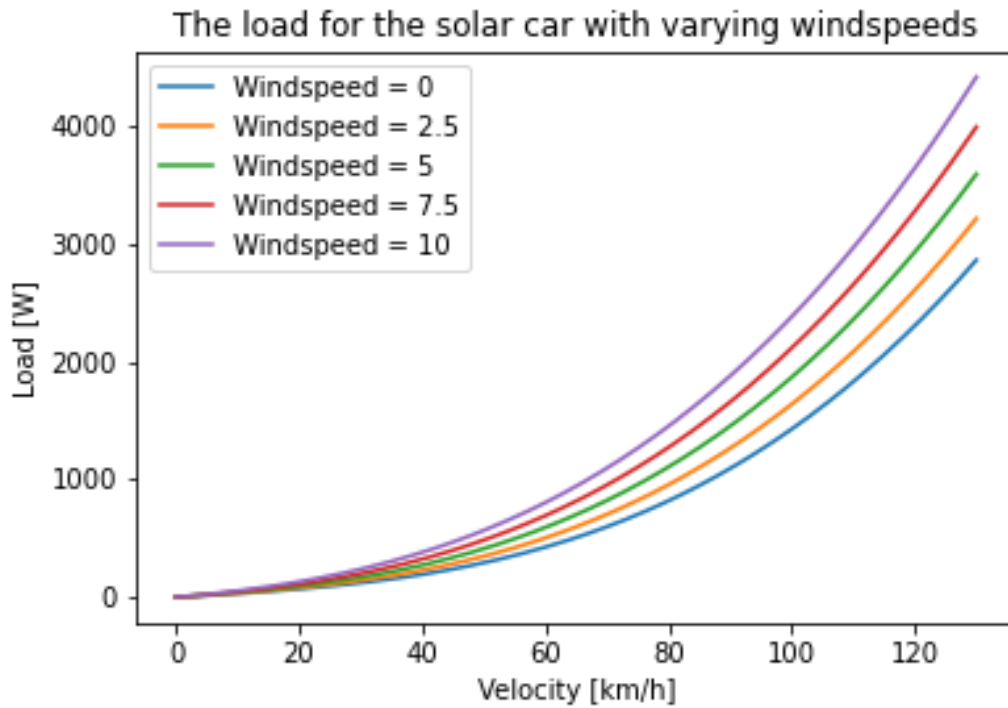


Figure 90: The load for the SC with steps in windspeed.

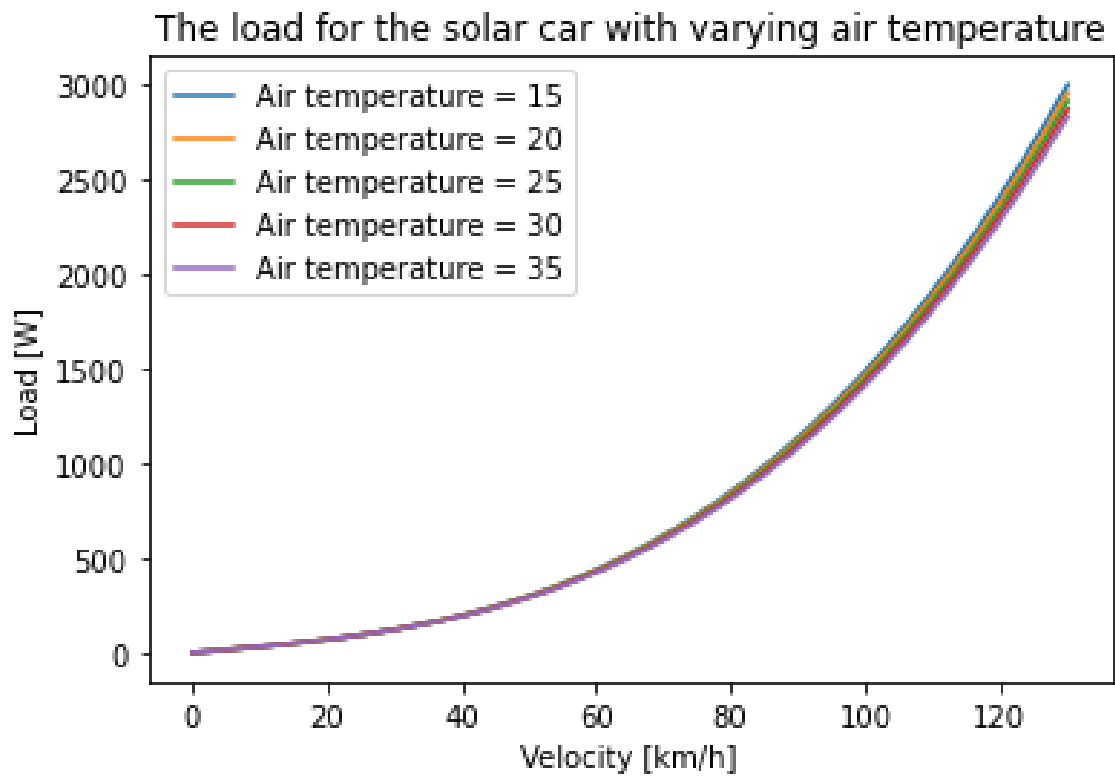


Figure 91: The load for the SC with steps in air temperature.



Norwegian University of
Science and Technology